STOCHASTIC DAMAGE EVOLUTION UNDER STATIC AND FATIGUE LOADING IN COMPOSITES WITH MANUFACTURING DEFECTS

A Dissertation

by

YONGXIN HUANG

Submitted to the Office of Graduate Studies of
Texas A&M University
in partial fulfillment of the requirements for the degree of

DOCTOR OF PHILOSOPHY

May 2012

Major Subject: Aerospace Engineering

Stochastic Damage Evolution under Static and Fatigue Loading in Composites with Manufacturing Defects

STOCHASTIC DAMAGE EVOLUTION UNDER STATIC AND FATIGUE LOADING IN COMPOSITES WITH MANUFACTURING DEFECTS

A Dissertation

by

YONGXIN HUANG

Submitted to the Office of Graduate Studies of
Texas A&M University
in partial fulfillment of the requirements for the degree of

DOCTOR OF PHILOSOPHY

Approved by:

Chair of Committee,	Ramesh Talreja
Committee Members,	Anastasia Muliana
	J. N. Reddy
	Vikram Kinra
Head of Department,	Dimitris Lagoudas.

May 2012

Major Subject: Aerospace Engineering

ABSTRACT

Stochastic Damage Evolution under Static and Fatigue Loading

in Composites with Manufacturing Defects.

(May 2012)

Yongxin Huang, B.S., University of Science and Technology of China;

M.S., Texas A&M University

Chair of Advisory Committee: Dr. Ramesh Talreja

In this dissertation, experimental investigations and theoretical studies on the stochastic matrix cracking evolution under static and fatigue loading in composite laminates with defects are presented. The presented work demonstrates a methodology that accounts for the statistically distributed defects in damage mechanics models for the assessment of the integrity of composites and for the structural design of composites.

The experimental study deals with the mechanisms of the formation of a single crack on a micro-scale and the stochastic process for the multiplication of cracks on a macro-scale. The defects introduced by the manufacturing processes are found to have significant effect on the matrix cracking evolution. Influenced by the distributed defects, the initiation and multiplication of cracks evolve in a stochastic way. The experimental study on the in-plane shear stress finds the detrimental effect of the shear stress on the fatigue performance of composite laminates. Combined with the transverse tensile stress,

the in-plane shear stress induces multiple inclined microcracks in the matrix, which enhance the initiation and propagation of the major matrix cracks.

Based on the experimental investigations, a statistical model for the stochastic matrix cracking evolution on the macro-scale is developed. Simulations based on the statistical model yield accurate predictions for both static and fatigue loading compared to the experimental data. The Weibull distribution of the static strength is estimated by the statistical model by comparing against the experimental crack density data. The estimated Weibull distribution of the static strength provides an efficient approach to characterize the manufacturing quality of composite laminates. Compared to deterministic approaches, the Weibull distribution of the static strength provides comprehensive information of the strength property of composite laminates.

ACKNOWLEDGEMENTS

I wish to thank my adviser Prof. Ramesh Talreja. It is a great honor for me to pursue my Ph.D. study under his supervising. I also thank my co-adviser Prof. Janis Varna for his guidance. I always enjoyed the discussion with Prof. Varna on any subject. I would like to thank the members of my dissertation committee: Prof. Anastasia Muliana, Prof. J. N. Reddy and Prof. Vikram Kinra for their suggestions and support.

I would like to thank Drs. Povl Brøndsted and Bent Sørensen for their support for my experimental work conducted at Risø DTU National Laboratory for Sustainable Energy. I want to thank Prof. Marino Quaresimin for his advice and support for my experimental work conducted at University of Padova.

I would like to thank all my research group members for their friendship and great help. They are Reding Derek, Chang Chen, Tessa DeCoite, Udaya Sunku, Linqi Zhuang. Special thanks to my collaborators and friends: Konstantinos Giannadakis and Loukil Mohamed at Lulea University of Techonology and Paolo Carraro at University of Padova.

Special thanks to Ms. Karen Knabe for her great help during my study in the Aerospace Engineering Department.

TABLE OF CONTENTS

Page

LIST OF FIGURES

Page

Page

Page

Page

Page

LIST OF TABLES

1. INTRODUCTION

In recent years, there has been a steady growth of the applications of fiber-reinforced composite materials not only for the aerospace industry, but also for some emerging fields such as the automotive, marine, and renewable energy industries. Thanks to the research and development in the aerospace industry for the past 60 years, abundant knowledge on the composites has been accumulated, and can be transferred to the fields outside of the aerospace industry. However, the different applications also mean quite different design methodologies, manufacturing processes, service environment, maintenance, and recycle strategies. It should be extremely cautious to extend the design methodologies and analytical tools developed for aerospace composite structures to other fields.

The applications of composite materials outside of the aerospace industry are often more sensitive to the cost. As a result, the tradeoff between the performance and cost usually yields low-cost composite structures with severer state of defects compared to high quality aerospace structures. The lacking of the understanding of the defects and their effect makes the structural design for the low-cost composites far from the optimal. The objectives of this study are to deepen this understanding and, based on this knowledge, to establish a modeling strategy for performance evaluation of composites with defects.

This dissertation follows the style of Composites Science and Technology.

In the second section of this dissertation, the current state of the art on defects and damage in composite laminates is reviewed and discussed. The damage modes under the external loading and the defects introduced by the manufacturing processes are firstly detailed. The available methods in treating defects are reviewed, followed by the discussion on a new approach, i.e. defect damage mechanics. Experimental observations and modeling strategies on the interaction between defects and damage are reviewed for this new approach, focusing on the statistical nature of defects. In the second part of this section, the stochastic matrix cracking evolution in composites is taken as an example to apply the new approach to evaluate the materials response for composites with defects. Section 3 presents experimental investigations on the stochastic matrix cracking evolution in composite laminates. The objectives are to identify the relevant mechanisms for modeling the cracking evolution, and to obtain experimental data for testifying the developed model. Section3.1 reports the effect of manufacturing defects on the multiplication process of matrix cracks in cross ply laminate. Section 3.2 presents a preliminary study on the effect of the in-plane shear stress on the fatigue performance of multidirectional laminates. Section 3.3 continues the study on the in-plane shear stress, focusing on its effect on the matrix cracking.

The stochastic matrix cracking evolution under the static loading is studied in Section 4. The objectives are to model the statistical process for the cracking evolution under the static loading and, based on the modeling, to characterize the effect of defects. The outcomes are: (1) the prediction of the cracking evolution, i.e. the crack density and the

statistical distribution of crack spacing, as functions of the static loading, and (2) the statistical distribution of the static strength resulting from the distributed defects. Section 5 presents the statistical model of the matrix cracking evolution under fatigue loading The objective is to extend the statistical model for the static loading to fatigue loading so that the modeling approach for different loading conditions can be unified. The outcome is the prediction of the crack density as a function of fatigue loading history.

Finally, conclusions are given, and the future direction is suggested in Section 6.

2. CURRENT STATE OF THE ART ON DEFECTS AND DAMAGE IN COMPOSITE LAMINATES

In this part of the dissertation, section 2.1 details the irregularities in fiber-reinforced polymeric composites including in-service damage and manufacturing defects. The experimental and theoretical study of damage and defects is firstly reviewed. The interaction between damage and defects is then discussed. Especially, the stochastic nature of damage evolution affected by the randomly distributed manufacturing defects is detailed. The importance of including the effect of manufacturing defects in damage mechanics models is explained, followed by some general modeling strategies in literature. In Section 2.2, matrix cracking evolution is taken as the example to detail the stochastic nature of damage evolution affected by defects, followed by a review of modeling efforts reported in literature. At last, a statistical modeling approach for the stochastic matrix cracking evolution is proposed.

2.1 Irregularities in composite laminates

2.1.1 In-service damage

In-service damage can be understood as irreversible changes by sorts of energy dissipation mechanisms before the catastrophic failure. In composite laminates, different damage modes exist as the irreversible changes under varied loading conditions. For the unidirectional laminate, fiber breakage, fiber debonding, and matrix cracking are the common damage modes under longitudinal tension.

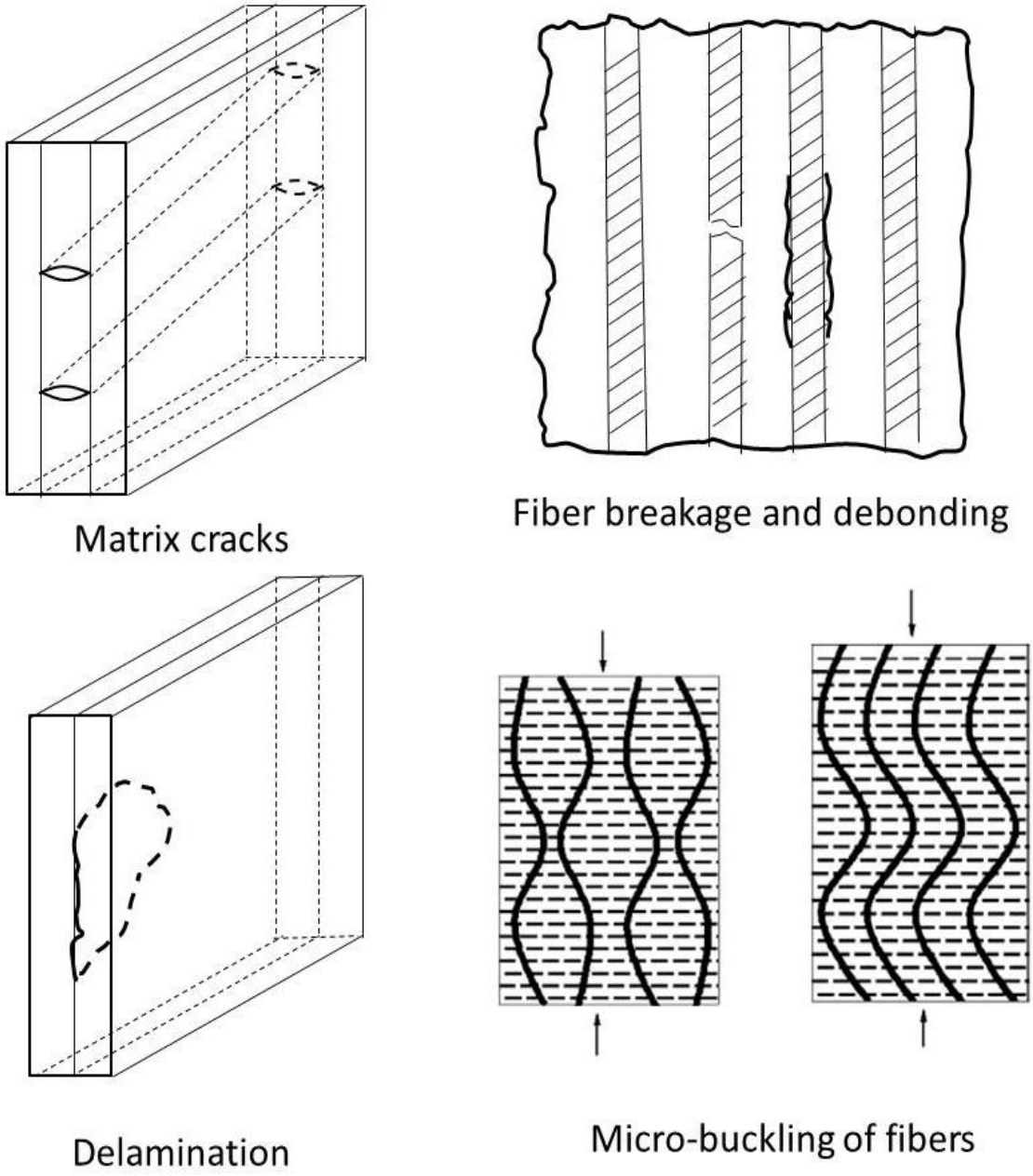

Fig. 2.1 The schematic of damage modes (replicated from [1])

Matrix cracking along the fiber direction is the major damage mode in a unidirectional laminate under transverse tension. Under longitudinal compression, microbuckling of fibers is the common damage mode. For multidirectional laminates, some additional damage modes are observed such as delamination. A schematic of different damage modes is shown in Fig. 2.1. For reviews on different damage modes, see Nairn[2] on matrix cracks, Garg [3] on delamination, Budiansky and Fleck [4] and Fleck[5] on micro-buckling of fibers.

As a well-established field, damage mechanics focuses on identifying important damage modes and studying the initiation and evolution of specific damage modes as well as their consequences on the response of the composites to external loading. The damage modes that are critical for the integrity of composite laminates are usually identified from experimental observation. As Fig. 2.2 shows, the damage development before the catastrophic failure of composite laminates under fatigue tension is clarified from extensive experimental investigations. Experimental observations also suggest that the initiation and evolution of damage usually accompanies the degradation of materials properties and leads to catastrophic failure. In Fig. 2.3, for example, the decreased effective stiffness is found to be accompanied by the matrix cracking evolution [6]. Based on the experimental observation, the modeling effort on damage has several objectives, which are not separated from each other; 1) predicting the damage development as response to the specific loading history; 2) predicting the property

degradation (strength or stiffness reduction) as the result of a given damage state; and 3) predicting the catastrophic failure caused by the damage accumulation.

The damage mechanics models may be classified in two categories: the micromechanics model and the continuum damage mechanics model. In micromechanics model, specific damage modes are usually directly modeled as discontinuous irregularities such as cracks. In contrast, continuum damage mechanics model treats damaged composites as a homogeneous continuum with the damage variables to represent the considered damage modes[7]. Despite of the differences, most of damage mechanics models share a common assumption that the material property is uniform within each pre-damaged layer. All factors that can affect the damage evolution have been lumped into the homogeneous lamina properties such as the lamina stiffness and strength. However, as the production and application of composite structures become increasingly diversified, the damage analysis based on homogenous lamina properties may be oversimplified for many cases. Especially, the composites manufactured by some low-cost processes are widely used outside of aerospace industry. They usually possess many defects. Those distributed manufacturing defects as pre-condition make the material property degrade in a random style. If the randomness in the resulted material property within lamina cannot be neglected, the homogeneous lamina property used in damage mechanics models is not valid anymore. For this consideration, the effect of manufacturing defects on damage development should be examined. As the first effort along this direction, information on manufacturing defects is presented in Section 2.1.2.

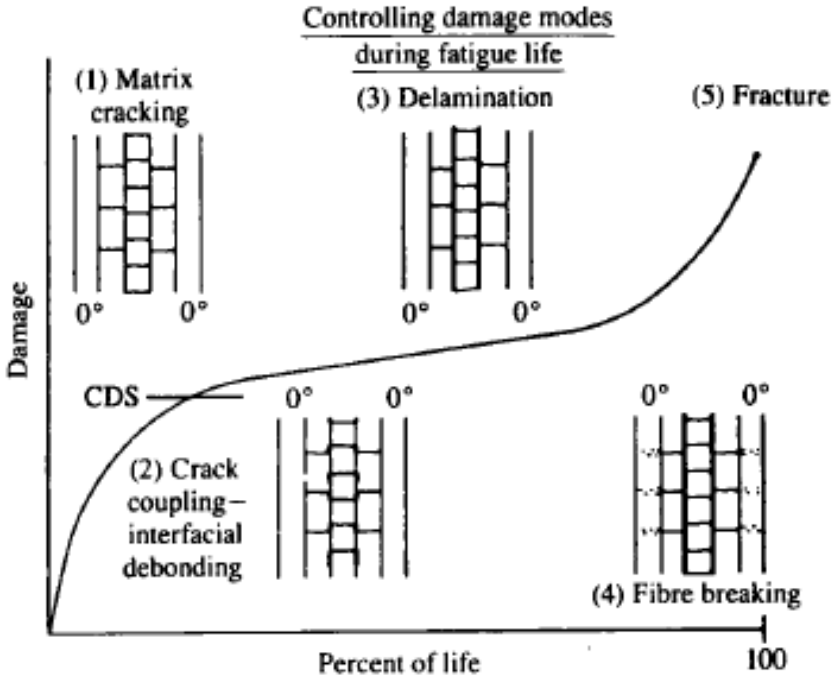

Fig. 2.2 The damage development leading to the catastrophic failure of laminates under fatigue tension [8].

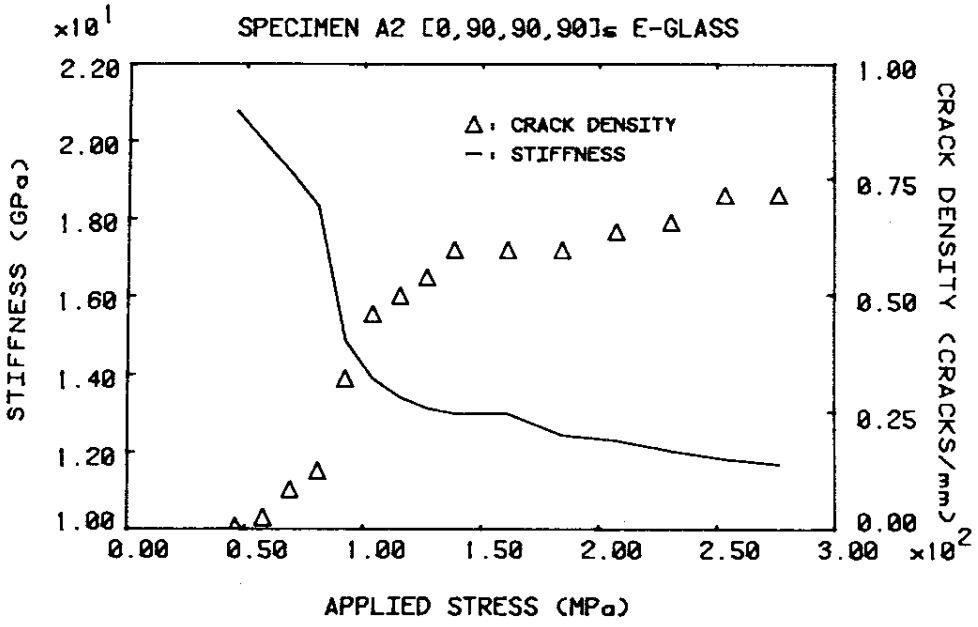

Fig. 2.3 The effective stiffness and matrix crack density vs. applied stress [6].

2.1.2 Manufacturing defects

Manufacturing-induced defects widely exist in fiber-reinforced polymeric composites though the severity varies with the manufacturing processes. Two major manufacturing processes are firstly described here as the background for understanding how defects are introduced through manufacturing processes. For more details on different manufacturing techniques, one can refer the textbook by Hoa [9].

The pre-impreg (prepreg) based autoclave molding is the standard process for manufacturing high quality composite structures in aerospace industry. The prepregs are the combination of fiber and partially cured resin in the form of tapes for unidirectional fibers and fabrics for woven. Fig 2.4 shows a roll of carbon/epoxy prepreg. For manufacturing laminates, the prepregs are cut and stacked according to the laminates design. The stacked layers are put on the surface of a mold surrounded or covered by ancillary materials (see Fig. 2.5). The bagged lay-up assembly is placed inside the autoclave for curing to complete the whole process as shown in Fig. 2.6. During the curing process, pressure and vacuum need to be applied to prevent defects such as fiber misalignment, resin rich area and voids. Although the manufacturing defects can be introduced at any step during the whole process, the autoclave curing is the critical step to introduce/reduce manufacturing defects. Insufficient pressure or vacuum is the major cause for the introduced defects.

Figure 2.4 A roll of carbon/epoxy prepreg

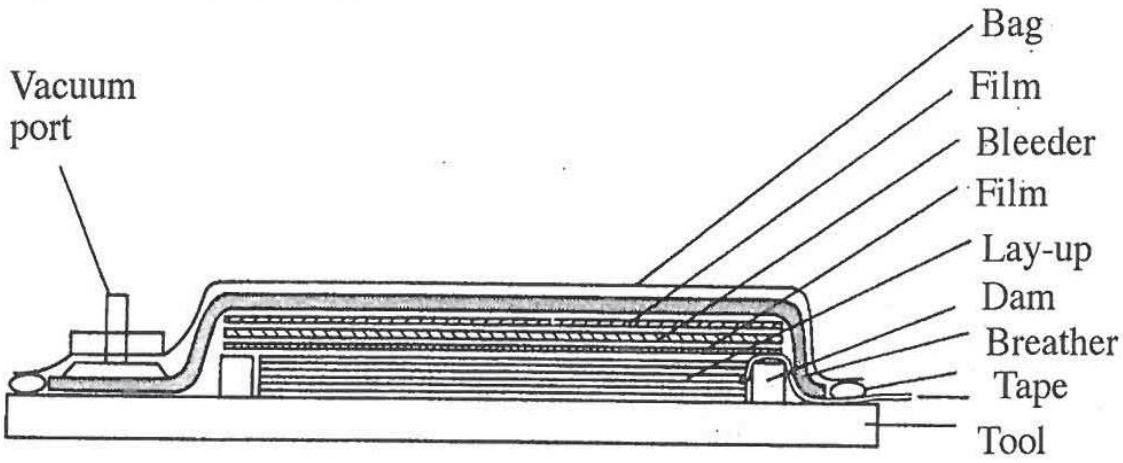

Fig. 2.5 The bagged lay-up assembly on the mold (Courtesy of J. Varna)

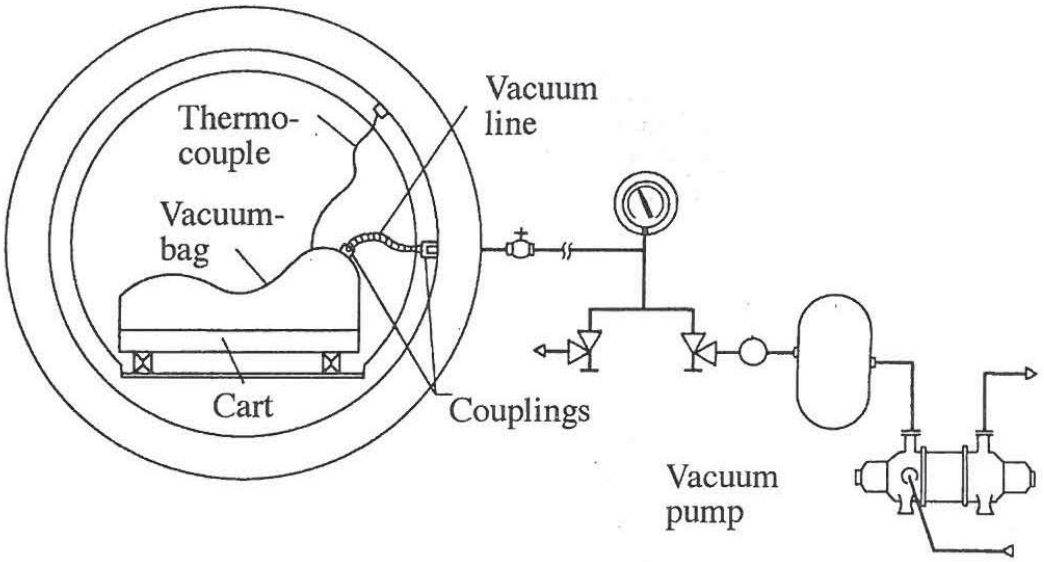

Fig. 2.6 Schematic of autoclave system for composite process.

Manufactured by the prepreg-based autoclave molding process, composite structures usually have very few defects. What's more, those defects usually distribute quite uniformly so that the materials properties are almost homogenous.

The Liquid composite molding (LCM) process is another widely used technique. Dry fibers are packaged forming the configuration of the part and put inside a tool. Then the liquid resin and catalyst are infused into the mold to wet the fibers and to eventually form the matrix during the curing process. The resin infusion is the critical step for the quality control. It usually introduces defects such as dry zone (not wet fibers), voids, and fiber misalignment. The distribution of those defects is not uniform. For this reason, the material properties might be highly inhomogeneous.

The use of prepregs and autoclave makes the cost of the autoclave molding process very high. For some large composite structures, the needed autoclave may be too large to be practical or economically sound. Large composite structures like wind turbine blades subject to strict restriction on cost are usually manufactured by low-cost processes such as the LCM process. Compared to the autoclave molding, low-cost processes usually introduce more defects into the final product. Therefore, as the composites see increasingly more applications outside of the aerospace industry, the trend of adopting low-cost processes like the LCM process make the study on the manufacturing defects especially urgent.

The most common manufacturing defects in composite laminates are listed in Table 2.1. Certain processes may eliminate some of the defects. For example, the use of prepreg in the autoclave molding process can get rid of the dry zone, which corresponds to inimpreganted fibers. Some of the defects are unavoidable in all available processes though the severity varies. The void as one of the most common defects found in any process is taken as the example to illustrate the origin and effect of defects.
Figure 2.8 shows the micrograph of voids in the matrix. Voids in the matrix may form during the curing process from two major origins; 1) the gas entrapped during laying up for prepreg based processes or during resin infusion for LCM processes, and 2) the volatiles and gas from the moisture forming at relatively high curing temperature. For the autoclave molding process, the applied pressure prohibits the formation of volatiles and gas bubbles from the moisture. It also drives the existing volatiles and gas to flow

through gas transport pathways and to be eventually removed by vacuum system. Lacking of applied pressure for LCM processes, more gas and volatiles are formed and kept in laminates as the origin of voids. Therefore, LCM processes usually yield much higher void content than the autoclave molding process. In addition, the gas transport system is harder to establish in textile laminates, and therefore more gas and volatiles are kept within the laminates to form voids, which is the case shown in Fig. 2.7.

Table 2.1 The common manufacturing defects in fiber-reinforced composite laminates

Location	**Manufacturing defects**
Matrix	void, porosity, resin rich area, incompletely cured matrix
Fiber	fiber misalignment, e.g. waviness, dry zone (unimpregnated fibers), fiber defects
Fiber/Matrix interface	debonding
Interface between plies	delamination

Fig. 2.7 The voids (black spots) in carbon/epoxy laminates [10].

The voids in the matrix can be characterized by their sizes, shapes and positions. For laminates manufactured by the autoclave molding process, the voids distribute quite uniformly, and their sizes have little variation. Under such conditions, it is reasonable to use the volume content to characterize the severity of voids, and to correlate the volume content to materials properties for describing the effect of voids.

There has been much research on the relationship between void content and different strength properties. By carefully controlling the curing process, plates with uniformly distributed voids but different void volume content can be obtained and subject to strength tests. Bowles and Frimpong [11] found that the interlaminar shear strength is decreased by about 20% when the void content increases from 1% to 10%. Liu [12] found that the transverse tensile strength is decreased by about 10% when the void content increases from 0.5% to 3%. Almeida and Neto [13] measured the flexural strength of carbon/epoxy laminates with the void content varying from 1% to 6%, and

found that the void has significant detrimental effect on the static strength of laminates once the void content surpasses certain threshold, i.e. 3% for their specimens. What's more critical, they revealed that the fatigue life of laminates is even more sensitive to the void content than the static strength. The fatigue life could be decreased by 90% when the void content increases from 1% to 6% for high fatigue stress levels. However, some strength properties are not affected by the void content. For example, Olivier et al. found that the longitudinal tensile strength is not sensitive to the void content [14].

For high quality composites, the current treatment of defects is to find the proper accept/reject criterion and to improve the process to satisfy such criterion. Firstly, the severity of the studied defects is quantified, and the important properties sensitive to the specific defects are identified. Then, the quantitative relationship between such properties and the defects is determined experimentally. The tradeoff between the manufacturing cost and materials properties involves and yields the proper accept/reject criterion for the detected state of manufacturing defects. In some cases, a threshold level can be found. If the degree of the defects is less than such threshold level, further reducing the defect will not significantly improve the quality. Then such threshold level is usually taken as the accept/reject criterion. For example, the volume content is identified as the characterization of homogeneously distributed voids, and the flexural strength and interlaminar shear strength (ILSS) are found to be sensitive to the void content. One accept/reject criterion for void content can be figured based on the

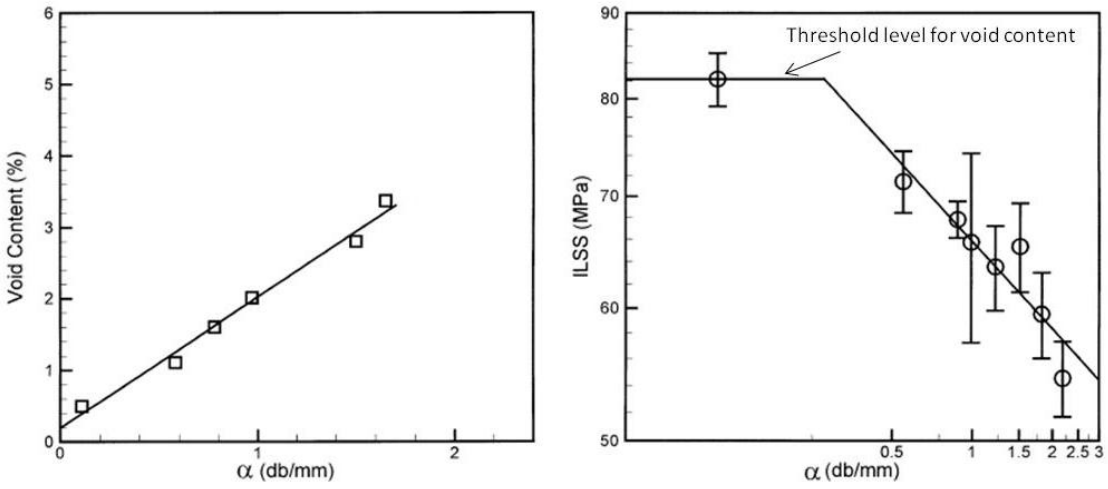

(a) (b)

Fig. 2.8 The relationship between void content and interlaminar shear strength (ILSS) correlated by the ultrasonic absorption coefficient. (a) The void content of laminated plate vs. the ultrasonic absorption coefficient and (b) the ILSS vs. the ultrasonic absorption coefficient [15]

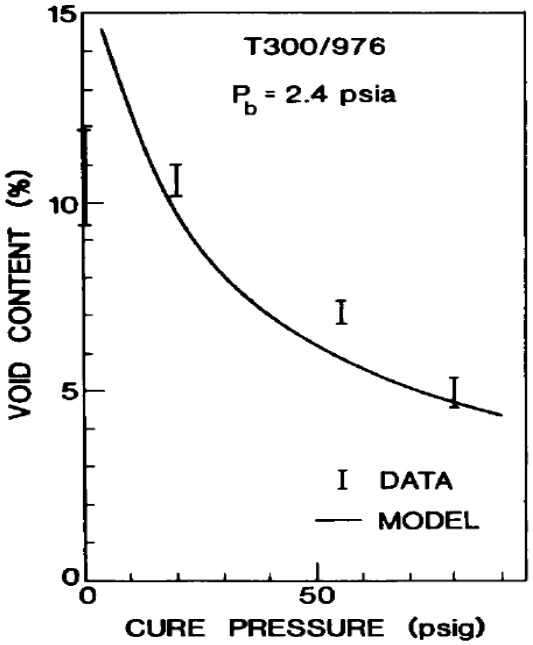

Fig. 2.9 The void content as a function of cure pressure for the autoclave molding process [16].

relationship between the void content and the corresponding ILSS shown in Fig. 2.8, for which such relationship is correlated by the measured ultrasonic absorption coefficient. Once the criterion is set, the process parameters are adjusted to satisfy it. For example, 5% is usually taken as the accept/reject criterion for the void content of aerospace structures. Based on the relationship between the curing pressure and void content, e.g. Fig. 2.9, the curing pressure can be easily determined to satisfy the criterion.

For composite structures manufactured by some low-cost processes such as the LCM process, the degree of defects is much higher. It usually sees large variation in the sizes and positions of defects. For such situation, the typical treatment is to find the critical state in terms of the sizes and positions and repair it. Usually, only large defects are detected by the non-destructive inspection (NDI) and repaired after production while small ones are assumed to be not important and left in the final product. To do that, an accept/repair criterion for the large defects is needed. An example is the treatment of delaminations introduced by manufacturing processes. The delamination will mainly reduce the compression strength of composite structures because the critical buckling load is reduced by the delamination. Depending on the position of delamination, local or global buckling may happen under compression as shown in Fig. 2.8 according to Short *et al.* [17]. The compression strength of a composite structure is therefore reduced as the critical buckling load is reduced. A critical size for the delamination at a given position may be obtained experimentally or theoretically based on the reduced compression strength and used as the accept/repair criterion for detected delaminations.

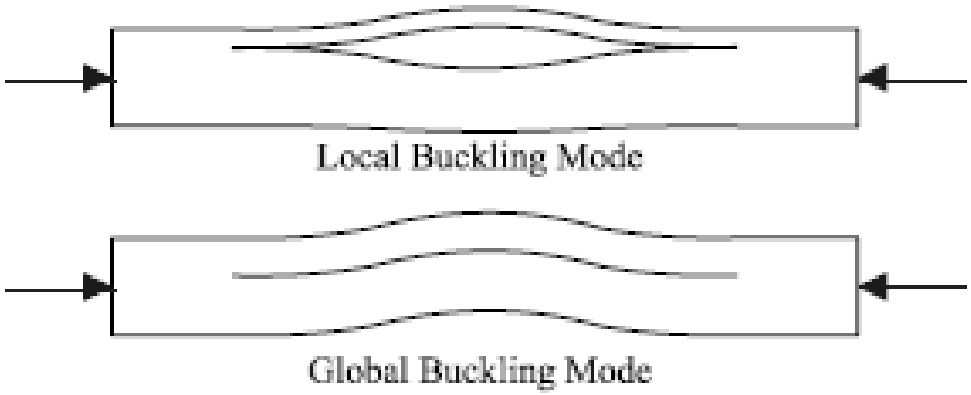

Fig. 2.10 Two buckling modes for delamination [17].

The statistical distribution of manufacturing defects in terms of sizes, shapes and positions has been widely observed especially in laminates manufactured by low-cost processes. However, neither the accept/reject approach or the accept/repair/reject approach is able to treat the defects by considering the statistical distribution of defects. In the traditional approach of designing composite structures, it is assumed that the manufactured composite laminates are free of defects and therefore possess homogeneous properties if they pass quality inspection. The effect of distributed defects and other uncertainties are accounted for by applying certain safety factor. In a recent report from Sandia National Laboratory[18], the authors recommended that new design methodology incorporating the statistics of manufacturing defects has to be adopted to assure the structural reliability, especially for composite structures such as wind turbine blades and ships those are manufactured by low-cost processes. One approach along this

direction is to directly model the specific defects. Toft *et al* [19] proposed a framework to study the statistics of manufacturing defects and its influence on the reliability of composite structures. The statistical information about defects such as defect type, size, position and shape is directly modeled in the proposed framework. Taking delamination as an example of manufacturing defects, the authors developed a statistical model to study the effect of the distributed delaminations on the reliability of a composite wind turbine blade. In the model, the statistical distribution of the size and position of delaminations is assumed while the shape is kept as circle. Their model reveals that the distributed delaminations greatly decrease the reliability, thus decreasing the load-carrying capacity of the structure. The parametric study also shows that such detrimental effect is intensified when the distributed delaminations tend to cluster with each other. As some pioneering work along this direction, the results from the statistical model offer some good evidence that illustrates the importance of the statistics of manufacturing defects. However, the statistical model quantifies the effect of the distributed delaminations by discounting the local strength in an empirical way. The whole failure process caused by the manufacturing induced delamination is not clear.

The gap between pre-existed manufacturing defects and the performance of composite structures under external loading can be filled by the study of the initiation and evolution of in-service damage. As mentioned in Section 2.1.1, for most cases, the failure process and property degradation under external loading in composites can only be understood through the study of damage development. Therefore, a mechanism-based approach to

study the effect of manufacturing defects on the integrity of composites must look into the interaction between defects and damage development.

2.1.3 The interaction between manufacturing defects and damage

Generally, the existence of manufacturing defects enhances the damage development under loading. Experimental observations of the damage development promoted by manufacturing defects have been reported in literature. Varna *et al.* [20] reported that the laminates with high void content possess more matrix cracks when they fail under transverse tension. The microscopic observation illustrates the interaction between cracks and voids shown in Fig. 2.11. The experimental observation suggests that voids promote the initiation and propagation of cracks.

Studying the effect of large waviness on compression strength of laminates, Adams and Hyer [21] reported that the failure mode is numerous delaminations near the waviness. This is confirmed by the observation on the edge of laminates shown in Fig. 2.13 cited from Cairns et al. [18]. It suggests that the large waviness can induce delaminations. For small fiber waviness, i.e. the order of fiber diameter, the waviness is usually the initiation site of fiber micro-buckling under longitudinal compression[5].

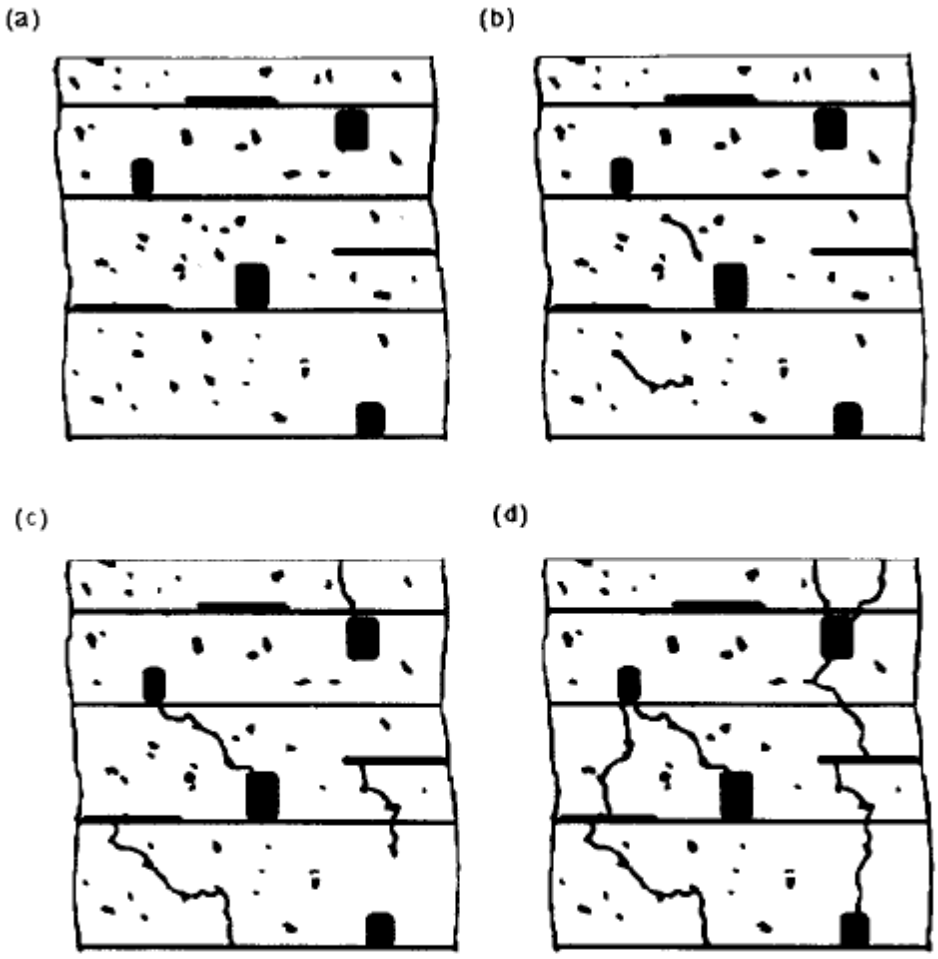

Fig. 2.11 Interaction between voids and matrix cracks (a) schematic of manufacturing defects in laminate (b)-(d) show the matrix cracking evolution affected by defects under external loading [20]

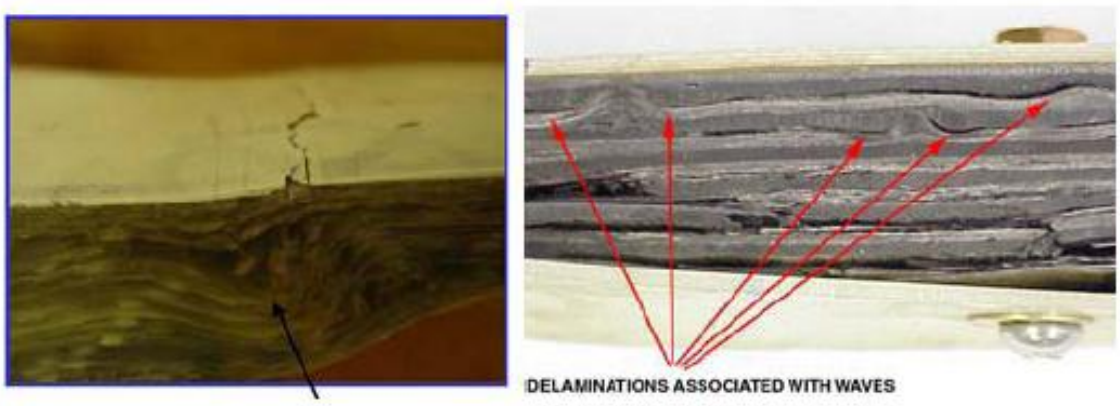

Fig. 2.12 Delaminations initiated from waviness [18].

The irregularity caused by manufacturing defects in composites usually induces some critical situations such as stress concentration under external loading to initiate damage. Also, manufacturing defects can deteriorate the local material property and therefore weaken the resistance to the damage development. Considering the important effect of manufacturing defects on the damage development, Talreja [22] recently proposed a new strategy of performance evaluation of composites called defect damage mechanics. Such a strategy requires including the defects in damage mechanics model for integrity assessment of composites. Some pioneering works have been done along this direction mainly through two approaches: 1) micromechanics models of the initiation and propagation of damage affected by local manufacturing defects; 2) statistical models of damage development affected by distributed manufacturing defects.

The first approach is an extension from some classical damage mechanics models that involves the interaction between damage and defects. For example, Ricotta *et al* [23]

studied the effect of voids on the fracture of woven fabric composites by positioning voids along the propagation path for delamination. According to the new model, the Mode I energy release rate increases as the dimension of the void increases. As the distance between void and crack tip decreases, the energy release rate also increases. The new model also reveals that the void shape plays an important role in delamination growth.

The first approach, which is extended from classical damage mechanics models, offers the fundamental understanding of the effect of defects on damage development and the quantitative characterization of the local effect of defects on damage development. However, the reliability of composite structures cannot be assessed through this approach due to the statistical nature of the distributed defects. The first approach focuses on the local interaction between defects and damage in a deterministic way, without considering the interaction of randomly distributed defects and damage.
The second approach adopts the results of the local effect of defects from the first approach and incorporates it into statistical models on a larger scale. Therefore, the second approach usually involves multi-scale models and yields the assessment of the reliability of structures based on the damage development affected by distributed defects throughout the whole structure, instead of a localized region. However, the multi-scale problem presents many challenges. Currently, such an approach can only be applied to some defects with simple variations. A good example of such a multi-scale model is given by Slaughter and Fleck [5] on the interaction of randomly distributed fiber

waviness and fiber microbuckling. The fiber micro-buckling under compression has been modeled by a kink band model [3] without considering defects, i.e. fiber waviness. Based on the kind band model, Slaughter and Fleck introduced the fiber waviness, which is characterized by the wave length and misalignment angle, into a micromechanics model. The micromechanics model can predict the fiber micro-buckling as a function of the two parameters of fiber waviness. This corresponds to the first approach studying the local effect of defects on damage development. Taking the results as inputs and assuming certain statistical distribution for these two parameters of the fiber waviness, Monte Carlo simulation was conducted to calculate the collapse compression stress controlled by the fiber microbuckling in laminates with fiber waviness.

The variation of most defects can be very complicated. For example, voids distributed in the matrix possess different sizes, shapes and locations. It may be possible to establish the quantitative relationship between defects and the relevant damage modes through micromechanics models (the first approach). However, it would be very difficult to incorporate the results into a statistical model (the second approach). What's more, some damage modes are affected by multiple defects. It would be extremely difficult, if not impossible, to include all relevant defects in a micromechanics model and yield a simple solution as the inputs of the statistical models. For those situations, the abovementioned multi-scale model cannot be implemented rigorously. But the strategy proposed here is believed to be very promising. In next section, the stochastic matrix cracking evolution

affected by the manufacturing defects is taken as the example to demonstrate such a strategy.

2.2 Stochastic matrix cracking evolution in composite laminates

2.2.1 Overview of matrix cracking evolution

The matrix cracks are generally caused by transverse tensile stress, which is perpendicular to the fiber direction, so the crack surface is parallel to the fiber direction (see Fig. 2.1). In laminates, the propagation of matrix cracks are arrested by the neighboring plies due to the change of the fiber orientation. Since the neighboring plies can share the loading, the matrix cracks usually do not cause the catastrophic failure of the whole laminates. Instead, the multiplication of matrix cracks is very common within the plies if the transverse stress increases for static loading or cycles for fatigue loading. In literature, matrix cracks are also referred as intralamina cracks, microcracks, ply cracks, and transverse cracks. Here, transverse cracks are used to specify the matrix cracks in 90^o plies of cross ply laminate while off-axis ply cracks are used to refer to the matrix cracks in off-axis plies of general multidirectional laminates.

Although the matrix cracks are not directly related to the catastrophic failure, they may cause functional failure of composite structures. For pressurized composite containers and pipelines, the matrix cracks may provide the leak path. For general composite structures, the multiple cracks cause stiffness reduction. For example, the multiple matrix cracks in some glass/epoxy cross ply laminates can degrade the stiffness up to

about 50%. Also, the matrix cracks may indirectly cause the catastrophic failure through inducing other damage modes such as delamination (see Fig. 2.2). Therefore, it is important to understand the cracking evolution for evaluating the integrity of the composite laminates in service.

The matrix cracking evolution is a multi-scale phenomenon including the development of single cracks on micro-scale and the multiplication of full cracks along the transverse direction on macro-scale. The matrix cracking evolution in cross ply laminate is one of the most extensively studied damage modes. Here, the review on the matrix cracking evolution is mainly based on studies of cross ply laminate.

Experimental observations show that the formation of a single crack is usually instantaneous without detectable stable growth except for laminates with very thin off-axis ply under low fatigue stress [24-26]. The experimental investigation reported in literature on the formation of the single crack focus on the first crack, which is followed by multiplication of cracks under further loading. Although the crack develops in the matrix, it is found that the static failure stress for first crack, σ_{tu}^{min} , is affected by the volume fraction of fibers, and usually much lower than the strength of the neat resin[27]. Stress analysis of the matrix between fibers shows large stress concentration. Such stress concentration has been taken as the reason for the low failure stress[28]. For low-cost composites, however, the introduced defects may also significantly deteriorate the local property and lower σ_{tu}^{min}. For example, the large variation of the transverse strength of

the unidirectional laminate shown in Fig. 2.14 may be better explained as the results of the random effect caused by the defects, instead of the stress concentration.

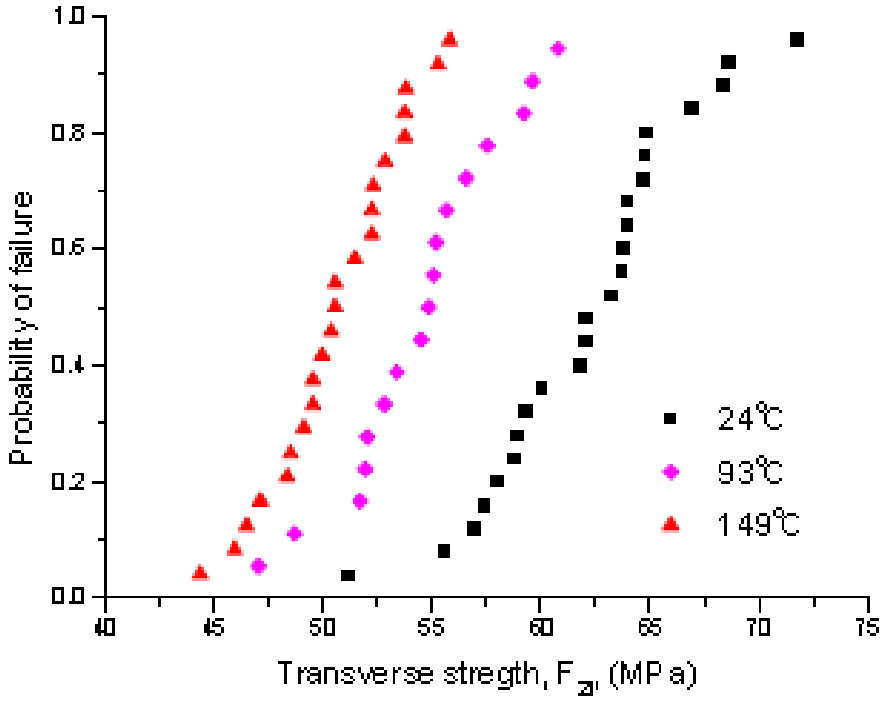

Fig. 2.13 Variation of transverse strength of unidirectional laminate at three temperatures[29].

The thickness effect on σ_{tu}^{min} is also reported in literature [30-32]. It describes the phenomenon that, as the thickness of the off-axis plies increases, σ_{tu}^{min} decreases until it is close to the transverse strength of the 90^{o} lamina (see Fig. 2.14). Two factors are related to such a thickness effect. The constraint effect from the neighboring plies is believed to improve the resistance to cracking process and thus increases σ_{tu}^{min}. A fracture mechanics analysis by Ho and Suo[33] verified such a constraint effect on the

cracking propagation. As ply thickness increases, the constraint effect decays and eventually becomes negligible, therefore σ_{tu}^{min} decreases and converges to the magnitude of the transverse strength of the 90^o lamina. Another factor, which may cause the thickness effect, is again relating to the manufacturing defects. The statistical nature of defects makes their effect volume-dependent. Thicker ply means larger volume and higher probability of possessing severer defects to lower σ_{tu}^{min}. This argument is supported by the study on the scale effect on the transverse strength of unidirectional laminate[34]. The reported experimental study shows that the measured strength decreases as volume increases.

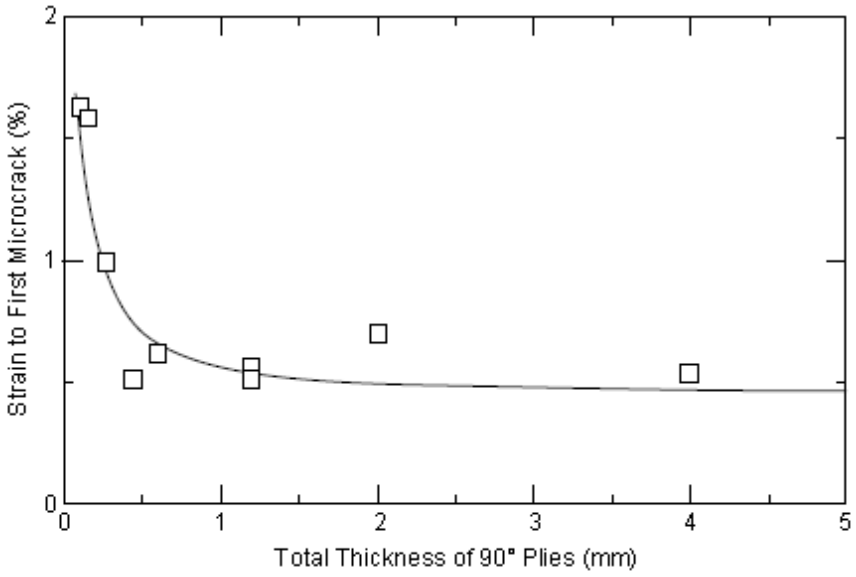

Fig. 2.14 Strain to initiate the first transverse crack in cross ply laminates for different thickness of 90^0 layer[2].

For modeling the cracking evolution, certain strength criterion is usually used to predict the formation of a single crack in the matrix. But the abovementioned experimental investigation on σ_{tu}^{min} suggests that the failure mechanism of constrained plies with defects is very complicated. It is noteworthy that the strength used for the matrix cracking is not the same as the transverse strength of the unidirectional laminate. For simplicity, all factors including the effect of defects have been lumped into one critical value, which is still named as the static transverse strength for constrained ply in literature.

The matrix cracking evolution on a macro-scale, or the multiplication of cracks, is quite clear according to extensive experimental studies reported in literature [27, 30, 35]. Through microscopic observation techniques, it is found that the multiplication of cracks starts with the first crack under σ_{tu}^{min}. For fatigue loading, the failure stress becomes lower as the fatigue cycles increase. As applied stress increases for static loading or cycles for fatigue loading, more cracks start to form in a random style while the pattern of new cracks remains the same. The number of cracks over unit length, i.e. crack density, is usually used to characterize the multiplication of cracks. The average crack spacing, which is the average distance between neighboring cracks, is also used. Fig 2.3 shows the crack density as a function of the loading history. The increase of crack density is fast after the first several cracks. Then the formation of additional cracks becomes increasingly harder until the crack density eventually saturates. After that, no more cracks can form under further loading for either the static or fatigue loading. A

saturation state independent of the loading history is found by Reifsnider and Highsmith [36]. Such a saturation state is purely determined by the laminate properties and therefore named as Characteristic Damage State (CDS).

The random formation of new cracks at the early stage makes the distribution of cracks highly non-uniform. The statistics of such randomness is qualified by the statistical distribution of the crack spacing as Fig. 2.15 shows. From Fig. 2.15, crack spacing among the gauge length varies from 2mm to 10mm for low crack density. As crack density increase, the variation becomes smaller, though it is still not negligible, e.g. 1~3.5mm at very last stage of the evolution. Only when the multiplication process obtains the saturation, the distribution becomes almost uniform. Similar experimental investigation in literature[37, 38] confirms the stochastic nature of the matrix cracking evolution.

2.2.2 Deterministic models of matrix cracks

Most of damage mechanics models of matrix cracks in literature are deterministic, though the stochastic nature of the matrix cracking evolution has been widely found in experiments. In those models, a uniform distribution of cracks is assumed. This is mainly because most damage mechanics models consider the effect of the matrix cracks on stiffness reduction, instead of the cracking evolution. As an average property, stiffness may not be sensitive to the position of each individual crack. Also, the cracking evolution in high-quality composites with relatively homogenous property is quite

uniform and therefore is possible to be modeled in a deterministic way[39]. Besides, it is much easier to develop a deterministic model rather than a statistical model in an analytical way. As already discussed, the deterministic models are not suitable for cracking evolution in laminates with randomly distributed defects. But they can serve as the basis for developing statistical models. For example, the interaction of cracks, which is very important for the cracking evolution, has been well studied in deterministic models. Thus, the deterministic damage mechanics models of matrix cracks are reviewed here.

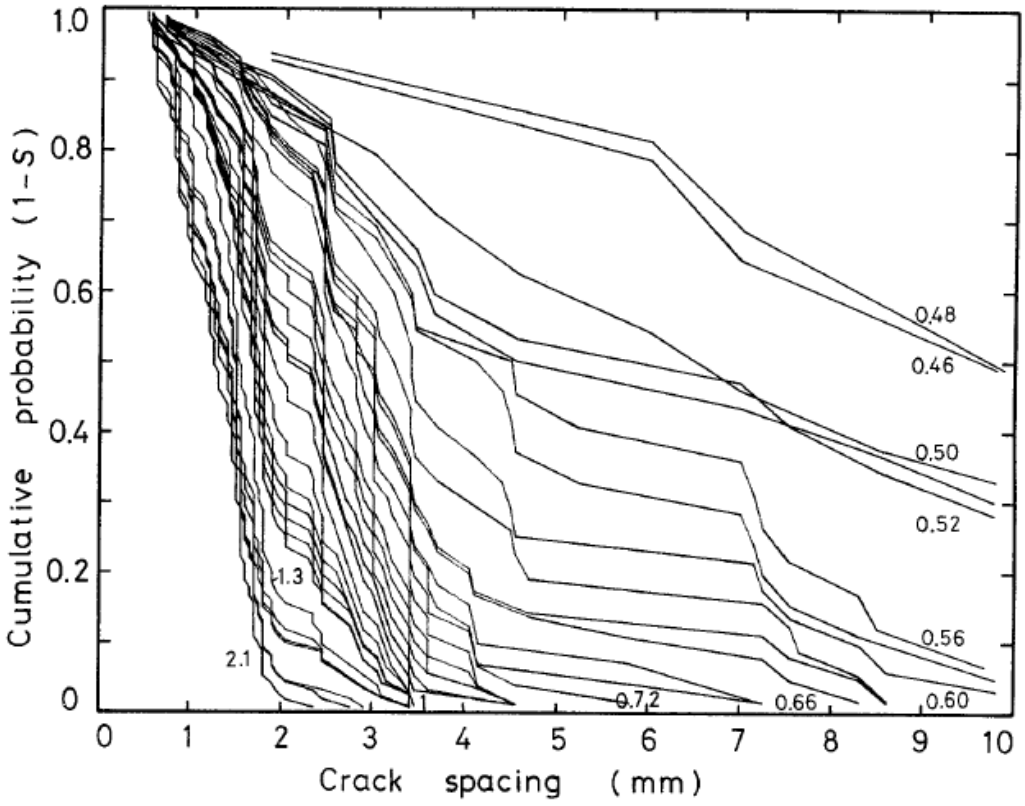

Fig. 2.15 The variation of crack spacing at different levels of applied strain[40].

The damage mechanics models of matrix cracks mainly have two objectives; 1) The effective thermomechanical properties for a given damage state characterized by the crack density, and 2) the multiplication process of cracks driven by loading, i.e. the crack density as a function of loading history. In deterministic models, the two problems are solved by assuming homogenous properties within each layer as well as a regular pattern for matrix cracks. Therefore, a unit cell with length as the average crack spacing is usually used to represent the damaged laminates as Fig. 2.16 shows.

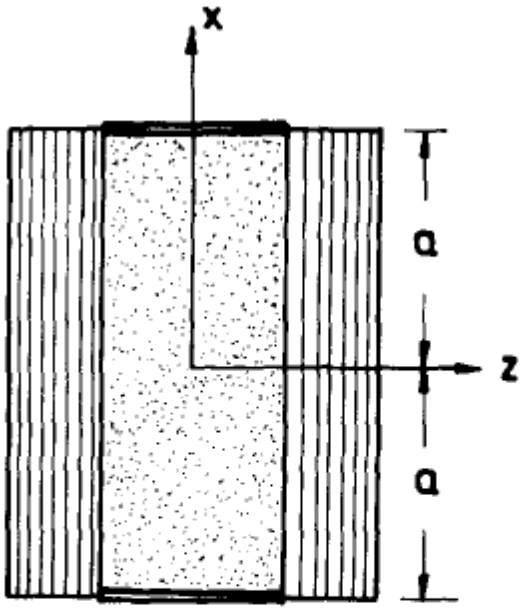

Fig. 2.16 Unit cell of cracked cross ply laminates[41]

The effective thermomechanical properties are obtained through stress analysis of cracked laminates. Several analytical solutions such as shear lag model and variational

approach are developed for the stress analysis of cracked cross ply laminates [5, 27, 41-50]. The general pattern of stress distribution within the unit cell is illustrated in Fig. 2.17 for small and large crack spacing in spite of some minor differences predicted by different models. Due to the perturbation of cracks, the transverse tensile stress of 90^o ply in the vicinity of cracks drops as Fig. 2.17 shows. The loading corresponding to such drop is shared by the neighboring 0^o plies. As it is away from the cracks, the tensile stress in 90^o ply is recovered because the developed shear stress helps transfer the loading back to 90^o ply from neighboring plies. Since the distribution of cracks is assumed uniform, the effective thermomechanical properties calculated based on the stress state within the unit cell is the same as the average properties of the corresponding cracked laminates. For the stress state of multidirectional laminates with arbitrary off-axis angles, finite element method is usually applied [51, 52].

With the stress state in the unit cell solved, the cracking evolution under further loading can be updated by applying certain criterion to predict the formation of new cracks. Although the used cracking criteria may be fundamentally different, i.e. strength and energy criteria ([39, 44, 46], the general process for the multiplication of cracks in the deterministic models is very similar. The middle plane between two preexisting crack possesses the highest stress level as Fig. 2.17 (b) depicts, and thus being the location where the cracking criterion applies. Once the criterion is satisfied under further loading, the original unit cell is divided by the new crack into two identical unit cells with length

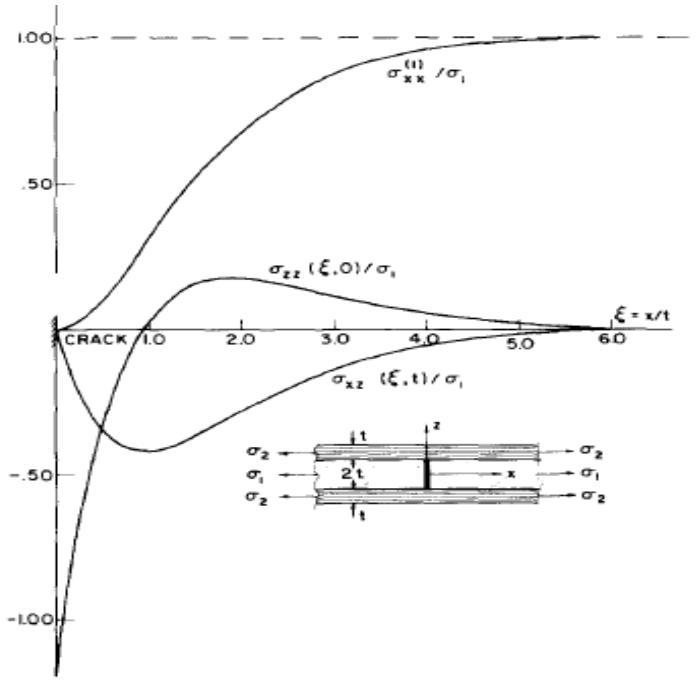

(a)

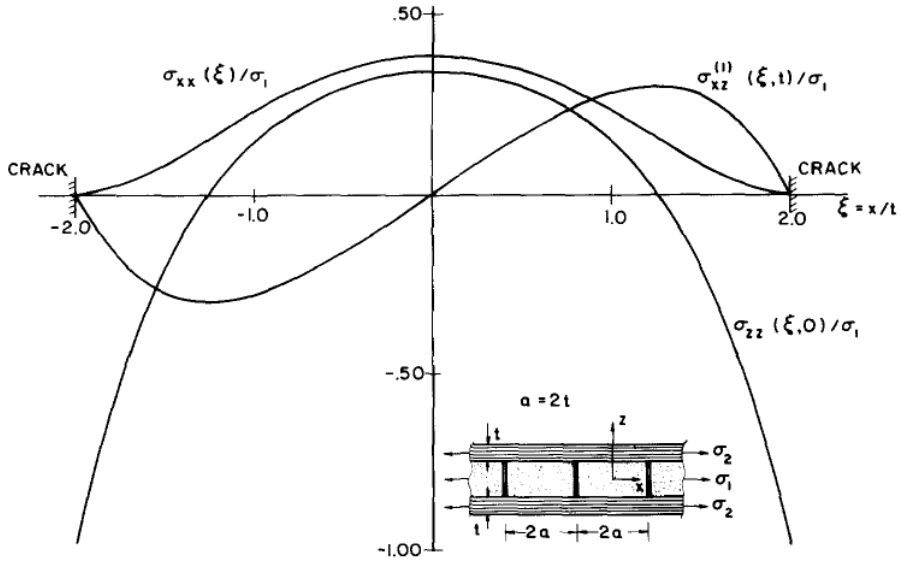

(b)

Fig. 2.17 Stress distribution perturbed by the cracks (a) large crack spacing; (b) small crack spacing[41]

as half of the previous one. Accordingly, the crack density doubles. Same procedures are repeated to the divided unit cell for further loading history. Fig. 2.18 shows the prediction of the crack density as a function of the applied stress using a strength criterion and different analytical stress solutions cited from [46]. The prediction correctly captures the trend of the matrix cracking evolution. But it is noteworthy that the modeled multiplication of cracks is actually a highly discrete process that the crack density doubles for every increment. The reason that the crack density predicted based on a discrete process is continuous in Fig. 2.18 is just because infinite number of initial damage states, i.e. the initial length of the unit cell used in the model, are simulated and plotted together. For a given sample, however, only one initial state exists. A simulation started from a fixed initial state must yield prediction that each increment of crack density is always equal to the current crack density according to the deterministic model that the crack spacing of unit cell is always reduced by half. This is actually against the experimental data in Fig. 2.18, which shows that the increment of crack density is much smaller. The deviation of the prediction from the experimental observation is caused by the unrealistic assumption of the uniform distribution of cracks. Fig. 2.19 shows an experimental observation on the cracking evolution under fatigue loading. It clearly shows that the crack spacing is not uniform and the new cracks only form in the region with lower crack density without doubling the overall crack density.

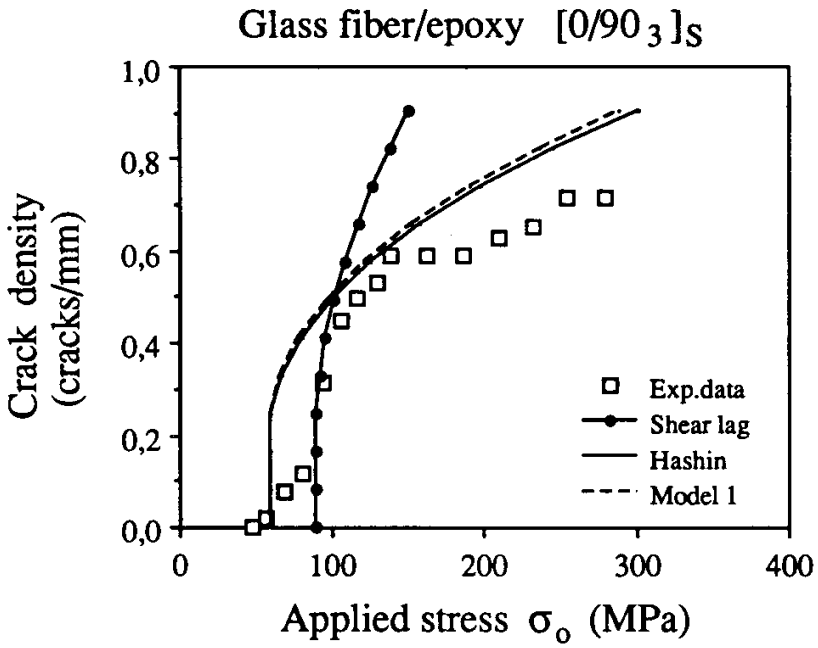

Fig. 2.18 Modeling predictions and experimental data for the crack density as a function of the applied stress [46].

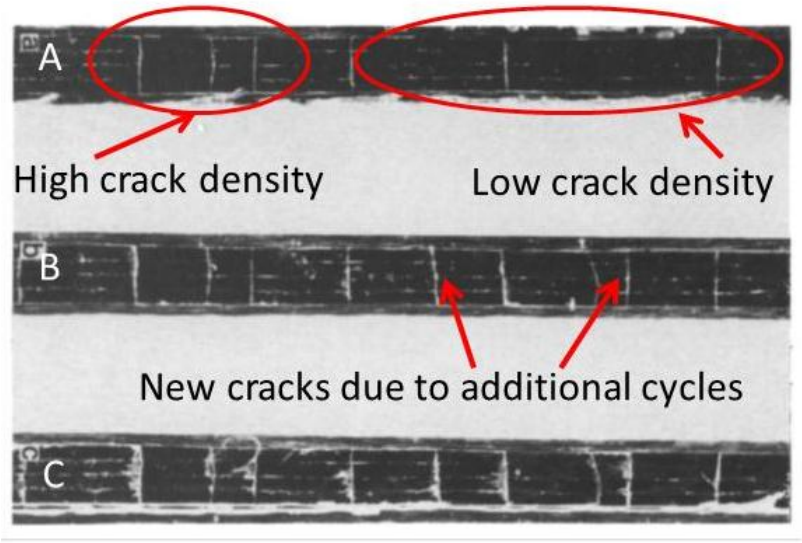

Fig. 2.19 Matrix cracking evolution in cross ply laminate under fatigue tension.

Another problem faced by the deterministic models is that the initial stage of cracking evolution cannot be properly modeled. As Fig. 2.18 shows, the deterministic model correctly predicts the prompt increase of crack density but misses the precedent stage. The initial stage is mainly controlled by the severest defects and cannot be explained in a deterministic way.

2.2.3 Weibull distribution

The Weibull distribution is a probability function which has been successfully applied to a wild field of problems including the defect-sensitive failure of brittle materials system. In his original work[53], Weibull explained his practicable approach formulating the probability density function as to "choose a simple function, test it empirically, and stick to it as long as none better has been found". Although empiric is the intrinsic nature of statistical analysis, some understanding of the theoretic basis of Weibull distribution is necessary to correctly apply it to specific problems. The fact that no better probability function than Weibull distribution has been found in the past half century to represent the strength of brittle materials system such as fiber is rooted in the statistical failure process represented by the Weibull distribution[54]. Here, the theoretic basis of Weibull distribution is briefly illustrated by taking the statistical transverse strength of a unidirectional laminate as an example.

In Fig. 2.20, the unidirectional laminate under transverse tension is modeled by the discrete elements under constant unidirectional tensile stress σ. The volume of the

discrete element ΔV is large enough to accommodate the local defects. Under the transverse tensile stress, failure of any element means the catastrophic failure of the laminate. Therefore, the reliability of the laminate is:

$$1 - P_f = \prod_{i=1}^{N} (1 - P_{f_i}) \tag{2.1}$$

where N is the number of elements, and $P_{f_i} = \Delta V \emptyset$. $\emptyset$ is the failure density function which is determined by all factors controlling the fracture such as the local manufacturing defects. Since the distribution of defects is assumed to be random, the

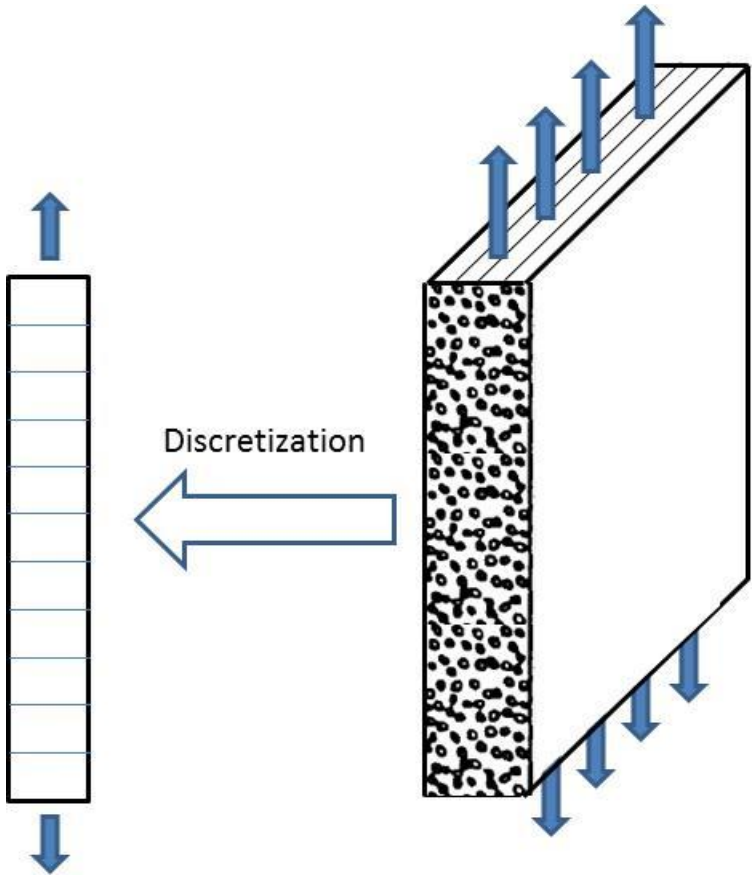

Fig. 2.20 Discretization of a unidirectional laminate into 2D elements

failure density function should be identical and independent to all elements. If $P_{f_i}$is close to 0, Eq. (2.1) is equivalent to:

$$P_f = 1 - e^{(-V\emptyset)} \tag{2.2}$$

where $V = \Delta VN$, the total volume of the laminate. The failure density function is proposed by Weibull:

$$\emptyset = \left(\frac{\sigma-\sigma'}{\sigma_0'}\right)^m \qquad \text{if } \sigma > \sigma' \tag{2.3}$$

where σ is the applied transverse stress, which is assumed as the only stress component important to the failure. σ_0' is the characteristic strength, m is the distribution shape constant, and σ' is the location parameter defining the lower bound for the applied stress. All the three parameters have to be determined in an empirical way. For applied stress lower than σ', the failure probability is zero.

The probability of failure of the laminate under transverse stress is same as the statistical distribution of transverse strength of the laminate. Plug Eq. (2.3) into Eq. (2.2), the expression of the probability function is obtained:

$$P_f = P(Strength < \sigma) = 1 - e^{\left(-V\left(\frac{\sigma-\sigma'}{\sigma_0'}\right)^m\right)} \tag{2.4.a}$$

Or the volume is absorbed into the characteristic strength parameter:

$$P_f = P(Strength < \sigma) = 1 - e^{\left(-\left(\frac{\sigma-\sigma'}{\sigma_0}\right)^m\right)} \tag{2.4.b}$$

Eq. (2.4) is the expression of the Weibull distribution. Eq. (2.4.b) is usually used for representing test data. But it should be emphasized that σ_0 is the extrinsic characteristic

strength that is volume-dependent. It can be estimated by the test data from samples with same dimensions. When applying to samples with different dimensions, the intrinsic characteristic strength in Eq. (2.4.a) should be used. The conversion between these two parameters is:

$$\sigma_0' = \sigma_0 V^{1/m} \tag{2.5}$$

For a unidirectional laminate, the strength is controlled by the weakest element. When it is embedded into laminates as the 90^o ply, the fracture happen at multiple locations rather than the single weakest spot. For multiple fractures, the statistical strength distribution for each element instead of the whole laminate is of interest. Such distribution can be obtained by replacing V with the element volume ΔV in Eq. (2.4). And the statistical process illustrated here can be readily modified and applied to modeling of the stochastic cracking evolution in constrained plies.

2.2.4 Stochastic models of matrix cracks

At the early stage of the cracking evolution, cracks form in the regions with severest defects. Because of the randomness of distributed defects, the resulted cracks are also randomly distributed. The random distribution of cracks further introduces the stress perturbation in a stochastic manner, together with the randomness of the remained defects, making the further cracking evolution very complicated. But the origin of this complicated stochastic process is simply rooted in the randomness of materials properties caused by the defects. Some statistical models have been developed to take account of such randomness to simulate the matrix cracking evolution.

Wang[55] assumed the statistic distribution of a conceptual defect in term of the length and location of the defect to represent the randomness of materials properties. The cracking process in the 90^o ply is treated by fracture mechanics. The model takes the length of the conceptual defect as the initial crack length. Through this way, the rational representation of defects provides a clear picture of the interaction between defects and matrix cracks, i.e. cracks initiate and grow from the conceptual defect driven by static or cyclic loading. This allows the developed model to unify the simulation of the cracking evolution for both static and fatigue loading in the same framework.

The second approach to represent the randomness of material property is through an energy approach[17, 56]. A threshold value for the energy release from the formation of a full crack has been used as the cracking criterion in some deterministic models[27, 39]. To extend it to a statistical model, the critical value for the energy release is assumed to follow certain statistical distribution. Like the deterministic model, it has the advantage of being able to deal with the thickness effect without changing the statistical distribution of the critical value. When converting from a deterministic model to a statistical model, however, one may face problem if a numerical solution for stress analysis of cracked laminates is used. This is because such method requires calculating the energy release of crack formation at any location, which may be too demanding for a numerical solution. This limitation may restrict the application of such method to general multidirectional laminates, for which the analytical solution of the stress state in cracked laminates may not be available.

The third approach to represent the randomness of material property is through a strength approach. The critical stress state, i.e. the static transverse strength, is assumed to follow certain statistical distribution [29, 37, 43, 57-59]. The problem of such method is the same as the corresponding deterministic model; the static transverse strength used in the model is not an intrinsic property like the strength of the neat resin. As Section 2.2.1 discusses, it actually reflects all the relevant effects such as the constraint effect from neighboring plies. Therefore, the statistical distribution of the strength has to be adjusted as the configuration of laminates changes. Due to this problem, the adaptability of the strength approach has been questioned in literature[2, 56]. However, the simplicity of a strength approach would be a great advantage for its application in statistical models. Especially, it would be much easier to be implemented for general multidirectional laminates for which no analytical solution of stress state in cracked laminates is available. For the problem that the used strength is not an intrinsic property, micromechanics models may be used to calculate the strength affected by the configuration of laminates. For example, it is well known that the transverse strength of unidirectional laminate is lower than the strength of the corresponding resin materials. Through micromechanics models analyzing the stress state in the matrix between fibers, the effect of stress concentration can be taken account for to obtain the effective strength of laminate using the intrinsic strength of resin[60]. Similarly, the constraint effect of neighboring plies can be somehow included into the static strength of the constrained ply. Actually, both for deterministic and statistical models, it has been shown that the

strength criterion is equivalent to the energy criterion judged by the correct prediction of the cracking evolution [38, 61].

With proper representation of the statistical distribution of materials properties, the stochastic matrix cracking evolution is usually simulated by the Monte Carlo simulation. The off-axis plies are discretized in a way similar to the unidirectional laminate in Fig. 2.20. Local fracture toughness or strength for the discrete element is generated by a random number generator according to certain statistical distribution such as the Weibull distribution. After the first crack forms at the weakest element, the local stress state affected by cracks is checked against the local fracture toughness or strength criterion at each increment of external loading.

The Monte Carlo simulation actually treats the stochastic cracking evolution in a deterministic way once the local strength or fracture toughness for each element is assigned. As a numerical testing, the Monte Carlo simulation can only yield the final results on the cracking evolution such as the crack density as a function of the external loading. It cannot reveal the statistical process of the cracking evolution. To better understand this problem, theoretical approach is needed. As the pioneer works, Manders[40] and Peters et al.[37] analyzing the initial stage of cracking evolution where the interaction between cracks can be neglected, finding the evolution is a Poisson process. For the further evolution where the interaction has to be considered, a simple theoretical solution is very difficult to obtain because the interaction between cracks

becomes very complicated when the non-uniform distribution of crack spacing has to be considered. Vinogradov and Hashin [56] developed a theoretical solution by assuming certain bound for the variation of crack spacings. Adersons et al. [38] separated the interactive regime from the initial stage and treated it as a classical fragment problem[62]. Both theoretical solutions need to be solved in a numerical way due to the complexity of the expression of the results. Similar to the problem faced by the Monte Carlo simulation, the two or three parameters in Weibull distribution is not easy to be fit at same time by comparing the numerical results against the experimental crack density data.

3. EXPERIMENTAL INVESTIGATION ON MATRIX CRACKS IN COMPOSITE LAMINATES

Experiments are conducted to investigate the matrix cracking evolution in composite laminates under static and fatigue loading. In Section 3.1, the effect of manufacturing quality on the stochastic matrix cracking evolution is studied by tracking the cracking evolution in carbon/epoxy cross ply laminate. The tested laminate plates are manufactured under different conditions to intentionally introduce different states of defects. Section 3.2 reports the preliminary experimental study on the effect of the in-plane shear stress on the fatigue performance of composite laminates. The experimental results imply that the in-plane shear stress may play role at different stages of damage accumulation under fatigue loading. Section 3.3 continues the study on the in-plane shear stress focusing on its effect on the matrix cracking evolution. Both the multiplication of cracks on macro-scale and the formation of a single crack on micro-scale are investigated through biaxial fatigue testing.

3.1 The effect of manufacturing quality on the stochastic matrix cracking evolution

For the results presented in this section, the manufacture of laminate plates, tensile testing, and microscopic observation were conducted by the author at Lulea Technology University collaborating with Konstantinos Giannadakis. Some optical microscopic observation was conducted at Texas A&M University by the author.

3.1.1 Manufacture of test specimens

The pre-impregnated (prepreg) based autoclave molding is used to manufacture test specimens. For details on such process, see Section 2.1.2. The standard process is as follows. The prepregs are cut and put into the desired layup sequence, and then enclosed in a vacuum bag. To cure the prepgregs, the enclosed laminate is placed in an autoclave. The curing parameters, which are the curing temperature and time, pressure, and vacuum condition, are given by the prepreg supplier.

Four laminate plates are manufactured through the autoclave molding process using carbon/epoxy unidirectional prepreg (HexPly M10/38%/UD300/CHS), with cured ply thickness as 0.32mm and fibre volume fraction as 52-53%. The curing process consists of one isothermal step at 120^{o}C lasting 60minutes for all plates. For the purpose of comparison, the layups of four plates are kept the same, i.e. [0/90]s.

During the curing process, certain pressure is applied on the vacuum bag to consolidate the layups and remove air and excessive resin. Vacuum is also applied within the vacuum bag to suck out the enclose air to reduce the void content. In the laboratory, such conditions can be easily satisfied. For actual manufacturing processes, however, pressure or vacuum may not be sufficiently applied. For example, actual composite structures such as wind blade are usually huge and curved. With few vacuum ports distributing around the laminate structure to be cured, the area far away from the vacuum ports may not have sufficient vacuum applied. For some low-cost processes such as resin infusion, which is widely used for ships and wind blades, no additional pressure rather than the

atmosphere is applied. Therefore, pressure and vacuum are chosen as two adjusted parameters to intentionally modify the manufacturing quality for the purpose of investigating the effect of manufacturing quality on the matrix cracking.

Four laminate plates are manufactured based on the autoclave molding process. Plate 4 is manufactured following the standard process recommended by the prepreg supplier; pressure (3 bars) and sufficient vacuum are applied during the curing process. Plate 1 is cured without applying either pressure or vacuum. Plate 2 is cured without vacuum while the 3 bars pressure is still applied. Plate 3 is cured without applied pressure while the sufficient vacuum is on. The code of specimens is given corresponding to the pressure/vacuum condition as follows: Plate 1(NV-NP), Plate 2 (NV-P), Plate 3 (V-NP), and Plate 4 (V-P).

Due to the different processes, the four plates have different quality. One obvious difference is illustrated by comparing the edge of the plates. As Fig. 3.1 shows, the transparent part along the edge of Plate 4 (P-V) is the excessive epoxy, which has been driven out of the plate by the pressure and vacuum during the curing process. Although it is not visible here, it is reasonable to think that some enclosed air is also removed like the resin. Therefore, it should have low void content.

Plate 1 (no vacuum; no pressure)

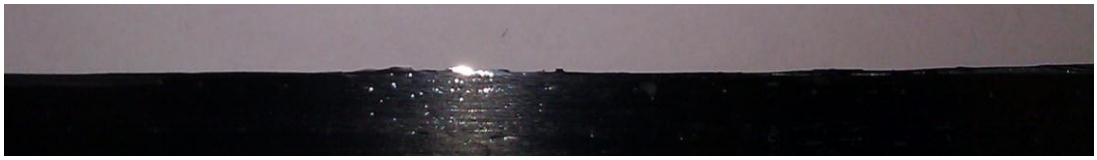

Plate 2 (no vacuum; pressure applied)

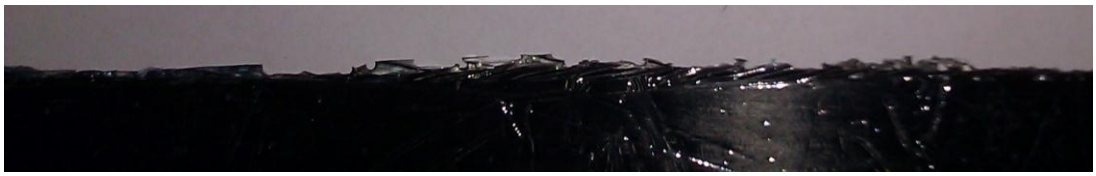

Plate 3 (vacuum applied; no pressure)

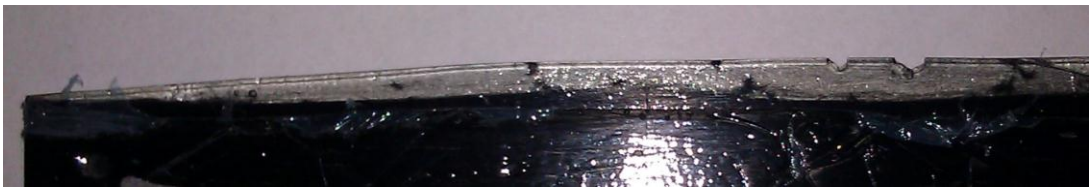

Plate 4 (no vacuum; no pressure)

Fig. 3.1 The edges of four plates: the excessive epoxy is removed from plates by applying vacuum and pressure, and clustered along the edge.

For Plate 1 (NV-NP), the edge seems to be free of the excessive epoxy due to the lack of any driven force. The enclosed air has been kept within plates after cure to become voids. For Plate 3 (V-NP), some excessive epoxy is observed along the edge while no epoxy exists for Plate 2 (NV-P). This simple observation illustrates the role played by

pressure and vacuum as the driven force removing the enclosed air and consolidating the laminate. What's more, the observation may suggest that the applied vacuum is more critical for removing excessive epoxy and air. Further microscopic observation will be reported later. In general, plate 4 (V-P) manufactured following standard process is expected to possess best quality while the other three plates may see different degree of property degradation due to the deviation from the standard one.

3.1.2 Measurement of the cracking evolution under static tension

The manufactured plates are cut into specimens for tensile testing. The typical dimension of the specimen is 210x10x1.2 mm. The edges of the specimens are polished for counting cracks and microscopic observation. 8 specimens from each plate were tested. Each specimen was subjected to a loading-unloading ramp under static tension. The maximum strain levels applied are: 0.35, 0.5, 0.65, 0.8 and 1.05%. After each loading the edge of the specimen is observed under an optical microscope for counting transverse cracks in the 90^o ply. For first several specimens, both sides are subjected to examination to make sure that the transverse cracks cross through the width direction of specimens. The gauge length is 70mm. In each case, the number of counted cracks in the 90^o ply is divided by the gauge length to calculate the crack density. The crack density measured at different strain levels is taken as the measurement of the cracking evolution. Fig. 3.2-3.5 shows the crack density as a function of the applied strain for four plates. The crack density data measured from all specimens are plotted to clearly see the

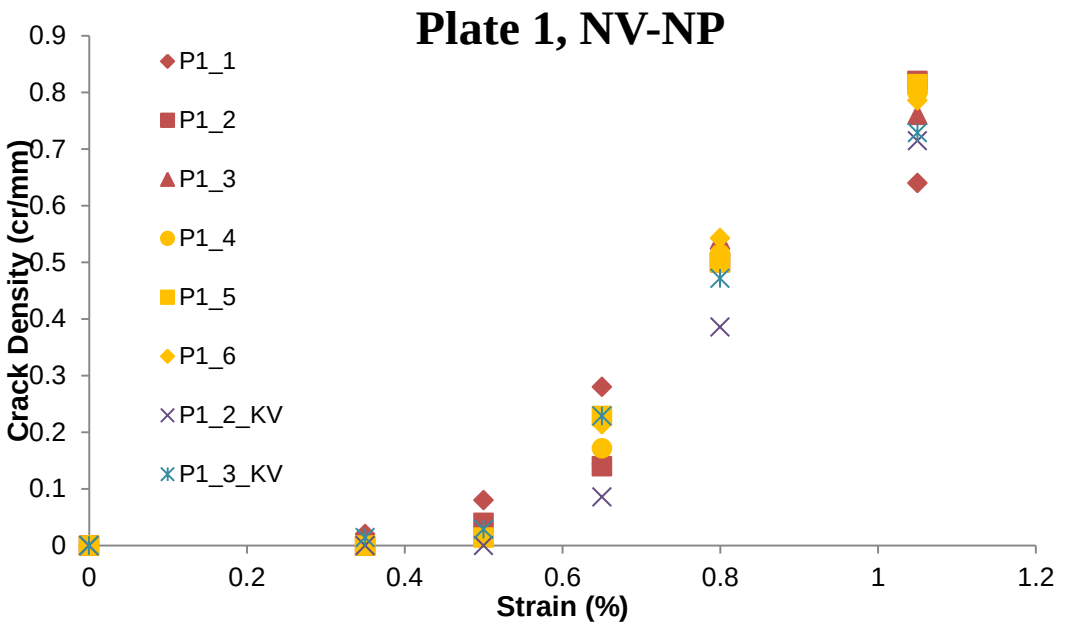

Fig. 3.2 Crack density as function of applied strain for specimens from plate 1

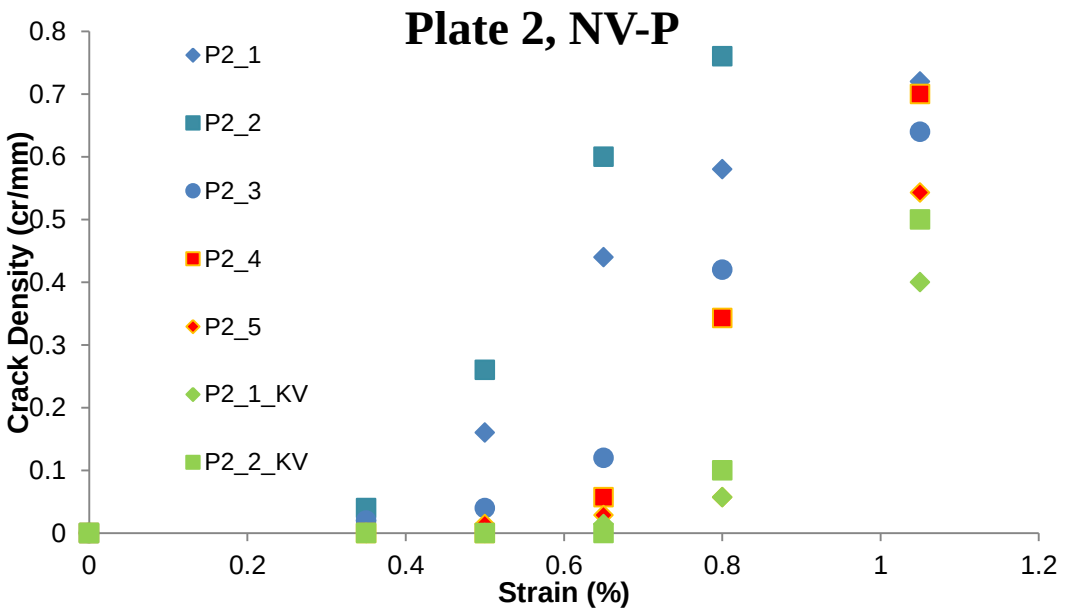

Fig. 3.3 Crack density as function of applied strain for specimens from plate 2

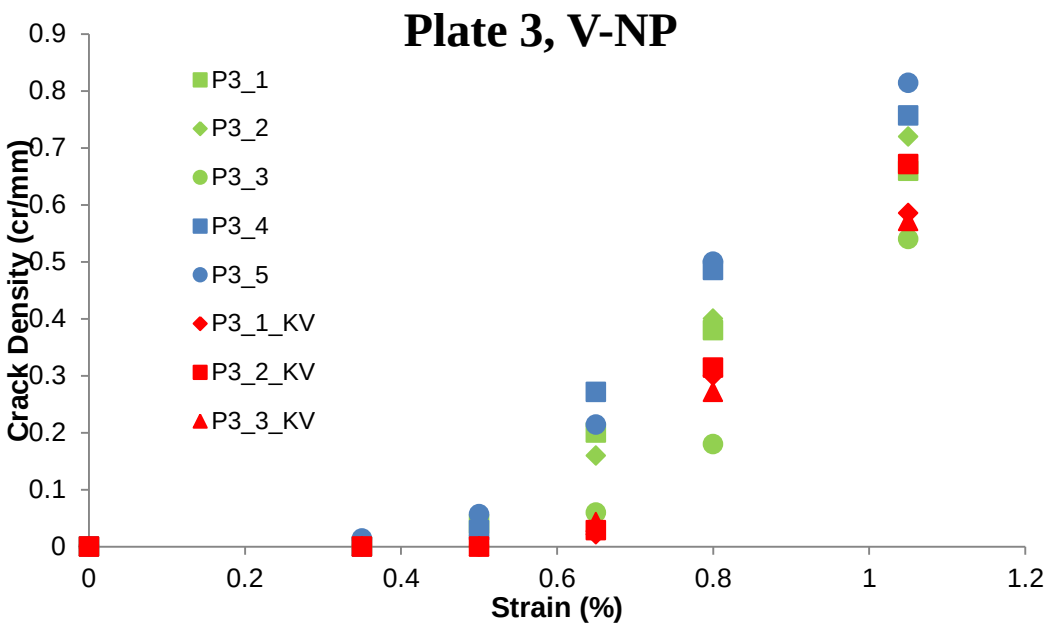

Fig. 3.4 Crack density as function of applied strain for specimens from plate 3

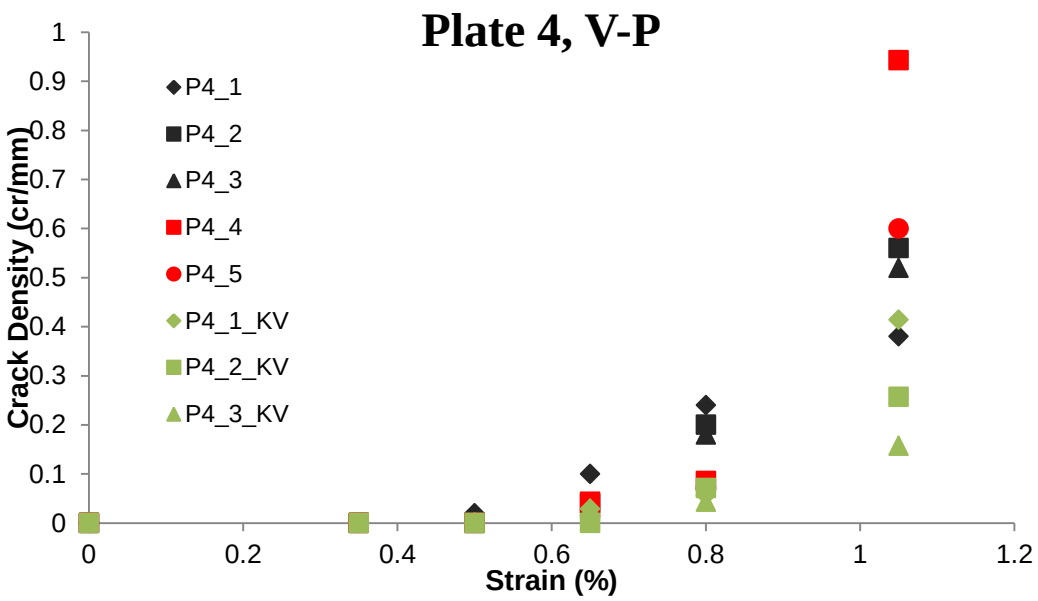

Fig. 3.5 Crack density as function of applied strain for specimens from plate 4

statistics. The data denoted as Pi_j_KV are measured from specimens cut from the middle of the plates. Others are from specimens cut from random locations. Fig. 3.6 shows the average crack density as a function of the applied strain for all four plates. The effect of manufacturing quality on the matrix cracking evolution is clearly shown in Fig. 3.6. It can be seen that the plate manufactured following the standard process, which is supposed to possess the best quality, yields lowest crack density at each strain level. In contrast, Plate 1 (NV-NP) which is manufacured by the process deviated from the standard process by removing both the applied pressure and vacuum, yields highest crack density at almost every strain level.

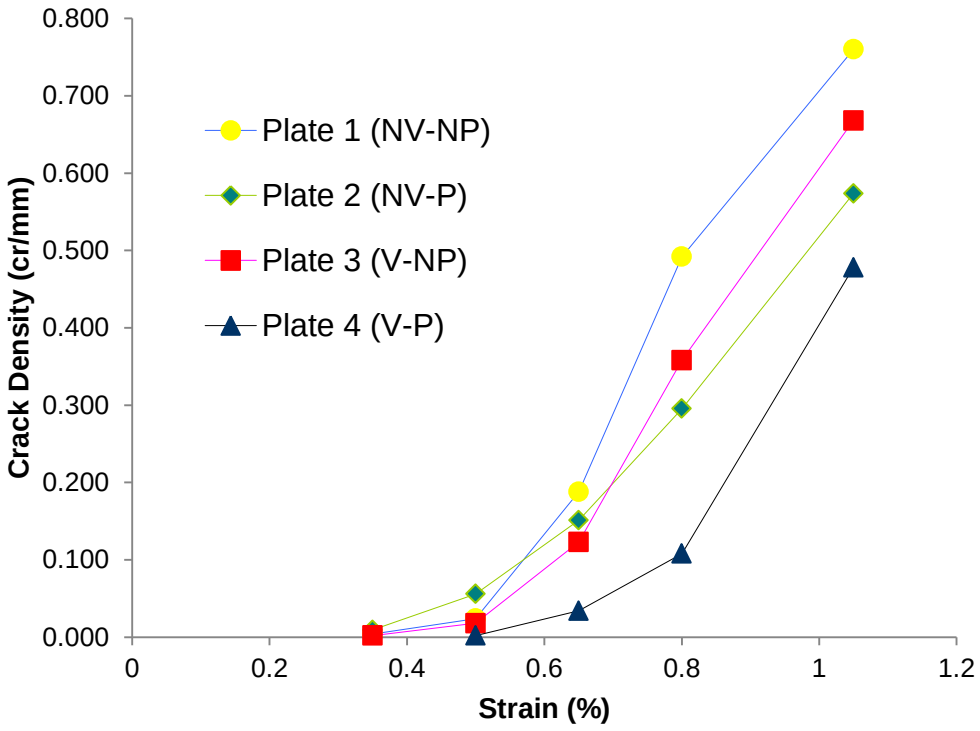

Fig. 3.6 Average crack density as a function of the applied strain.

The manufacturing process affects the quality of laminate plates mainly through introducing defects. Through these ramdonmly distributed defects, the effect of manufacturing quality on cracking evolution is natrually a stochastic problem. Therefore, the cracking evolution cannot be fully described by the crack density. In addtion, the statistical distribution of cracks must be measured.

Fig. 3.7 shows the location of each crack along 70mm gauge length measured from one specimen from Plate 2 (NV-P). At lower crack density, the distribution of cracks is highly non-uniform while it tends to be relatively uniform as crack density increases.

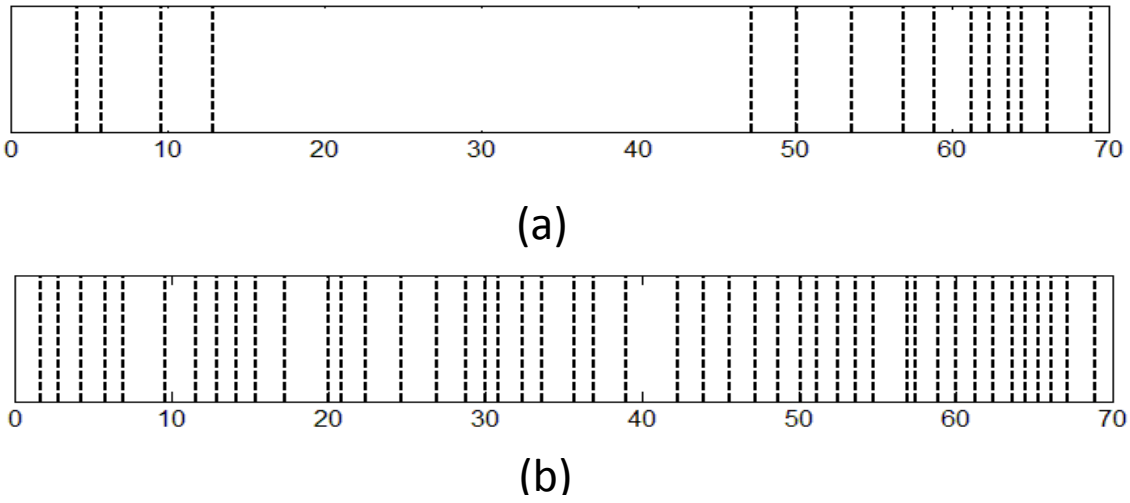

Fig. 3.7 Distribution of cracks along the 70mm gauge length. Each vertical dash line represents one matrix crack (a) low crack density (b) high crack density.

To quantitatively study the statistics of the cracking evolution, the probability distribution of the crack spacing which is the distance between two neighboring cracks,

is chosen as the characterization of the non-uniform distribution of cracks. In another word, the relative location of one crack to the neighboring cracks or the crack spacing is important while the location of each crack along the gauge length is not considered. This is because the crack spacing is important for the stress distribution in cracked laminates as illustrated in Section 2.2.2.

The crack spacings are measured under the optical microscopy by tracking the distance for the microscopy travelling from one crack to the next one until the full gauge length is examined by the microscopy. The probability distribution of crack spacing, i.e. the cumulative probability, is calculated as follows:

$$P_L(L < L') = \frac{N_{L'}}{N} \tag{3.1}$$

where N is the total number of measured crack spacings along the gauge length which is less than the number of cracks by 1. $N_{L'}$ is the number of crack spacings which are equal to or less than L' along the gauge length. Fig. 3.8 shows $P_L(L < L')$ measured from multiple specimens for two crack density levels. At the relatively low crack density level, the crack spacing varies from 1mm to about 30mm while it concentrates in the range of 1~10mm for high crack density. However, no evidence shows that the variation of crack spacings falls into a very narrow range, e.g. $l \sim 2l$, as some theoretical works suggested in literature[56, 63]. It also suggests that when the crack density is low, the random nature of manufacturing defects plays more important role in the formation of cracks. In Fig. 3.8, no significant difference can be observed for the distribution of crack spacings for specimens from different plates.

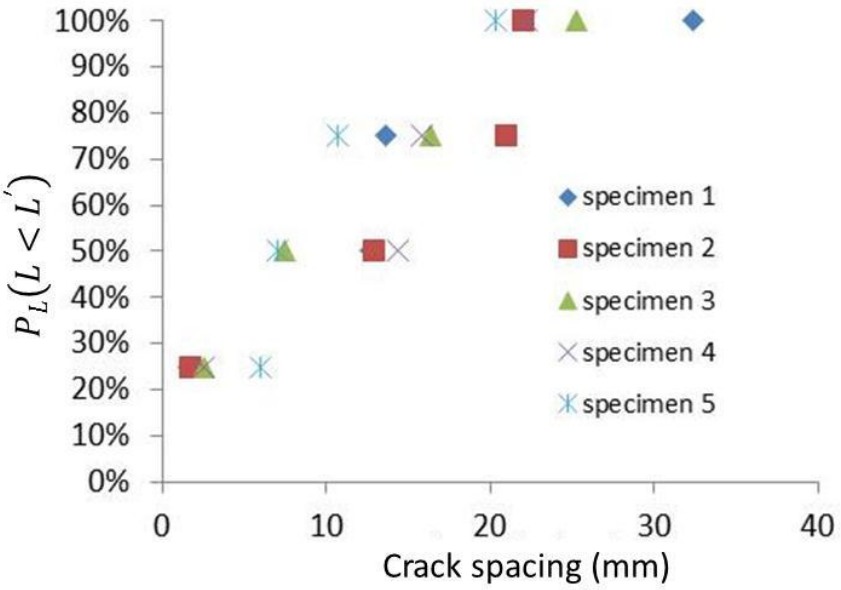

(a)

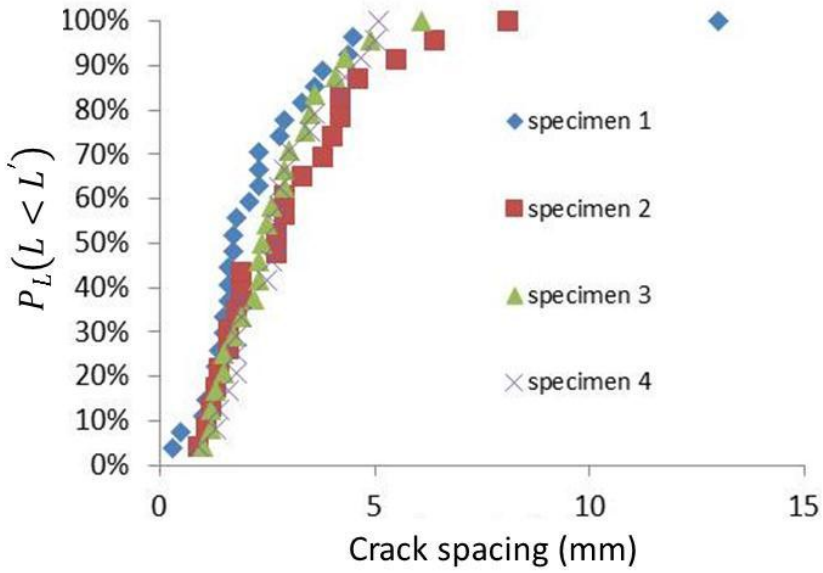

(b)

Fig. 3.8 Cumulative probability distribution of crack spacing measured from different specimens. (a) low crack density (b) high crack density

3.1.3 Microscopic observation

The optical microscopic observation along the polished edge of specimens is conducted. The voids in matrix is firstly observed before the specimens are subjected to testing. In Fig. 3.9, the microscopic observation of the 90^o ply in Plate 2 (NV-P) and Plate 4 (V-P) are compared, showing much higher void content in Plate 2 (NV-P) than in Plate 4 (V-P). This difference is directly caused by the different manufacturing processes. All black spots in Fig. 3.9 are identified as voids through the following procedures: (1) after polishing, the surface is carefully washed using ethonal to remove debris; (2) after taking digital pictures under microscope, the surface is subject to polishing for less than 1 minute, and another microscopic picture is taken for the same location. Two pictures are compared and all black spots are expected to remain if they are voids insteand of debris. It is known that the source of such voids is the gas trapped between prepregs during stacking the prepreg and the volatiles within prepregs. During the curing process, gas transport pathways are established by the vacuum system to transfer the gas and volatiles out of laminates. The remaining gas and volatiles form voids in the matrix after the curing process. The role of the applied vacuum in reducing void content and the corresponding gas transport pathways is of great interest to a new manufacturing process called out-of-autoclave molding. For more information, one can refer to references [10, 64, 65]. The difference in the void content shown in Fig. 3.9 is due to that all gas and volatiles have been kept within Plate 2 (NV-P) in the form of voids while most of

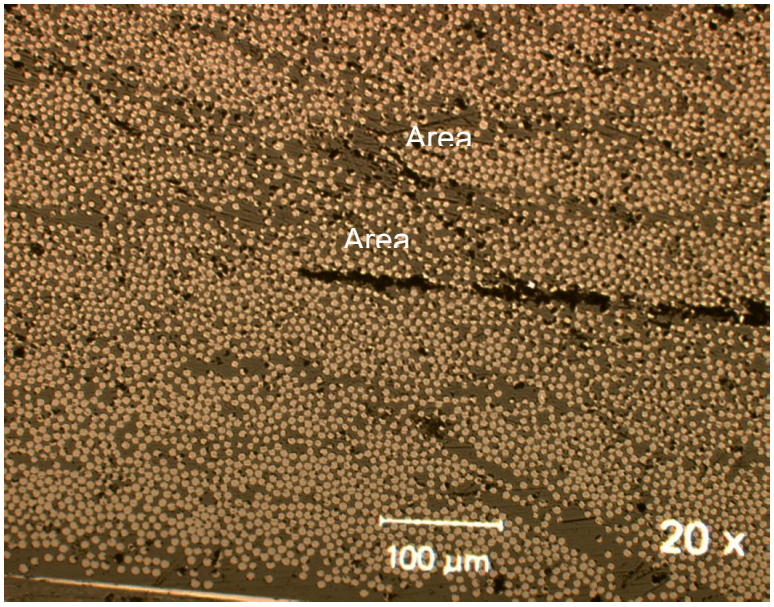

(a)

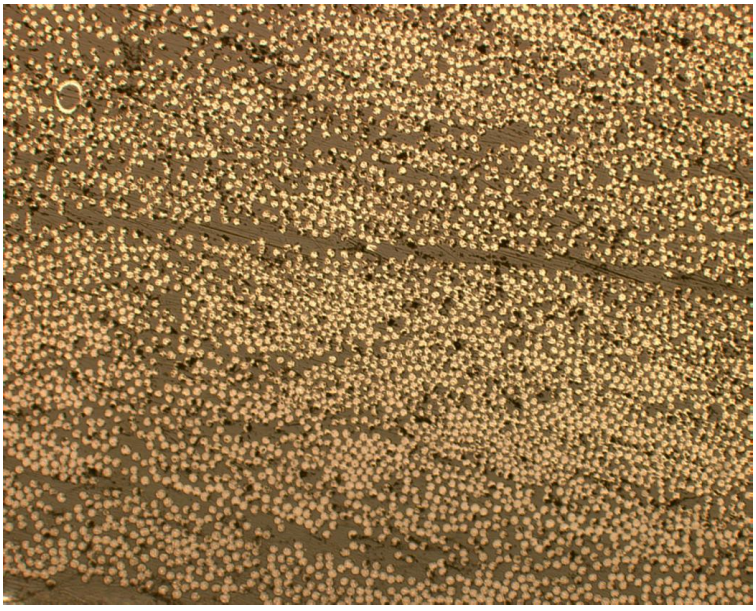

(b)

Fig. 3.9 Microscopic observation of voids in matrix (a) plate (b) manufactured with vacuum applied

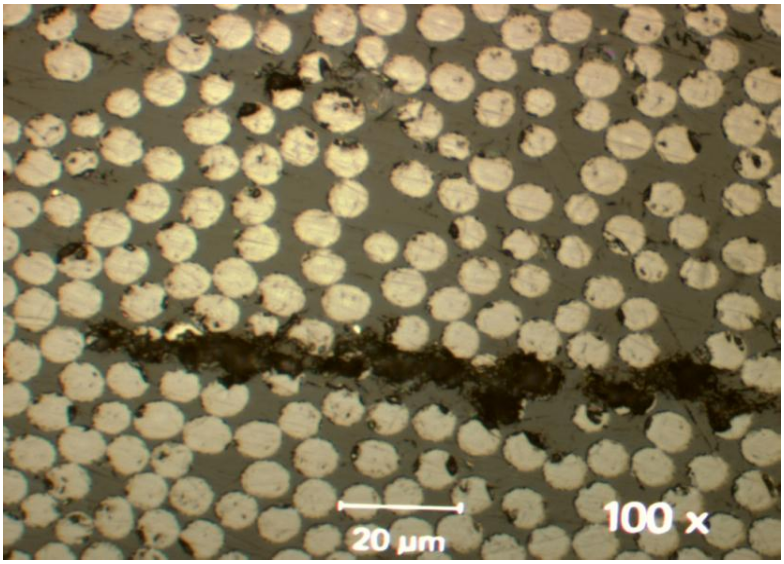

(a)

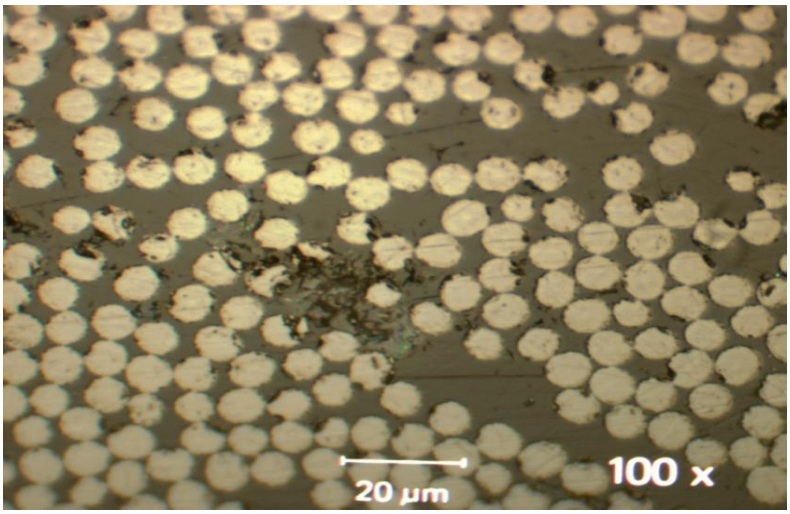

Fig. 3.10 The close-up view of voids at different locations for Plate 2 (NV-P): (a) voids between two layers of 90^{o} plies (area 1 in Fig. 3.9), and (b) voids within one layer (area 2 in Fig. 3.9).

them have been removed by the applied vacuum in Plate 4 (V-P). In Fig. 3.9 (b), the resin rich band in the middle between two 90^o layers should be the result of the transport payway for transfering gas.

The close-up views of the voids in Fig. 3.10 show that the morphology of voids varies with the location. The largest ones exist between the two layers of 90^o plies as Fig. 3.10 (a) shows. They are formed from the air trapped between prepregs during stacking. Under the applied pressure during the curing process, the trapped air is squeezed into the cluster of voids in the 2D plane between layers. For valatiles and moisture trapped in pregreg, they remain within layers in the form of mush smaller voids as Fig. 3.10 (b) shows. The applied pressure may collapse them or even dissolve them into resin. It is believed that for the same void content, the smaller size caused by high applied pressure can improve the strength property of laminate[66].

Under external loading, the voids can be the initiation site for the matrix cracking. This process has been caputred during the tensile testing and microscopic observation as shown in Fig. 3.11. Under relatively high applied strain, one crack forms and connects two voids. The microscopic observation suggests that this crack may initate from the corner of one void. The experimetnal observation on the interaction between defects and matrix cracking qualitatively explains that Plate 2 (NV-P) with more voids yields much higher crack density than Plate 4 (V-P) at the same loading level.This observation offers strong evidence of the effect of manufacturing defects on matrix cracking evolution.

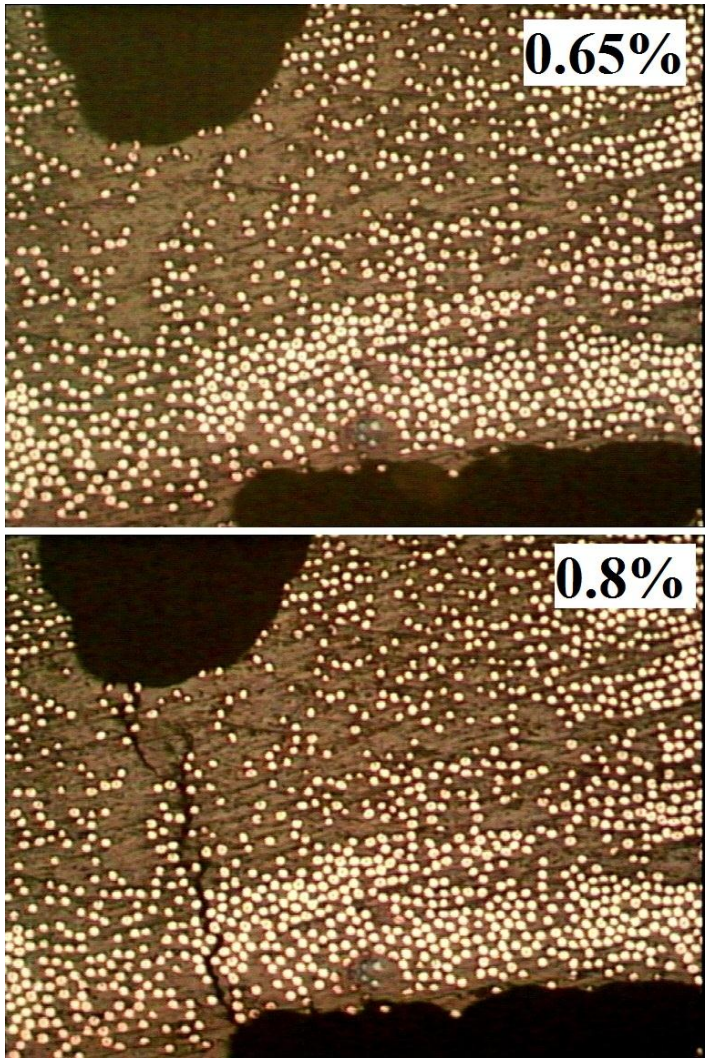

Fig. 3.11 One matrix crack forms between two voids.

One way to study such an effect is based on the extensive information of the relevant manufacturing defects. For example, the void is one of the critical defects for the matrix cracking evolution, so the information on the void content, size and distribution in laminates resulting from certain manufacturing process must be collected. Similar information is also needed for other relevant defects such as resin rich area, delamination,

and so on. Based on the collected information of relevant defects, their effect on the initiation and propagation of matrix cracking may be explicitly studied through micromechanics models. However, collecting such information is very difficult, if not impossible. An alternative way is through probilistic strength approach which directly studies the total effect of all revelant defects on the material property relating to the ability of laminate resisting the matrix cracking process. More about applying the probabilistic strength approach in studying matrix cracking evolution is explained in next section. Here, the microscopic observation just presents some evidence as the physical fundamental for using the probabilistic strength to represent the effect of manufacturing defects on matrix cracking evolutionn.

3.2 The effect of shear stress on the fatigue performance of composite laminates

The test specimens are taken from the project OPTIMAT of the fatigue performance of wind turbine blades. The dimensions of the specimen are shown in Fig. 3.12. The materials system is glass/epoxy with layups as $[\pm 45, 0°]_4;\pm 45]$**.** GFRP fabric is bonded to the both sides of the gripping area.

Specimens are subject to tension and torsion loading. The adoption of rectangular specimens for the combined tension/torsion testing is suggested in [67]. For rectangular specimens under torsion, a relatively homogenous stress state can be obtained in the region away from the four corners of the specimens. Although the stress state is not

strictly uniform, it is sufficient for the purpose of a preliminary study on the effect of shear stress.

The axial fatigue tension is applied by controlling the applied force to keep the maximum applied strain as constant for all tests. The torsion is applied by controlling the twisted angle, i.e. 0, ±1, ±1, ±2, ±3, ±4, ±5 degree. The frequency of fatigue loading is set as 5 Hz for both tension and torsion loading. Fig. 3.13 shows the setup of the tension/torsion fatigue testing.

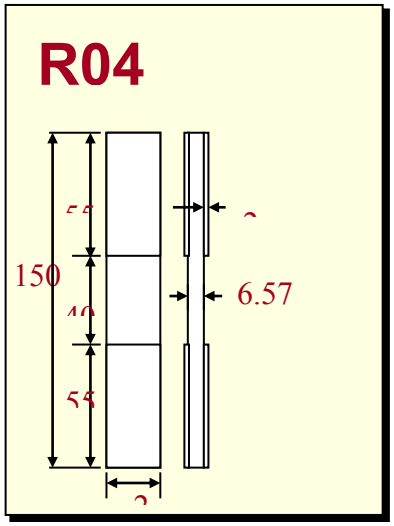

Fig. 3.12 The dimensions of the test specimen (code R04 in OPTIMAT project).

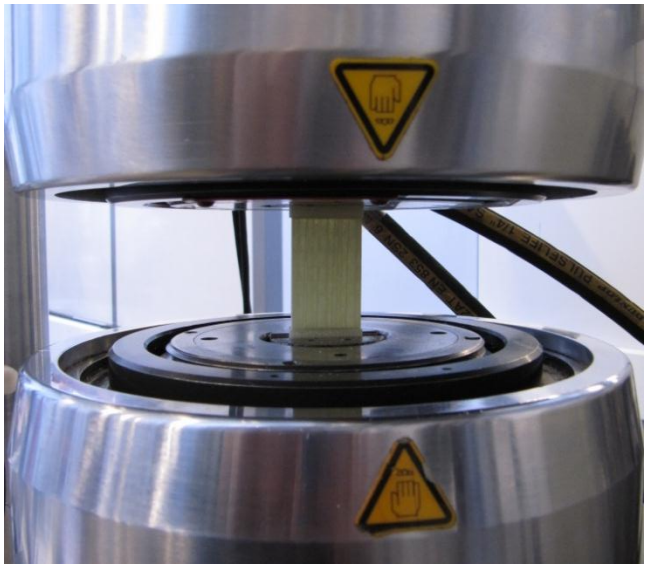

Fig. 3.13 The tension-torsion testing of rectangular specimen.

Table 3.1 shows the fatigue life of the test specimens under different magnitudes of torsion while the cyclic tension remains unchanged. It clearly illustrates the negative effect of torsion, or shear stress, on the fatigue life of composite laminates.

The fracture surface is shown in Fig. 3.14. Multiple matrix cracks are observed on the surface of $\pm 45^{o}$ plies, and the fracture surface is along the fiber direction. For the 0^{o} plies, fiber breakage occurs, and the fracture surface is like a brush head. Following the critical element model proposed by Reifsnider [68], the failure process is expected to start with multiple matrix cracks in $\pm 45^{o}$ plies followed by the delamination. Finally, the failure of the 0^{o} plies caused by fiber breakage happens and causes the catastrophic failure. All failure modes can interact with each other. For example, the delamination can be initiated from the matrix crack tip.

Table 3.1 Fatigue life decreases as the magnitude of torsion increases.

Axial tensile stress (MPa) (Max value corresponding to 0.8% strain)	Max/min twisted angle (degree)	Fatigue life (cycles)
124.9±102.2	0	64737
123.7±101.4	±1	39517
123.3±100.8	±2	38009
119.9±98.1	±3	22245
124.8±102.1	±4	8755
125.2±102.5	±5	7096

The role played by the shear stress may be further studied by examining its effect on the observed damage modes including matrix cracks. As a preliminary study, the experimental observation that shear stress greatly reduces the fatigue life can be taken as indirect evidence proving the effect of shear stress on matrix cracking.

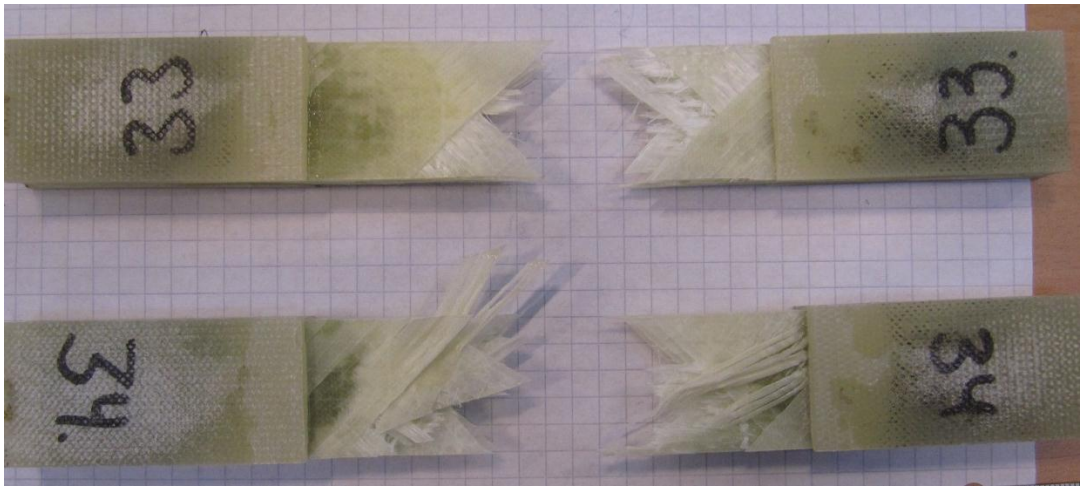

Fig. 3.14 Failure modes of laminates under tension/torsion fatigue

3.3 The effect of shear stress on the matrix cracking

Section 3.2 reports the preliminary study on the effect of shear stress. In this section, the further experimental investigation of the effect of shear stress focuses on the matrix cracking evolution under biaxial fatigue. The design of tubular specimens for the biaxial fatigue testing is reported firstly. Then the experimental study on the matrix cracking evolution in unconstrained and constrained plies under biaxial fatigue is detailed. The experimental study presented in this section was conducted by the author at University of Padova collaborating with Paolo A. Carraro.

3.3.1 Design of tubular specimens for biaxial fatigue testing

Several testing technologies have been developed to obtain uniform multiaxial stress state in plate or tubular specimens to study the behavior of materials under complex stress state [69]: (1) axial loading with internal pressure on tubular specimens, (2) axial

loading with torsion on tubular specimens [70], (3) flat cruciform specimens with biaxial loading applied to the arms, and (4) plate specimens under biaxial bending moments. For the purpose of studying the effect of shear stress on the matrix cracking, the fatigue testing, which applies the combined cyclic axial tension and torsion loading on tubular specimens, is conducted. Fig. 3.15 shows the schematic of the loading conditions. The glass/epoxy laminate tube is unidirectional hoop wound. Since the fiber direction is perpendicular to the axial direction, the specimen is designated as a [90] laminate tube.

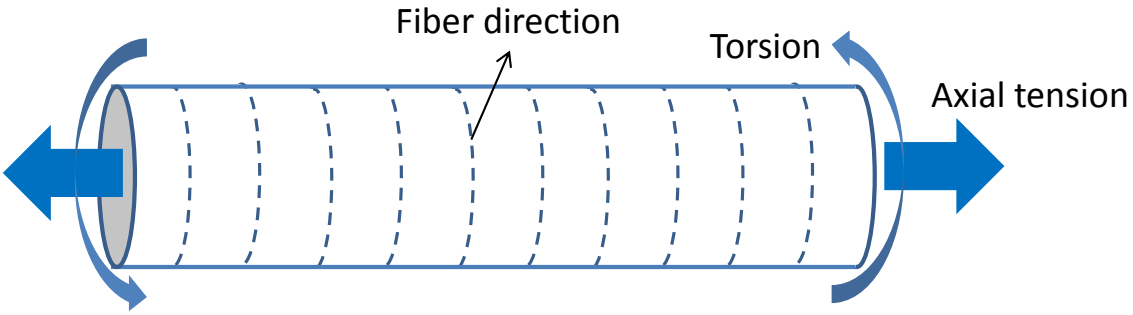

Fig. 3.15 The schematic of the tension/torsion fatigue testing using tubular specimens

Similar to the homogenous materials subjected to multiaxial fatigue, there are certain requirements for the geometry of the laminate tube in order to obtain reasonably uniform stress state in gauge section. The anisotropic nature of composite laminates, however, makes the problem more complicated. It can raise not only the non-uniform stress field, but also end effect and size effect [71]. Since the degree of anisotropy varies with the tested composite specimens, it is very hard, if not impossible, to design a universal specimen for all configurations to prevent those problems. Therefore, some geometric

parameters of the [90] laminate tube used for the testing must be designed based on stress analysis to assure that the desired uniform biaxial stress state, which are the transverse tension and in-plane shear, can be obtained.

Analytical stress analysis and the finite element simulation are conducted for the [90] laminate tube under the combined tension and torsion loading. The stress fields under axial tension and torsion are separately solved, and the combined multiaxial stress state can be obtained through the superimposition of the two solutions. For the problem of the [90] laminate tube under torsion loading, analytical solution for isotropic materials can be readily modified and applied to orthotropic materials, e.g. the [90] laminate. The applied torsion develops in-plane shear stress as Fig. 3.16 shows with the variation along the thickness of the tube:

$$\sigma_{z\theta}(r) = G_{z\theta} r \frac{\Delta\theta}{L} \tag{3.2}$$

where $G_{z\theta}$ is the in-plane shear modulus, L is the gauge length, and $\Delta\theta$ is the twisted angle for the gauge section. From Eq. (3.2), a desired pure shear stress state is obtained by applying torsion on the tubular specimen. However, the stress state is not strictly uniform through the tube thickness. The maximum shear stress exists on the outer surface of the tube while the minimum value is obtained on the inner surface. Here, the maximum/minimum ratio is used to evaluate the non-uniform degree of the stress distribution along the thickness:

$$\frac{Max(\sigma_{z\theta}(r))}{Min(\sigma_{z\theta}(r))} = \frac{\sigma_{z\theta}(r_2)}{\sigma_{z\theta}(r_1)} = 1 + \frac{t}{r_1} \tag{3.3}$$

where t is the thickness of the tube, and r_1 is the inner radius. Eq. (3.3) suggests that a reasonably uniform stress state can be obtained by reducing the thickness/diameter ratio. It also suggests that the degree of anisotropy for the elastic property of the [90] laminate tube has no effect on the stress state.

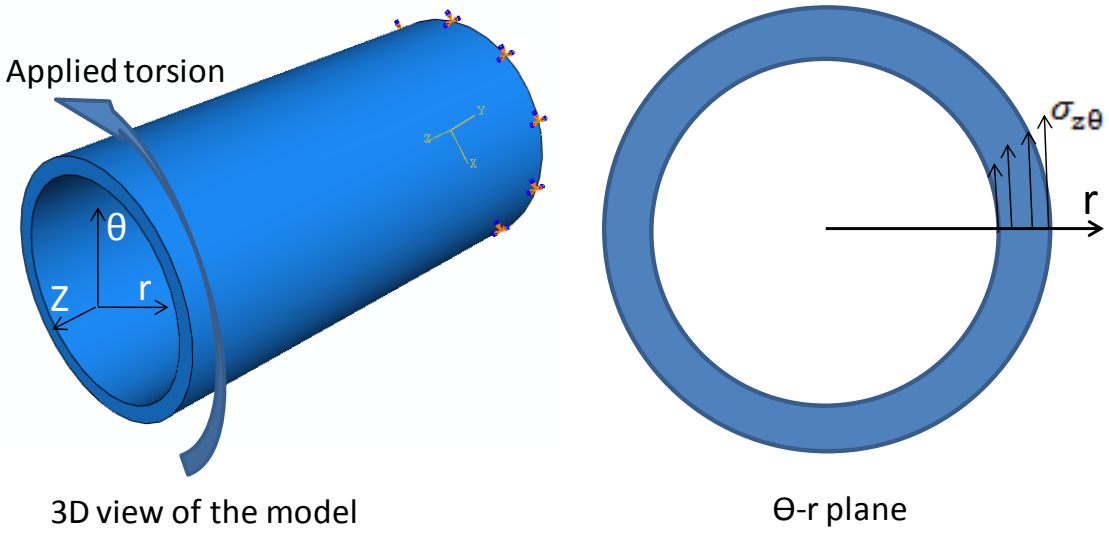

Fig. 3.16 Stress state in tubular specimen under torsion

When it is subject to axial tension, the [90] laminate tube will contract along the radial direction. This contraction induces displacement along the radial direction. Considering the symmetry of the problem, the displacement field is:

$$u_r = u(r) \tag{3.4a}$$

$$u_\theta = 0 \tag{3.4b}$$

$$u_z = \epsilon_0 z \tag{3.4c}$$

where the uniform strain ϵ_0 along the axial direction is caused by the axial tension and can be calculated by Eq. (3.4c) if the displacement boundary condition is given. And the corresponding strain field is:

$$\epsilon_{rr} = \frac{du_r}{dr} \tag{3.5a}$$

$$\epsilon_{\theta\theta} = \frac{u}{r} \tag{3.5b}$$

$$\epsilon_{zz} = \epsilon_0 \tag{3.5c}$$

Since there is no shear strain, the stress-strain relation is simplified as:

$$\begin{pmatrix} \sigma_{rr} \\ \sigma_{\theta\theta} \\ \sigma_{zz} \end{pmatrix} = \begin{bmatrix} C_{11} & C_{12} & C_{13} \\ C_{12} & C_{22} & C_{12} \\ C_{13} & C_{12} & C_{11} \end{bmatrix} \begin{pmatrix} \epsilon_{rr} \\ \epsilon_{\theta\theta} \\ \epsilon_{zz} \end{pmatrix} \tag{3.6}$$

where $[C_{ij}]$ is the stiffness matrix of the [90] laminate with transversely isotropic property.

From Eqs. (3.5-3.6), the equilibrium equation yields a differential equation:

$$C_{11}u'' + C_{11}u' - \frac{C_{22}u}{r^2} + (C_{13} - C_{12})\frac{\epsilon_0}{r} = 0 \tag{3.7}$$

The general solution with undermined constants for Eq. (3.7) is:

$$u(r) = A_0 r^{\sqrt{\frac{C_{22}}{C_{11}}}} + A_1 r^{-\sqrt{\frac{C_{22}}{C_{11}}}} + \frac{C_{12}-C_{13}}{C_{11}-C_{22}}\epsilon_0 \tag{3.8}$$

The unknown constants, A_0 and A_1, can be solved by applying the boundary conditions (the surfaces of the tube are traction free). Once the displacement field is solved, the stress field can be obtained through Eq. (3.5-3.6).

The analytical solution finds that the hoop stress $\sigma_{\theta\theta}$ is also developed under the axial tension. The existence of such hoop stress is confirmed by the finite element model. Fig. 3.17 shows the distribution of $\sigma_{\theta\theta}$ through thickness from both the analytical solution and FE results. The hoop stress, which is the longitudinal stress along the fiber direction, should be as small as possible because the aim is to study the effect of shear stress on the matrix cracking under transverse tensile stress.

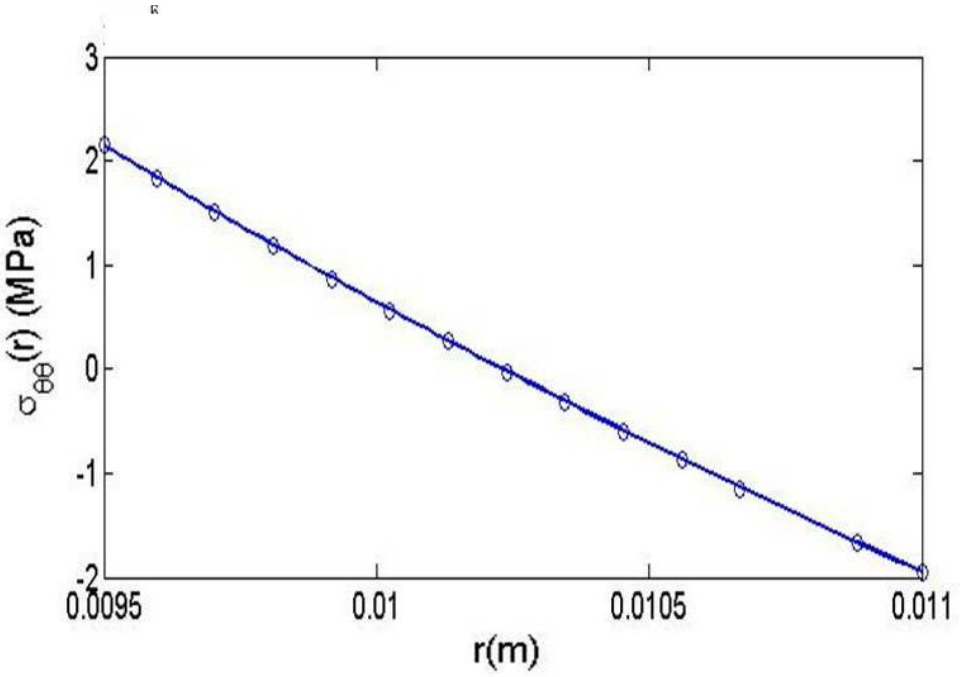

Fig. 3.17 Distribution of hoop stress through thickness when [90] laminate tube is subject to applied axial strain as. (dot: FEM result; line: analytical solution).

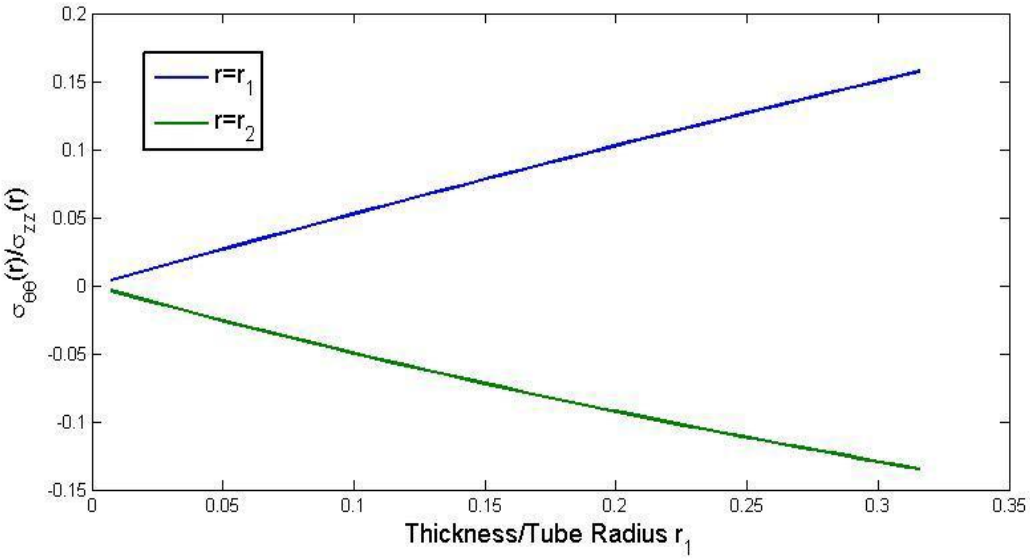

Fig. 3.18 The variation of hoop stress as a function of the ratio of the thickness to the inner radius of the [90] laminate tube.

The analytical solution shows that the magnitude of the hoop stress is inversely proportional to the thickness/diameter ratio (see Fig. 3.18). It suggests that the undesirable hoop stress may be reduced by decreasing the thickness/diameter ratio. As a summary, the desirable uniform stress state, i.e. the combined transverse tensile stress and in-plane shear stress, can be obtained by controlling the ratio of thickness to the inner radius of the [90] laminate tube. Also, the size of the hydraulic grips of the testing machine may put some additional restriction on the geometry of the tubular specimen. Considering all requirements, the thickness of the tube is set as 1.5mm and the inner radius is 9.5mm. Under such conditions, the degree of non-uniform distribution of the shear stress is 1.158 by Eq. (3.3), and the undesirable hoop stress is ±6% of the corresponding axial tensile stress.

The laminate tube is manufactured by wrapping and then autoclave molding. Fig.3.19 shows the setup of the biaxial fatigue testing using MTS 809. The cyclic tension and torsion is applied proportionally with frequency as 5Hz. For the observation of any damage initiation and progression, a LED light is positioned inside of the tube taking the advantage of the transparency of the glass/epoxy laminates.

Fig. 3.19 The setup of the biaxial fatigue testing.

3.3.2 Matrix cracking in unconstrained plies under biaxial fatigue

The fatigue test is firstly conducted using the [90] laminate tube. The biaxial ratio is defined as:

$$\lambda_{12} = \frac{\tau}{\sigma_2} \tag{3.9}$$

where τ is the in-plane shear stress and σ_2 is the transverse tensile stress. For different biaxial ratios, i.e. 0, 1, 2, the observed failure mode is always matrix cracking. The

cracking process is very fast. No crack initiation or propagation has been observed during the fatigue testing. Since epoxy as the matrix is very brittle, the instantaneous cracking process in the matrix is understandable. One may view the failure under such conditions as a process controlled by the crack initiation. Once the crack is initiated from a defect, there is no mechanism to dissipate the energy except propagating the crack unstably. Since there is no stable crack growth, S-N curve is used to characterize the matrix cracking under fatigue loading as Fig. 3.20 shows. In Fig. 3.20, the transverse tensile stress level is chosen as Y axis while the effect of shear stress is shown by plotting multiple S-N curves for different biaxial ratios. It clearly shows the significant effect of shear stress on the fatigue life of unconstrained plies that is controlled by the matrix cracking process.

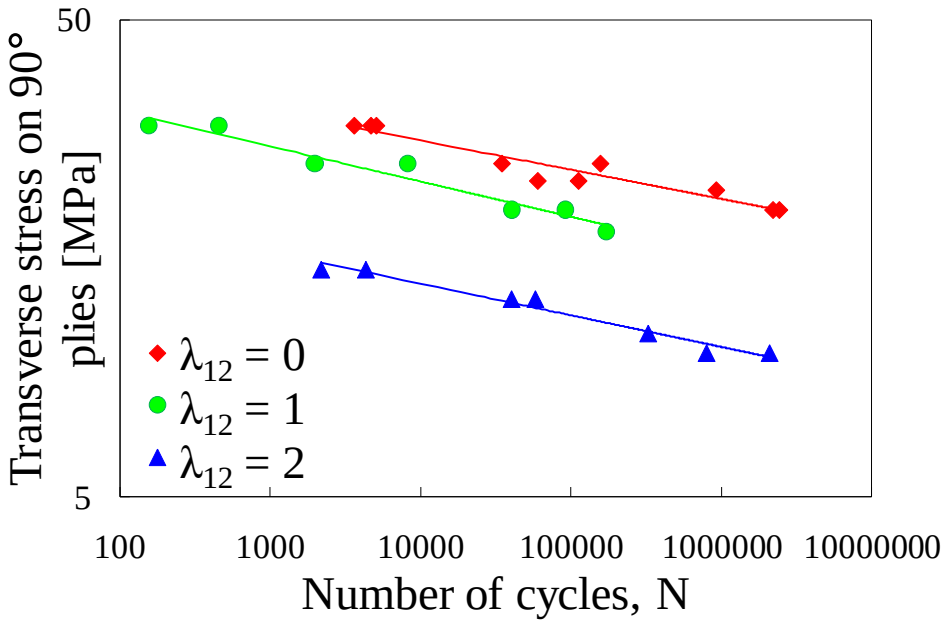

Fig. 3.20 S-N curves of the [90] laminate under the pure tension and biaxial fatigue

An empirical way to quantitatively describe the effect of shear stress is through enforcing certain polynomial fatigue failure criteria to fit the experimental data. For example, Hashin and Rotem[72] proposed the following criterion for fatigue failure of unconstrained plies caused by matrix cracking:

$$\left(\frac{\sigma_2}{\sigma_2^u}\right)^2 + \left(\frac{\tau}{\tau^u}\right)^2 = 1 \tag{3.10}$$

where σ_2 and $\tau$are the maximum transverse tensile stress and in-plane shear stress for fatigue loading, respectively. σ_2^u and τ^u are the fatigue failure stress for the transverse tension and in-plane shear, respectively, They are determined by the relevant fatigue parameters:

$$\sigma_2^u = \sigma_2^u(\sigma_{2,max}, \sigma_{2,min}, ; N; n) \tag{3.11.a}$$

$$\tau^u = \tau^u(\tau_{max}, \tau_{min}, ; N; n) \tag{3.11.b}$$

where the subscripts *max* and *min* denote the bound of fatigue stress, N is the number of cycles to failure, and n is the frequency. By enforcing Eq. (3.10) to the experimental data obtained from the off-axis unidirectional laminate under cyclic axial tension, Hashin and Rotem found the fitted value for σ_2^u and τ^u as functions of the failure cycles (see Fig. 3.21). It can be seen that both failure stresses decrease as fatigue cycles increase. For low fatigue cycles (high stress fatigue), τ^u is higher thanσ_2^u. When fatigue cycles increase as the fatigue stress decreases, τ^u decreases faster than σ_2^u. Similar trend for the decrease of σ_2^u and τ^u as fatigue cycles increase was also reported by Sims and Brogdon[73] by applying a similar polynomial fatigue failure criterion to their experimental data.

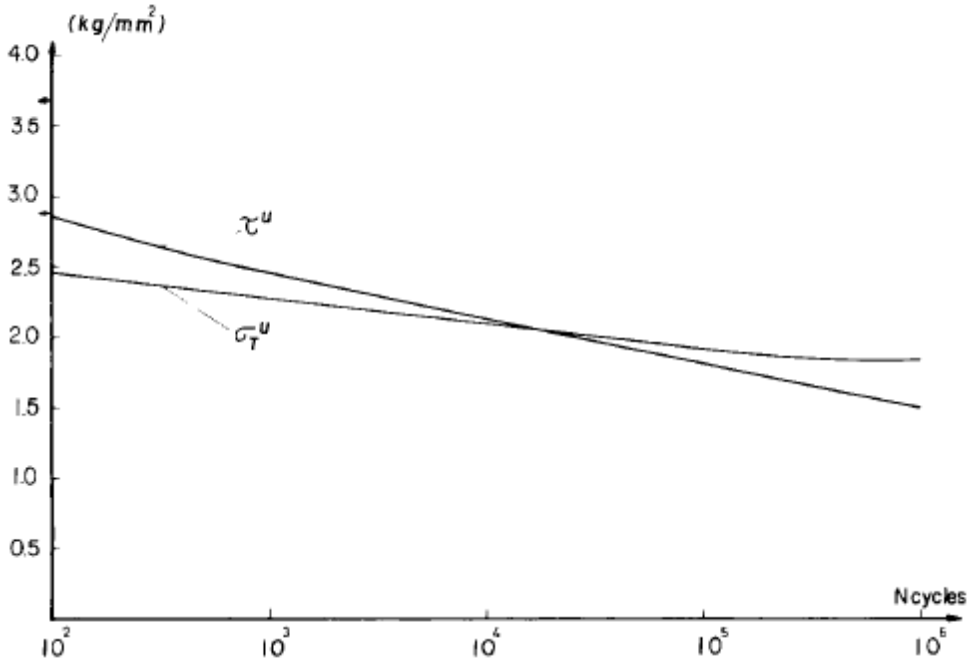

Fig. 3.21 σ_2^u and τ^u vs. the number of cycles to failure.

Although named fatigue failure stress, the physical meaning of σ_2^u and τ^u is not clear for the failure under biaxial fatigue. However, these two terms do offer a quantitative way to illustrate the effect of the corresponding stress components on the fatigue failure caused by the matrix crack. A larger value for the failure stress means that the matrix cracking is less sensitive to the corresponding stress component. For example, it is known that the axial tension along fiber direction play no role in the matrix cracking, therefore, the term $\left(\frac{\sigma_1}{\sigma_1^u}\right)^2$ is eliminated in Eq. (3.10) by setting the failure stress for axial tension σ_1^u as infinite. In Fig. (3.21), τ^u starts with relatively large value but decreases faster as the number of cycles increases. It suggests that the effect of the shear stress becomes more important for the failure caused by matrix cracking under high cycle fatigue.

3.3.3 Matrix cracking in constrained plies under biaxial fatigue

When the off-axis plies are embedded into multidirectional laminates, the matrix cracking process under on-axis tension is constrained by neighboring plies. From the point view of fracture mechanics, the constraint effect keeps the energy release rate as constant after the initiation of a crack. For static loading, it requires higher loading to propagate the crack. For fatigue loading, stable crack growth independent of the crack length is usually observed. For some composite structures undergoing extremely high cycles of fatigue, the stable growth of matrix cracks is of interest. Therefore, the stable crack growth in the constrained ply under biaxial fatigue is studied here. Especially, the role of shear stress in the stable cracking growth is examined.

Cross ply laminate tubes are manufactured using filament winding process and subject to tension-torsion fatigue testing. With the constraint from the 0^o plies, the matrix cracks in the 90^o ply grow steadily as shown in Fig. 3.22. The growth is characterized by the crack growth rate:

$$CGR = \frac{\Delta L}{\Delta N} \tag{3.12}$$

where ΔL is the crack propagation for one tip of the crack, and ΔN is the corresponding cycles for that propagation.

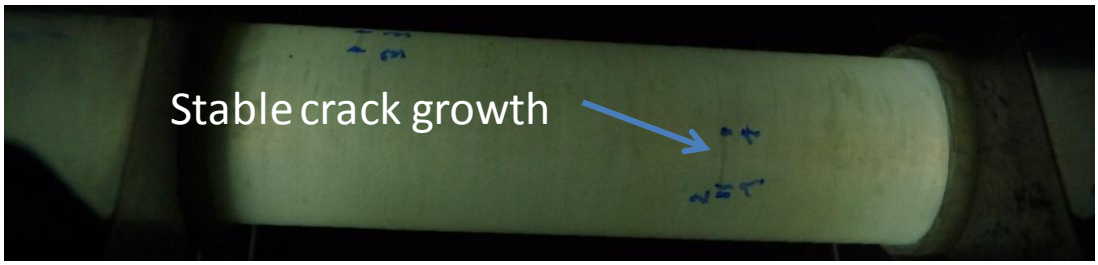

Fig. 3.22 Stable crack growth in the 90^o ply under tension and torsion fatigue loading

In Section 3.3.2, it has been shown that the fatigue failure caused by the matrix crack in unconstrained plies become more sensitive to the shear stress for high cycle fatigue. To examine whether similar trend exists for the matrix cracking process in constrained ply, the measurement of crack growth rate is conducted for two transverse tensile stress levels at different biaxial ratios. The high transverse tensile stress for the 90^o ply is set as 30MPa (maximum stress for fatigue) while the lower one is set as 20MPa (maximum stress for fatigue). The biaxial ratio is set as 0, 0.5, and 1.0. For the low cycle fatigue testing, multiple cracks are usually initiated within thousands of cycles under high stress level. For high cycle fatigue, the stress level is too low to initiate a crack within one million cycles. An alternative way is adopted here; cracks are initiated under a relatively high stress level. After that, the fatigue stress level is switched to the designed lower level for the measurement of crack growth rate. For measuring the growth rate, the corresponding increment of cycles ΔN is recorded when the crack tip propagates 1 mm ($\Delta L = 1mm$).

The measured crack growth rate under different stress levels is summarized in Table 3.2. For both stress levels, the added cyclic shear stress increases the crack growth rate. What's more, such increase is more significant for the high cycle fatigue. This finding is similar to the situation for unconstrained plies.

Table 3.2 Crack growth rate increased by adding shear stress

Biaxial ratio	Crack growth rate* ($\sigma_2 = 20MPa$, Low stress/high cycle	Crack growth rate* ($\sigma_2 = 30MPa$, High stress/low cycle)
0.5	97.5	3
1	675	10

* normalized by the crack growth rate under the corresponding pure tension fatigue.

The microscopic observation of the fracture surface may help explain the role played by the shear stress during the matrix cracking process under fatigue. In Fig. 3.23, the fracture surface is along the fiber direction, indicating that the failure is caused by the matrix crack. Some serration is observed along the fracture surface. The degree of serration is higher when the shear stress is higher. The observed serration is caused by the microcracks between fibers. Unlike the major matrix cracks along the fiber direction, these inclined microcracks are arrested by fibers. They are probably formed under the combined transverse tensile and in-plane shear stress considering that no obvious

serration is observed for the pure transverse tension case. Also, the higher degree of serration under higher biaxial ratio suggests that higher shear stress yields higher density of microcracks for a given number of cycles. Therefore, the added shear stress is critical for the formation of such microcracks. Assisted by such microcracks, the initiation and propagation of major matrix cracks may become easier. For unconstrained plies, it

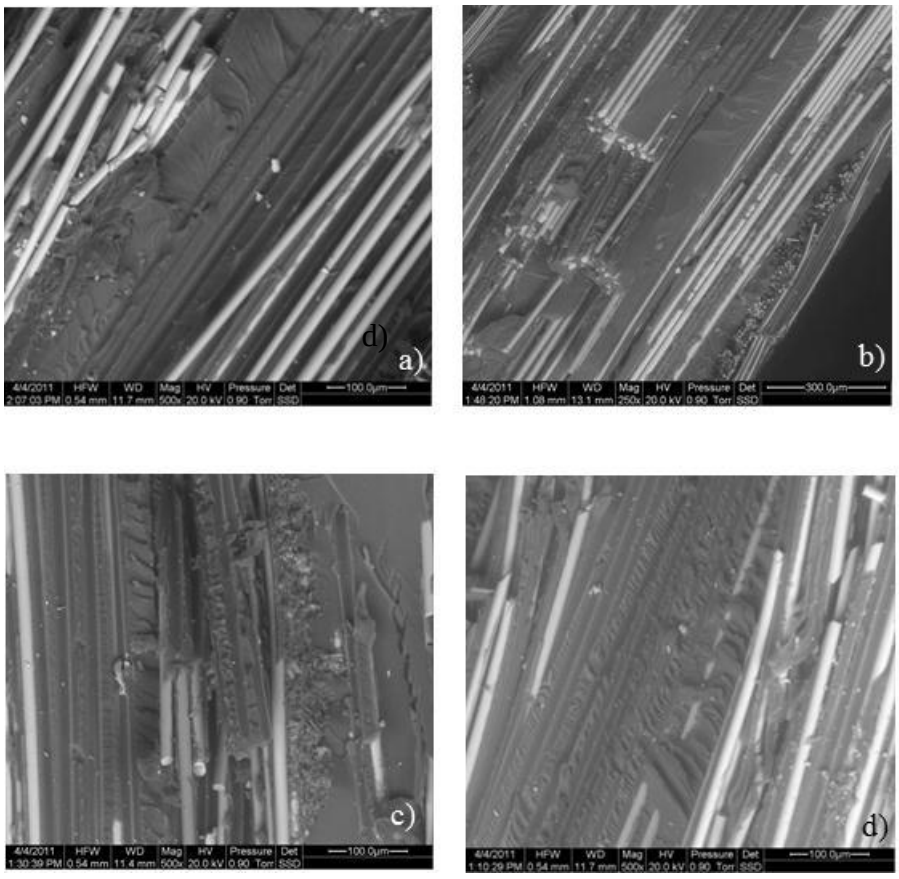

Fig.3.23 Fracture surfaces for a) $\lambda_{12} = 0$, b) $\lambda_{12} = 0.5$, c) $\lambda_{12} = 1$, and d) $\lambda_{12} = 2$ (courtesy of P.A. Carraro)

means shorter fatigue life, which is controlled by the initiation of the crack. For constrained plies, the stable crack growth rate controlled by the cracking propagation becomes higher. The above analysis suggests that the shear stress plays important role in the matrix cracking under biaxial fatigue by causing the microcracks.The experimental results also show that the matrix cracking becomes more sensitive to shear stress for high cycle fatigue. This is probably because the abovementioned mechanism on microcracks is more active for high cycle fatigue. According to the observation from Awerbuch and Hahn[74], the degree of serration becomes much higher for high cycle fatigue. For higher fatigue stress level, very few serrations are found along the fracture surface. The major matrix cracking process is mode 1 cracking, which is mainly driven by the transverse tensile stress. When the transverse tensile stress is relatively high for the low cycle fatigue, the cracks develop without the assistance of the microcracks. For the high cycle fatigue, the very low transverse tensile stress is not enough to drive the cracking process. The shear stress assisted microcracks become more important for the cracking process. Therefore, the cracking process is more sensitive to the shear stress for the high cycle fatigue.

4. STOCHASTIC CRACKING EVOLUTION IN LAMINATES UNDER STATIC LOADING

4.1 Modeling of cracking evolution in cross ply laminate

4.1.1 Weibull distribution of static transverse strength

As Fig. 4.1 shows, the 90^o layer is discretized into elements. The element size satisfies the following criteria: 1) it must be large enough to contain typical manufacturing defects critical for cracking, and 2) it must be small enough so that the stress level may be assumed constant within each element. If these two requirements are satisfied, each element is assumed to possess a single static transverse strength (σ_s), thus accommodating at most one crack. The failure of one element when the strength criterion is satisfied is equivalent to the formation of one crack in the 90^o layer.

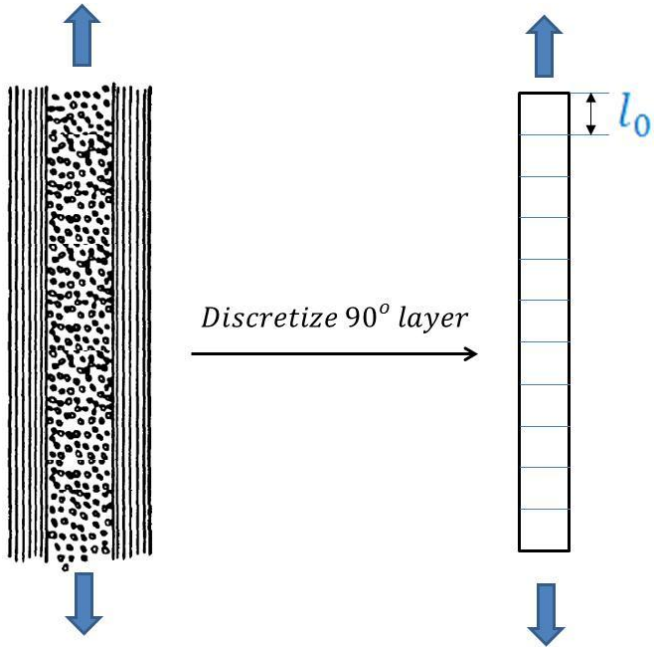

Fig. 4.1 Discretization of the 90^o layer for distributed static transverse strength

The static transverse strength of each element is assumed to follow the same Weibull distribution to reflect the non-uniform material property of resisting cracking:

$$P_s(\sigma_s \leq \sigma) = 1 - \exp\left(-(\frac{\sigma}{\sigma_0})^m\right) \quad (4.1)$$

where σ_0 and m are two Weibull parameters called the characteristic strength and distribution shape constants, respectively. The location parameter σ' in Eq. (2.4) is assumed to be zero. Such independent and identical distribution of σ_s for different elements is the result of the assumption that the manufacturing defects are randomly distributed, e.g. no cluster of defects. In the Monte Carlo simulation, random numbers are generated according to Eq. (4.1) and assigned to elements as the local strength. After σ_s is assigned a deterministic value for each element, the rest of the simulation is conducted in a deterministic way. In contrast, the developed statistical model keeps the statistical nature of σ_s and models the stochastic cracking evolution in a statistical way. It should be emphasized that the static transverse strength of the 90^o layer and its distribution in Eq. (1) is very different from the statistical distribution of transverse strength of the stand-alone unidirectional laminate shown in Fig. 2.14. As Section 2.2.1 discussed, the cracking process in the constrained 90^o layer is not the same as the one in the unconstrained layer. But the threshold value for the cracking in constrained layer is still named as the static transverse strength for the simplicity. Also, the statistical distribution of strength expressed as Eq. (4.1) is dependent on the discrete element size as Section 2.2.2 shows while the statistical distribution of transverse strength of unidirectional laminate is dependent on the volume of the tested specimens. Due to these two considerations, it may require additional examination of some modeling work in

literature such as Sun et al. [29] that applies the experimental data from the unidirectional laminate to the stochastic cracking evolution in constrained layer.

4.1.2 Stress analysis of cracked cross ply laminate

The variational approach by Hashin[41] is used for calculating the transverse stress distribution in the cracked 90^o layer. The solution is based on the unit cell, which is the region between two pre-existing cracks (see Fig. 2.18). It consists of the original stress for uncracked laminate and the perturbation caused by cracks. Through equilibrium equations and boundary conditions, all stress components can be expressed as functions of a single unknown function. By applying the principle of minimum complementary energy, the only unknown function can be solved to obtain the solution for the stress state in cracked laminate. One important assumption for this method is that there is no stress variation through the thickness within each layer.

Fig. 4.2 shows the transverse stress distribution between cracks. It can be seen that the stress perturbation from cracks becomes dominate as the crack spacing decreases. For large crack spaces, the stress perturbation is highly localized, and most parts undergo the unperturbed stress level.

4.1.3 Non-interactive regime of cracking evolution

During the initial stage of the cracking evolution, most cracks distribute far away from each other. With very few cracks randomly distributed along the length, most crack

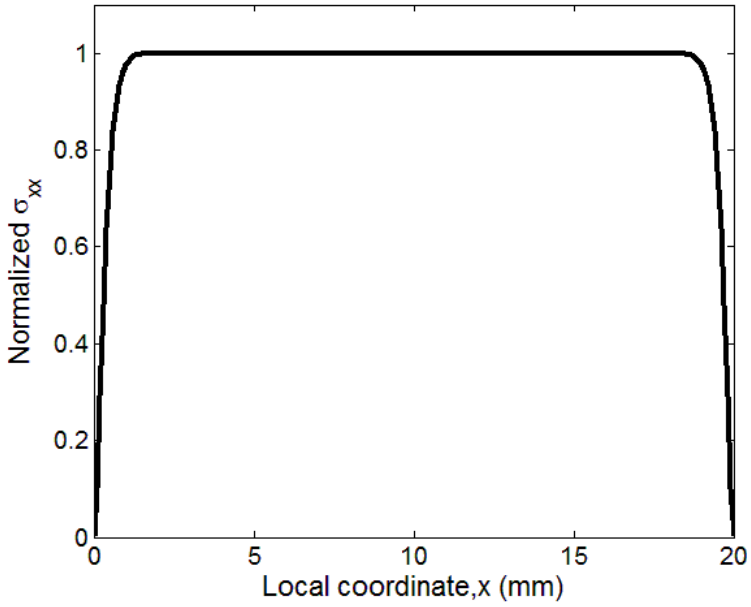

(a)

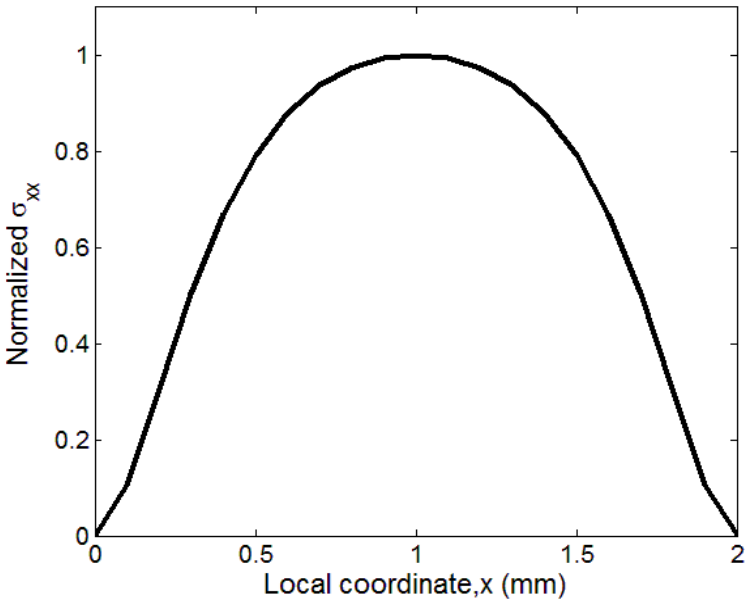

(b)

Fig. 4.2 Transverse stress distribution between two pre-existing cracks. (the stress is normalized by the maximum value) (a) large crack spacing, and (b) small crack spacing

spacings are very large (see Fig. 4.2(a)). The stress perturbation by preexisting cracks is highly localized and therefore can be neglected for the formation of new crack between pre-existing cracks. This stage is named as the non-interactive regime of the cracking evolution in the sense that the formation of cracks is independent from each other.

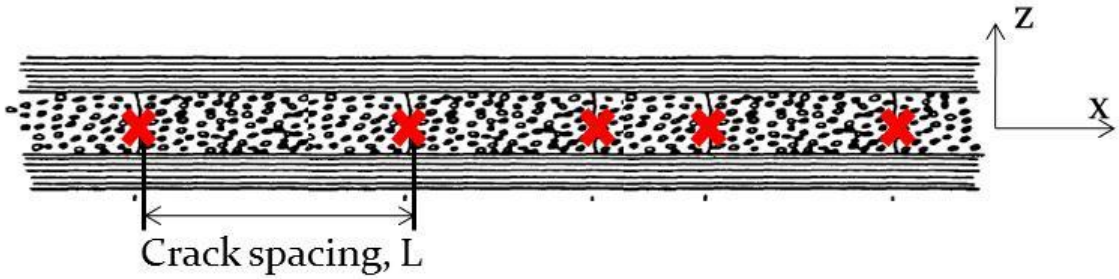

Fig. 4.3 The 90^o layer divided into blocks with varied length by the cracks

For the non-interactive regime, the transverse stress remains constant as the ply stress $\sigma_{xx}$for the uncracked 90^o layer, which can be calculated from external loading through CLT. The number of cracks per unit length is the number of failed elements of which the element strength is not higher than the longitudinal tensile stress:

$$\rho = \frac{1}{l_0} * P_s(\sigma_s \leq \sigma_{xx}) \tag{4.2}$$

Manders[40] found that the independent formation of cracks along the the 90^o layer is actually a Poisson process. For a Poisson process, it can be shown that the crack spacing L, which is the distance between neighboring cracks (see Fig. 4.3), is exponentially distributed with an accumulative probability:

$$P_L(L \le L') = 1 - exp(-\rho L') \tag{4.3}$$

So far, the analytical solution for the stochastic cracking evolution in the non-interactive regime has been obtained. Crack density as a function of applied stress is given by Eq. (4.2) as the averaged quantity. The statistical distribution of the crack spacing given by Eq. (4.2) corresponds to the variation for a statistical process.

4.1.4 Interactive regime of cracking evolution

According to Eq. (4.2), the 90^o layer has been divided by the cracks into blocks with varied length in the non-interactive regime (see Fig. 4.3). For the non-interactive regime, most blocks fall into the situation as Fig. 4.2 (a) shows. As the applied loading keeps increasing, more cracks form and they tend to be close to each other. The stress distribution as Fig. 4.2 (b) shows becomes increasingly common. The cracking evolution therefore gets into the interactive regime where the stress perturbation by the neighboring cracks has to be considered for predicting the formation of new cracks. For the interactive regime, an iterative numerical procedure was developed based on the discretized 90^o layer (see Fig. 4.1) to track the formation of new cracks at each increment of applied stress. Firstly, the probability or percentage of the block length L_i, or crack spacing among all blocks, is obtained by discretizing the $P_L(L \le L')$ in Eq. (4.3) at the end of the non-interactive regime,

$$P_{L_i}^{(0)} = \begin{cases} P_L(L_i) - P_L(L_{i-1}) & i = 1,2,\dots,N-1 \\ 1 - P_L(L_{i-1}) & i = N \end{cases} \tag{4.4}$$

where $L_i = i * l_0$, and N should be large enough so that $P_L(L_N)$ is close to 100% for including most of possible cases. As new cracks form under additional loading, the

probability distribution of the block length is changing; long blocks are divided by new cracks and eventually become small ones. If the fraction of block length $P_{L_i}^{(n)}$ at each step can be tracked, the cracking evolution, i.e. the average crack spacing and the variation, is simulated.

For a general block with length L_i shown in Fig. 4.4, the formation of a new crack at each element, or the process of becoming short ones, is predicted as follows. The element at x_j within the block L_i is denoted as $x_{i,j}$.The transverse stress for element $x_{i,j}$ at step n is denoted as $\sigma_{i,j}^{(n)}$. At next step of the iterative, of which the external loading is increased, the local stress is increased to $\sigma_{i,j}^{(n+1)}$ as shown in Fig. 4.4. Such increase may cause the element that has survived from the previous loading to fail at step n+1. The probability for the failure can be calculated from the given strength distribution:

$$\lambda_{\mathrm{ij}}^{(\mathrm{n+1})} = \frac{\mathrm{P_s}\left(\sigma_{i,j}^{(n+1)}\right) - \mathrm{P_s}\left(\sigma_{i,j}^{(n)}\right)}{1 - \mathrm{P_s}\left(\sigma_{i,j}^{(n)}\right)} \tag{4.5}$$

If the strength is lower than $\sigma_j^{(n)}$, the element has failed in previous steps. For the survived elements, the strength probability distribution cannot be the same as the initial Weibull distribution. An adjustment to the distribution has been made in Eq. (4.5) to address this problem. A similar treatment can be found in[56].

With the failure probability for every element $\lambda_{\mathrm{ij}}^{(\mathrm{n+1})}$ under the additional loading, three scenarios are considered in the simulation: 1) no crack forms, which is equivalent to that

all elements survive under the additional loading, 2) only one crack forms, and 3) more than one crack form.

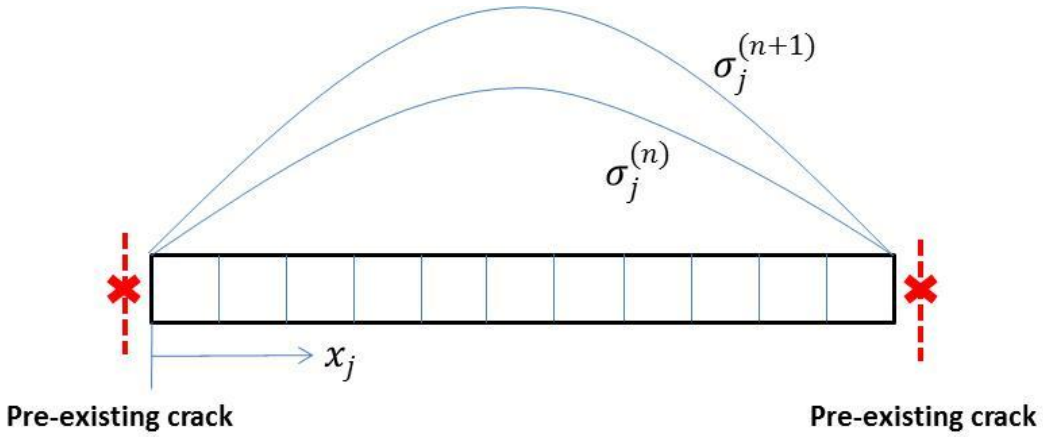

Fig. 4.4 Schematic of the stress distribution at steps n and n+1 for a block.

For the first scenario that all elements survive within block L_i, the probability can be calculated as a conditional probability problem:

$$P0_{L_i}^{(n+1)} = P_{L_i}^{(n)} * \prod_{j=1}^{i} \left(1 - \lambda_{ij}^{(n+1)}\right) \tag{4.6}$$

Such probability is also the percentage among all blocks that will remain the original length L_i.

The second scenario actually includes a group of cases with variation in the crack location. For only one crack form at an arbitrary location x_j within block L_i, the probability is still a conditional probability problem:

$$P1_{x_{i,j}}^{(n+1)} = P_{L_i}^{(n)} * \frac{\lambda_{ij}^{(n+1)}}{1-\lambda_{ij}^{(n+1)}} * \prod_{j=1}^{i}\left(1-\lambda_{ij}^{(n+1)}\right) \quad (4.7)$$

Such probability is also the percentage among all block lengths that the original block L_i is divided by the new crack into two blocks with shorter length as x_j and $L_i - x_j$.

If the increment of the applied stress is kept small, the third scenario that more than one crack form within one block can be neglected. In the simulation, this is assured by the following criterion at each step:

$$\sum_{i=1}^{N} P0_{L_i}^{(n)} + \sum_{i=1}^{N}\sum_{j=1}^{i} P1_{x_{i,j}}^{(n)} \geq 99\% \quad (4.8)$$

If Eq. (4.8) is satisfied, then almost all possible scenarios have been examined by applying Eqs. (4.6-4.7) to $P_{L_i}^{(n)}$. The probability distribution of the crack spacing at step n+1 is therefore updated:

$$P_{L_i}^{(n+1)} = P_{L_i}^{(n)} P0_{L_i}^{(n+1)} + \sum_{k=i+1}^{N} 2\, P_{L_i}^{(n)} P1_{k,i+1}^{(n+1)} \quad (4.9)$$

where the first part of the right side is corresponding to the fraction of the blocks surviving from the additional loading, and the second part is corresponding to the fraction of those short blocks forming from the process that long blocks are divided by the new crack. Since one long blocks will generate two short blocks, there is a factor 2 in the second part. It will cause the sum of $P_{L_i}^{(n)}$ not remained as 100%. Therefore, $P_{L_i}^{(n)}$ has to be normalized at the end of each iterative. Once the probability distribution of the block length is updated at step n, the crack density can be easily calculated:

$$\rho^{(n)} = \frac{1}{\sum_{i=1}^{N} L_i * P_{L_i}^{(n)}} \quad (4.10)$$

The interactive regime of the stochastic cracking evolution is simulated based on Eqs. (4.9-4.10), yielding the crack density and the variation of crack spacing under the given applied loading. The initial state for the simulation is given by Eq. (4.4). Together with the analytical solution for the non-interactive regime, the whole stochastic cracking evolution in cross ply laminate under static loading is simulated.

4.2 Results and discussion

As explained in Section 4.1, the multiplication of cracks can be viewed as the process that long blocks are divided by new cracks to form smaller blocks. Fig. 4.5 shows such process in the form of the probability density function of crack spacing as the applied stress increases in the simulation. The probability or percentage of longer blocks decreases and shifts to the lower range of the probability distribution as the applied stress increases. From such a distribution, the average crack spacing, or crack density, can be calculated at every stress level. Fig. 4.6 shows the crack density as a function of the applied stress predicted by the developed semi-analytical model. The experimental data of each carbon/epoxy plate manufactured by different processes (see Section 3.1.2) is used to estimate the corresponding Weibull parameters for the simulation. The simulation results agree well with the experimental data. Especially, the effect of manufacturing quality on the cracking evolution is correctly predicted by adjusting two Weibull parameters.

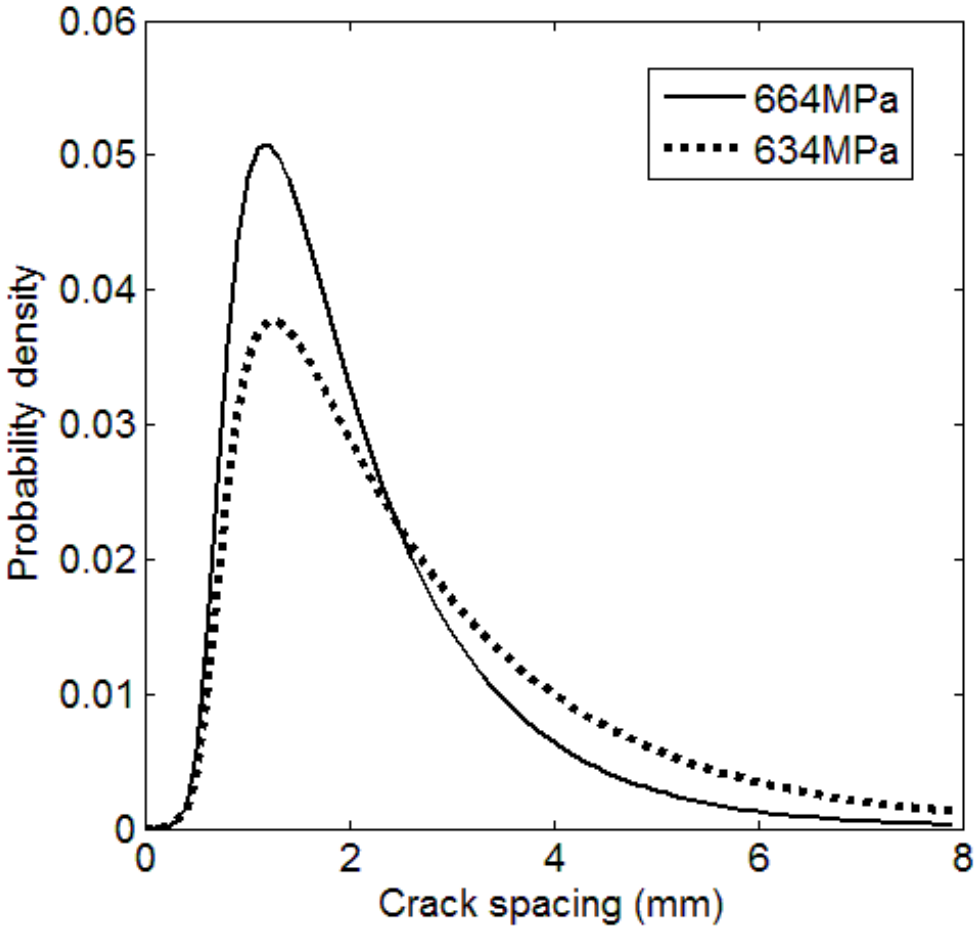

Fig. 4.5 Evolution of the statistical distribution of crack spacing as applied stress increases.

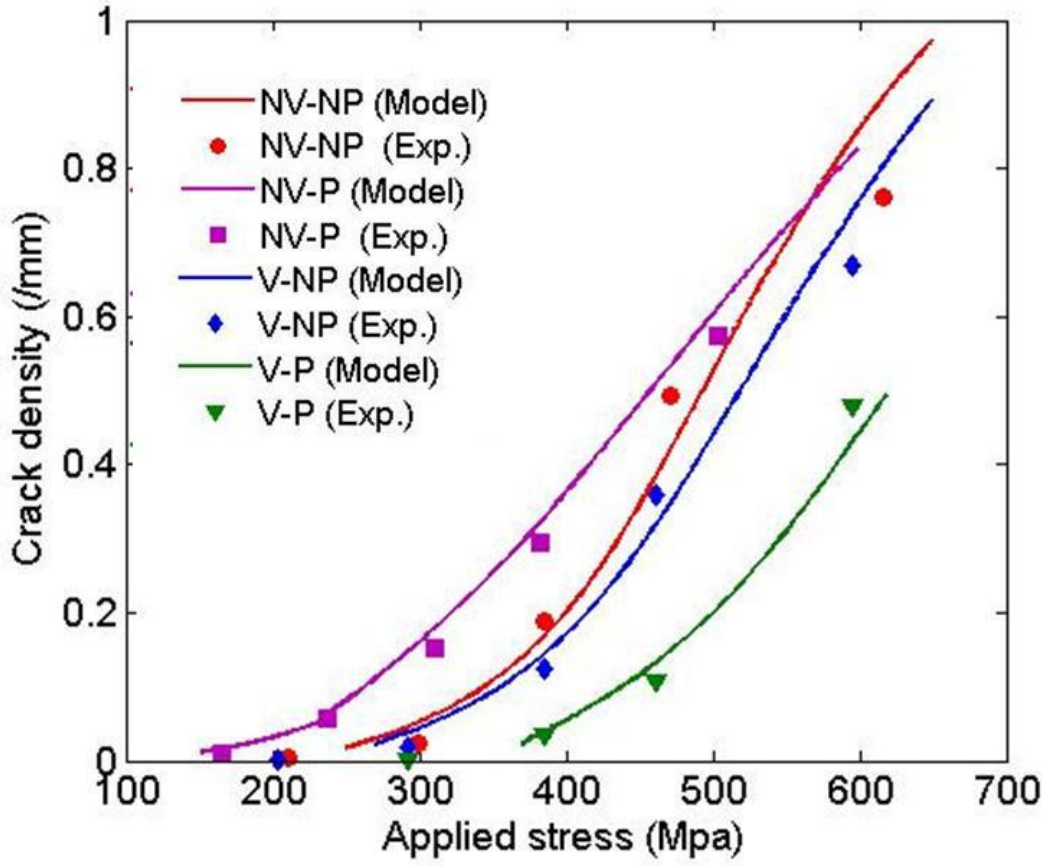

Fig. 4.6 Modeling prediction and experimental data for the crack density as a function of the applied stress (see Section 3.1 for the information on the experimental data).

To better validate the model, the distribution of the crack spacing from the simulation is compared against the experimental data. In Fig. 4.7, the distribution of crack spacing in the interactive regime is shown. For the non-interactive regime, the experimental data is well fitted by the exponential distribution (see Manders[40]). For the interactive regime, the distribution of crack spacing deviates from the exponential distribution with higher fraction for large blocks. This is because that the stress perturbation from preexisting cracks prohibits the formation of new cracks in shorter blocks. As fig. 4.7 shows, the

simulated distribution agrees well with the experimental data, which can be taken as the evidence that the statistical model correctly simulates the stochastic process of the cracking evolution in the interactive regime.

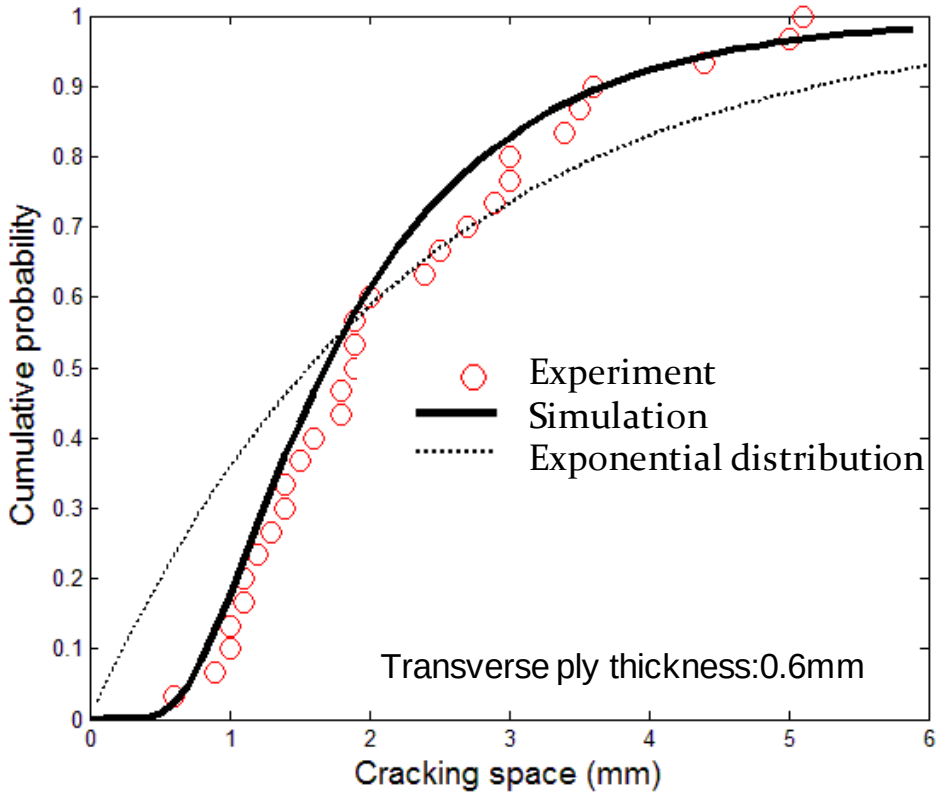

Fig. 4.7 Probability distribution of crack spacing

According to the Weibull parameters estimated by the experimental crack density data, the statistical distribution of the static transverse strength for different plates can be obtained (see Fig. 4.8). From Fig. 4.8, plate 4 (V_P) manufactured by the standard process possesses the best quality with its strength distributed in the higher range while

plate 1 (NV_NP), which is one largely deviated from the standard process, possess the worst quality with its strength distributed in the lower range. The strength distribution for Plate 2 (NV_P) and Plate 3 (V_NP) fall in between the two extreme cases.

Fig. 4.8 (a) gives the overall strength distribution. But it is noteworthy that only the lower range of the strength distribution is accurate. This is rooted in the nature of the Weibull distribution as a weakest-link model. The experimental data of crack density used to calibrate the Weibull distribution of strength only includes the information of the weakest elements of the 90^{o} layer. Logically, the strength of elements can only be measured if they fail under certain stress level. For elements with higher strength do not fail during the cracking evolution, there is no way to know the exact strength. The calculated strength distribution in the higher range is merely mathematical result enforced by the specific formula of the Weibull function. The strength distribution in the lower range is taken from Fig. 4.8(a) and shown in Fig. 4.8 (b), which is the useful information on the manufacturing quality affecting the cracking evolution. As Fig. 4.8(b) shows, plate 1 (V_P) has lowest fraction in the lower strength range, which means it has least defects thanks to the best controlled process.

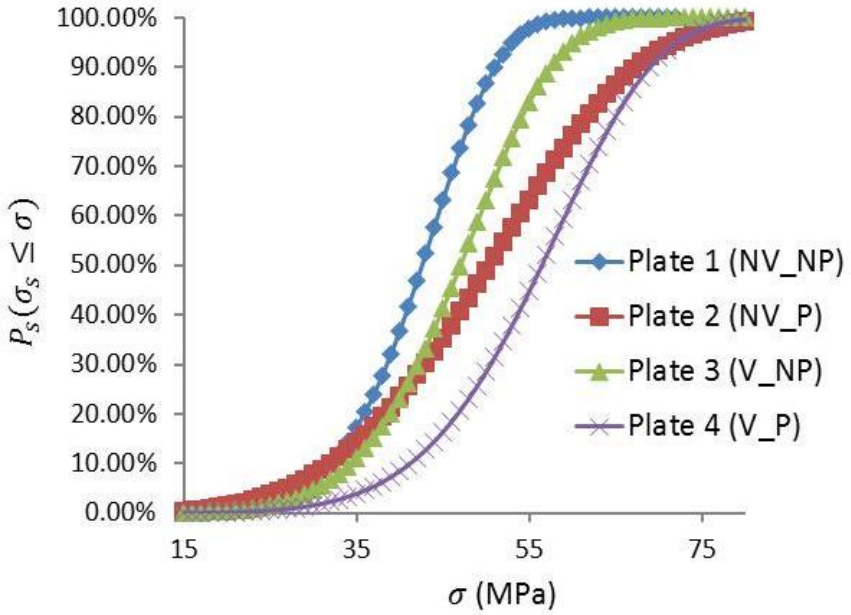

(a)

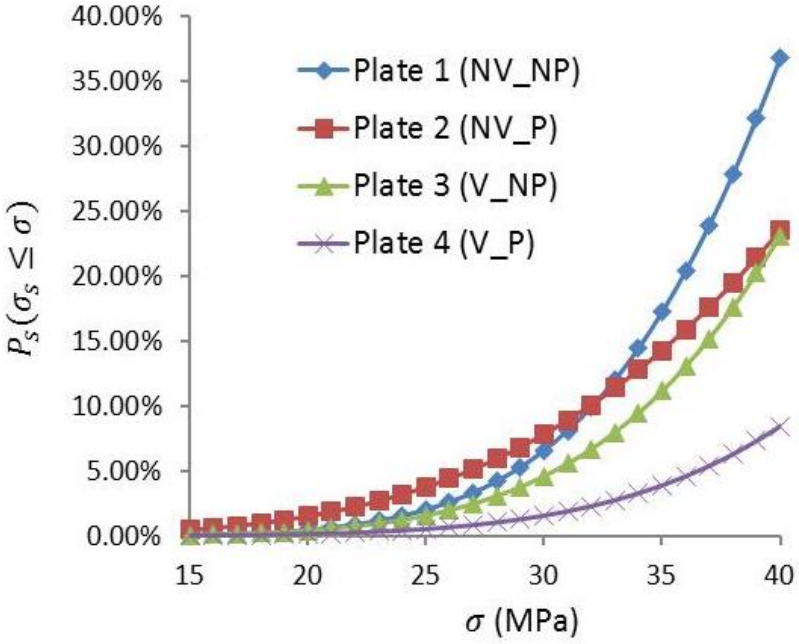

(b)

Fig. 4.8 The statistical distribution of static transverse strength of four plates manufactured by different processes. (a) full range, (b) lower range of the distribution.

It is very interesting to see plate 2 (NV_P) instead of plate 1 (NV_NP) has highest fraction in the lower strength range, i.e. $P_s(\sigma_s \leq 30Mpa)$. One explanation is that, in plate 2 (NV_P) under the manufacturing condition with only pressure applied during the curing process, the gas gather together driven by the applied pressure. Lacking of vacuum system, the gathered gas form large voids and largely reduced the local strength. In plate 1 (NV_NP), though it cannot be removed due to the lack of vacuum system, the gas will not gather to form large voids because there is no applied pressure. Instead, the gas forms many small voids to reduce the strength distribution of the plate moderately but more extensively. This has been supported by the higher fraction of relatively low strength (around 35MPa) for plate 1 (NV_NP).

The statistical distribution of static transverse strength obtained from the crack density data through the developed model offers a power tool to assess the manufacturing quality. As the above analysis demonstrates, it quantifies the manufacturing quality in a deliberate way. Unlike the statistical strength of unidirectional laminate which only has the information on the weakest element, the statistical strength of static transverse strength obtained from multiple cracks offers much more information on the distributed material property. This is very important for studying the damage evolution in composites, of which distributed damage entities instead of a single dominating crack are of interest. In Section 5, the application of such strength distribution will be shown in modeling the cracking evolution under fatigue loading.

4.3 Extension of the statistical model for multidirectional laminates

When apply the developed statistical model to the off-axis ply cracking evolution in multidirectional laminates, there are two major challenges. First of all, the in-plane shear stress plays a role in the cracking process as the experimental investigation indicates in Section 3.This has not been considered in the statistical model for cross ply laminate because no in-plane shear stress exists for that problem. Secondly, the analytical solution for the stress state of the cracked cross ply laminate cannot be extended to a general multidirectional laminates.

For the role played by the in-plane shear stress, some experimental observation such as the micro-cracks associated with the shear stress has been reported in Section 3.3. But for the statistical model of the cracking evolution which focuses on the multiplication of cracks, the mechanism on the micro-scale for the formation of a single crack under biaxial stress state is less interested. Generally, the additional shear stress will decrease the critical value for the transverse stress at failure. Like treatment that the constraint effect and the effect of defects are lumped into the static transverse strength, the effect of the in-plane shear stress can also be included by properly decreasing the static transverse strength. Therefore, the criterion for off-axis cracking is still given in the form of the static transverse strength. It should be emphasized that this treatment is for any given off-axis angle with fixed biaxial ratio. The purpose of doing so is to simply testify the application of the developed statistical model for multidirectional laminates. For the

second problem about the stress analysis of cracked laminates, it is solved by a finite element model.

4.3.1 FE model of cracked multidirectional laminates

3D finite element analysis of periodic structures saw wide success in micromechanical analysis of unidirectional fiber-reinforced composites[75],particle-reinforced composites[76], and textile composites[77]. Recently, this method has been introduced into damage analysis of composites. For example, Li et al. [6] constructed a 3D unit cell of cracked laminates to calculate the stiffness reduction as a function of the crack density. That model is capable of analyzing laminates with off-axis cracks along two arbitrary directions, e.g. $[0/\theta_1/\theta_2/0]_s$. A similar FE model developed to study the stress state in the cracked off-axis laminates is briefly described here.

Firstly, a grid system is introduced to divide the cracked laminates into unit cells. As Fig.4.9 (a) shows, two groups of gridlines are set along the ply cracks in two off-axis layers, i.e. θ_1 and θ_2. The gridlines in each group are spaced at the crack spacing of the corresponding array of cracks, i.e. a_1 and a_2. This configuration is consistent with the experimental observation in Fig.4.9 (b). As Fig.4.9 (a) shows, all patches created by the grid system are identical to each other. Taking any patch as the master cell, one can reproduce the rest by translational transformation, and therefore, to form the whole plane of the laminates. Fig.4.10 shows the 3D view of one single unit cell as the master cell.

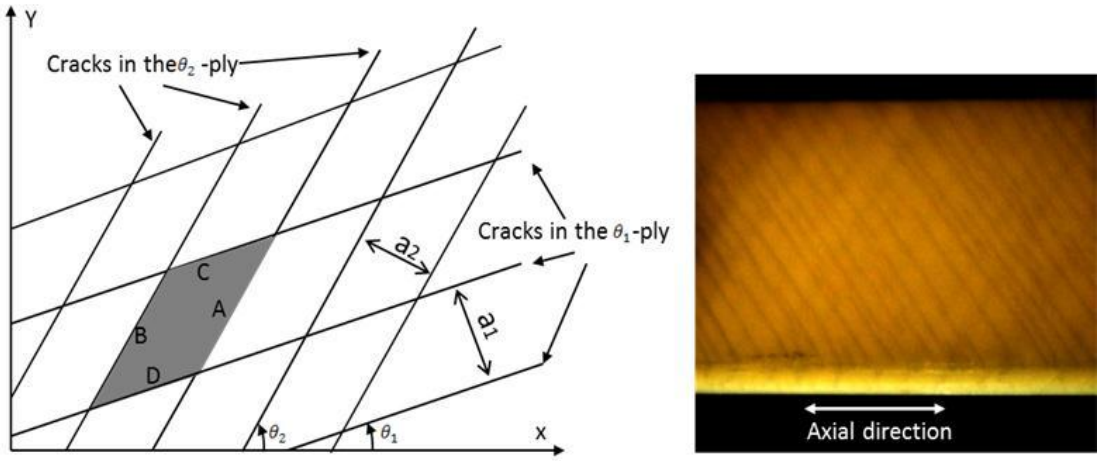

(a) (b)

Fig. 4.9 Cracked multidirectional laminates a) A planner view of a cracked laminate with cells tessellated by the grid system b) Top view of two arrays of off-axis ply cracks observed in $[0/60_2/-60_2/0]_s$ laminates

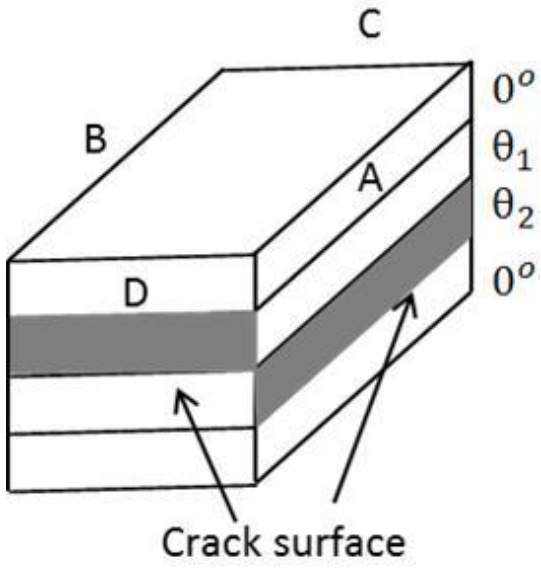

Fig.4.10 The 3D view of one unit cell

To replace the cells surrounding the master cell, periodic boundary conditions have to be applied by constraining paired nodes in the FE model. In Fig. 4.10, the paired node (x', y', z') on Face B and C corresponding to any point (x, y, z) on Face A and C, respectively, is defined as:

$$x' = x + a_1 cos\theta_1 + a_2 cos\theta_2 \quad (4.11.a)$$

$$y' = y + a_1 sin\theta_1 + a_2 sin\theta_2 \quad (4.11.b)$$

$$z' = z \quad (4.11.c)$$

For laminates subjected to a macroscopically uniform strain field under in-plane loading, the displacements of the paired nodes must satisfy the constraining equations;

$$u' - u = (x' - x)\varepsilon_x^0 + (y' - y)\gamma_{xy}^0 \quad (4.12.a)$$

$$v' - v = (y' - y)\varepsilon_y^0 \quad (4.12.b)$$

$$w' - w = 0 \quad (4.12.c)$$

where $(\varepsilon_x^0,\ \varepsilon_y^0, \gamma_{xy}^0)$ is the macroscopically uniform strain field, which can be taken as the direct input as loading in the FE model, or be replaced by the equivalent macroscopic stress.

All paired nodes are constrained following Eq. (4.12) expect the nodes on crack surfaces, which will be left unconstrained as free surface. To restrict rigid body translation, the node at one corner is fixed. For more details on constructing such unit cell with periodic boundary condition, one can refer to [52, 78].

Based on the developed unit cell, the FE simulation is performed using ABAQUS®. Unlike the analytical solution used for cross ply laminate, the stress variation through the ply thickness exists for the FE results. The stress on the mid-plane of the off-axis plies is output as the local transverse stress $\sigma_{i,j}^{(n)}$, to calculate the probability of the local failure according to Eq. (4.5) at each step. A python script is developed to automatically calculate the stress state for the different crack spacing L_i. Once the stress is known, the rest of the procedures are the same as Section 4.2 describes for cross ply laminate though the physical meaning of the static transverse strength for the off-axis ply is slightly different from that of the 90^o ply because it now includes the effect of the in-plane shear stress on cracking. Again, the effect of the non-uniform distribution of cracks on the stress state of the cracked laminates is neglected as other statistical models reported in literature [17, 56].

4.3.2 Results

The cracking evolution under static loading in -60^o plies of glass/epoxy $[0/+60_2/0/-60_2]s$ laminates is measured (See Fig. 4.13 for the experimental crack density data). To simulate the cracking evolution, the stress state of cracked laminates is firstly obtained from the abovementioned FE model. A Python script is developed to automatically run the FE simulation for all possible cases with varied crack spacing. It is noteworthy that, if the external loading is given as applied strain, the cracks in $+60^o$ ply do not affect the stress state in -60^o ply because of the much stiffer 0^0 ply, which separates these two off-axis plies. This has been validated by the FE model and used to simplify the stress

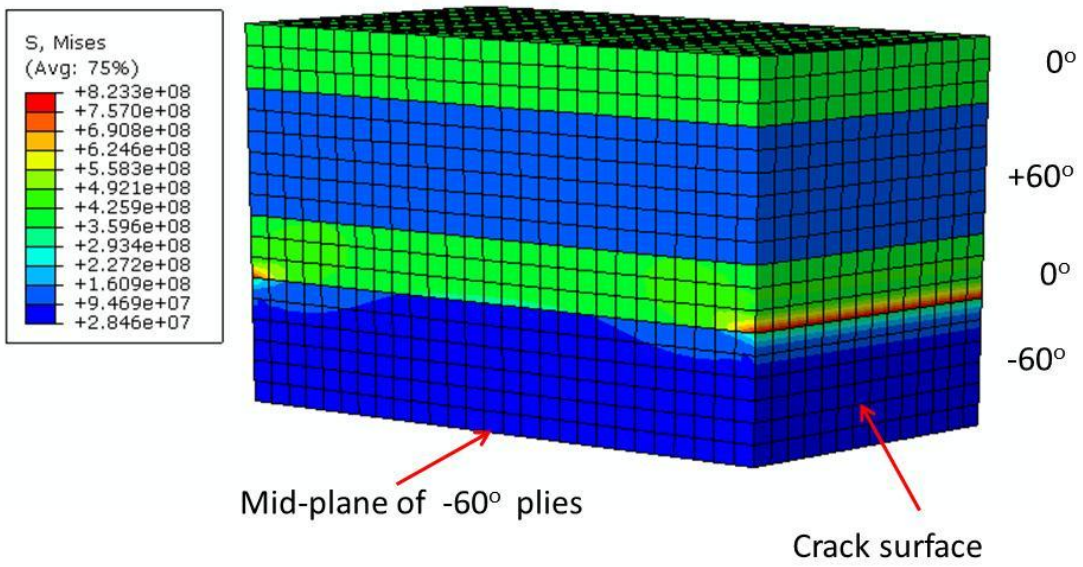

(a)

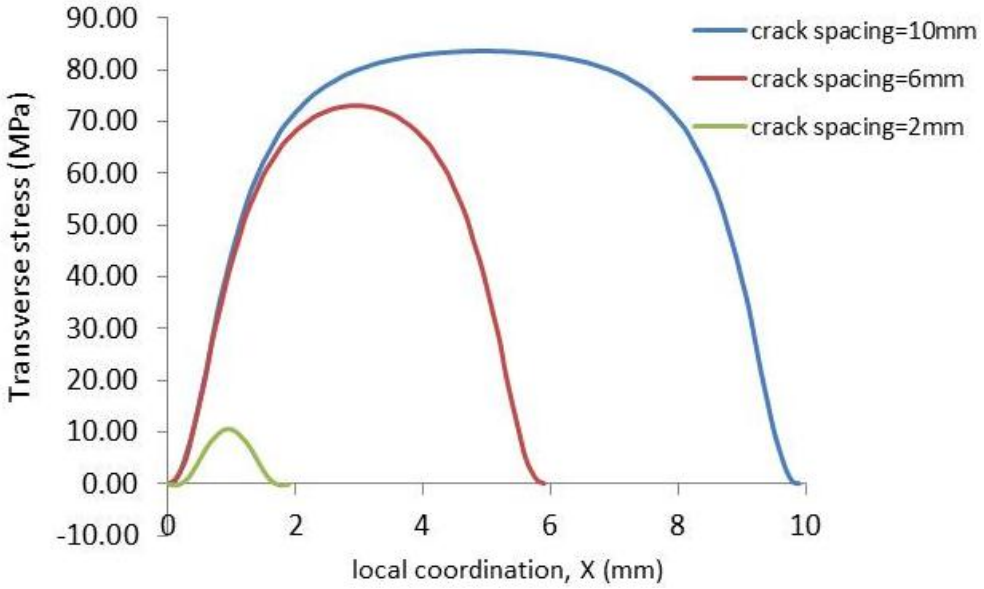

(b)

Fig. 4.11 Stress state of cracked laminates $[0/+60_2/0/-60_2]s$ laminates with cracks in -60^o plies. (a) stress contour plot. Half of the unit cell is simulated due to the symmetry. (b) the transverse stress distribution between cracks at different crack spacings. X direction is the axial direction shown in Fig. 4.9. The stress output from FE model is along X direction on the mid-plane shown in Fig. 2.11.

analysis. Fig. 4.11 shows the stress state of the laminates with cracks in -60^o ply from the FE model.

The predicted cracking evolution in -60^o plies is plot in Fig. 4.12, showing good agreement with the experimental data. The two Weibull parameters are estimated in the statistical model through the experimental crack density data. The corresponding Weibull distribution of the static strength is shown in Fig. 4.13. As the property of the constrained plies, these two parameters will be used for simulating the cracking evolution under fatigue loading in next section.

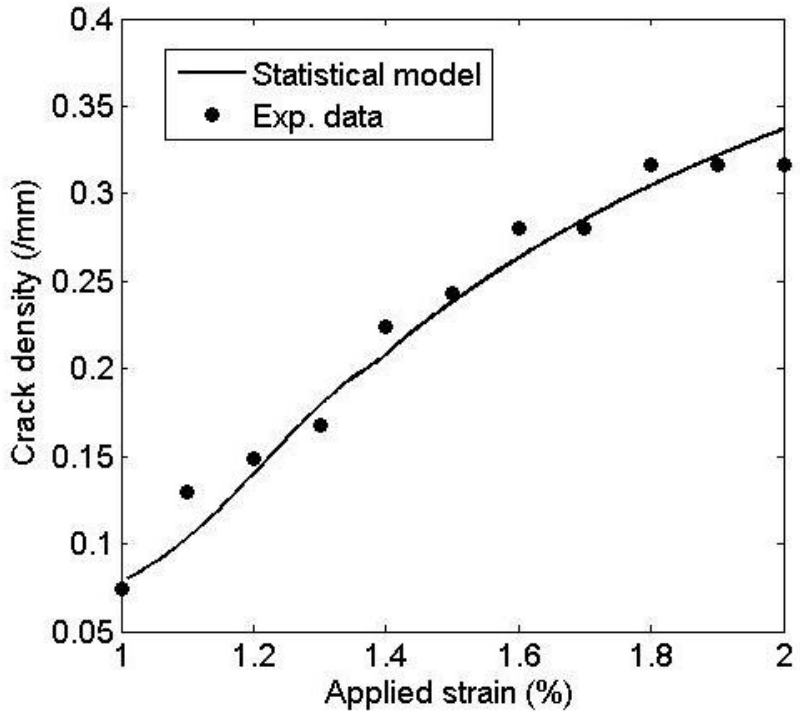

Fig. 4. 12 The cracking evolution in -60^o plies under static tension.

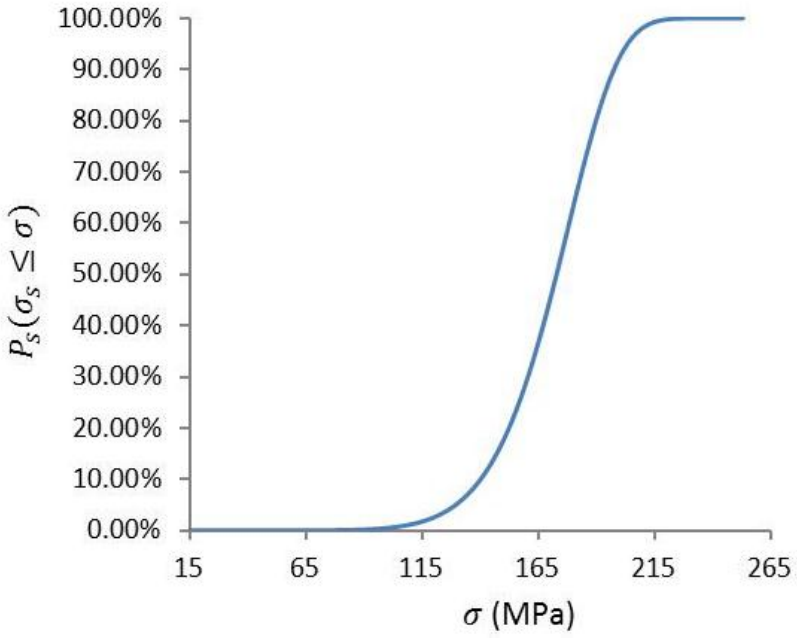

Fig. 4.13 Weibull distribution of static transverse strength.

5. STOCHASTIC CRACKING EVOLUTION IN LAMINATES UNDER FATIGUE LOADING

5.1 Introduction

The statistical model of the cracking evolution under fatigue loading is extended from the developed model for static loading reported in Section 4. The connection between static and fatigue loading is made through the strength-life equal rank assumption [79]. This widely used assumption states that for a given specimen its rank in static strength is equal to its rank in fatigue life. This assumption is applied to the discrete element in the statistical model to map the Weibull distribution of static transverse strength of each element to a statistical distribution of fatigue life.

Fatigue failure models of composite laminates can be classified in three categories [80]; (1) empirical models which simply utilize S-N curves, (2) phenomenological models based on the residual strength/stiffness, and (3) mechanistic models based on the progressive damage evolution. Due to the complexity of the fatigue failure of composite laminates, the empirical models generally are undesirable.. They usually require extensive testing for reliable prediction for composite materials. However, for the matrix cracking in off-axis plies, the failure process under fatigue tension is relatively simple. Although the multiple cracks form in off-axis plies during the fatigue loading, the formation of each single crack under fatigue loading is similar to the failure process in homogenous materials, which is just the initiation and propagation of a single crack.

Therefore, the formation of each crack during the stochastic cracking evolution is modeled in an empirical way in the statistical model.

5.2 Modeling of cracking evolution in laminates under fatigue loading

5.2.1 The probability of failure for a given fatigue loading history

Still discretizing the off-axis plies into elements as Section 4.1 describes, and recall the Weibull distribution of the static transverse strength that is followed by all elements independently and identically:

$$P_s(\sigma_s \leq \sigma) = 1 - \exp\left(-(\frac{\sigma}{\sigma_0})^m\right) \tag{5.1}$$

A fatigue function which is an approximation of the S-N curve (see Fig. 5.1) is usually used to correlate the fatigue strength with the static strength in an empirical way. According to Charewicz and Daniel[81], the S-N curve for 90^o lamina under transverse tension can be approximated by the following fatigue function:

$$\sigma^u = \sigma_s N_f^a \quad \text{for } \sigma^u > \sigma_{f.l.} \tag{5.2}$$

where N_f is the cycles to failure under fatigue stress σ^u, and a is the fatigue parameter controlling the slope of the simulated S-N curve. Eq.(5.2) is also applicable to the S-N curves for unidirectional laminate loaded along off-axis direction[72]. $\sigma_{f.l.}$ is the fatigue limit. If the fatigue stress is below the fatigue limit, no fatigue failure can occur. It is noteworthy that the static strength σ_s is not a deterministic value. Instead, it follows the Weibull distribution. Accordingly, N_f has certain statistical distribution.

Due to the perturbation on the local stress from cracks, elements may undergo varied fatigue stress levels even if the external fatigue loading remains unchanged. For this multi-stage fatigue, the number of cycles to failure is difficult to obtain from Eq. (5.2) because the maximum stress σ^u cannot be not changed. A damage parameter D is therefore introduced , and Miller's rule[82] is adopted as the simplest damage accumulation model:

$$D = \sum \frac{n_i}{N_f^i(\sigma_i^u)} \tag{5.3}$$

where D is the damage parameter, σ_i^u is the local fatigue stress at stage i, $N_f^i(\sigma_i^u)$ is the failure cycles as a function of the fatigue stress, and n_i is the number of cycles at stage i. The cracking occurs under the multi-stage fatigue when D=1, and the corresponding failure cycles is the summation of cycles at every fatigue state, i.e. $\sum n_i$.

Since the damage parameter D is eventually dependent on σ_s, D follows certain statistical distribution, which can be obtained from Eq.(5.1-5.3):

$$\mathrm{P_D(D)} = \mathrm{Exp}\left(-\left(\frac{\mathrm{D^a}}{\sigma_0\left(\sum\frac{\mathrm{n_i}}{(\sigma_i^u)^{1/a}}\right)^{\mathrm{a}}}\right)^{\mathrm{m}}\right) \tag{5.4}$$

To get Eq. (4), the strength-life equal rank assumption is applied.

The failure probability under the fatigue loading equals to the probability for D≥1:

$$\mathrm{P_D(D \geq 1)} = 1 - \mathrm{Exp}\left(-\left(\frac{1}{\sigma_0\left(\sum_{\mathrm{i}}\frac{\mathrm{n_i}}{(\sigma_i^u)^{1/a}}\right)^{\mathrm{a}}}\right)^{\mathrm{m}}\right) \tag{5.5}$$

If we define a parameter representing the fatigue loading history as:

$$H = \sum \frac{n_i}{(\sigma_i^u/\sigma_0)^{1/a}} \tag{5.6}$$

Then Eq. (5.5) becomes:

$$P_D(D \geq 1) = 1 - \text{Exp}(-H^{am}) \tag{5.7}$$

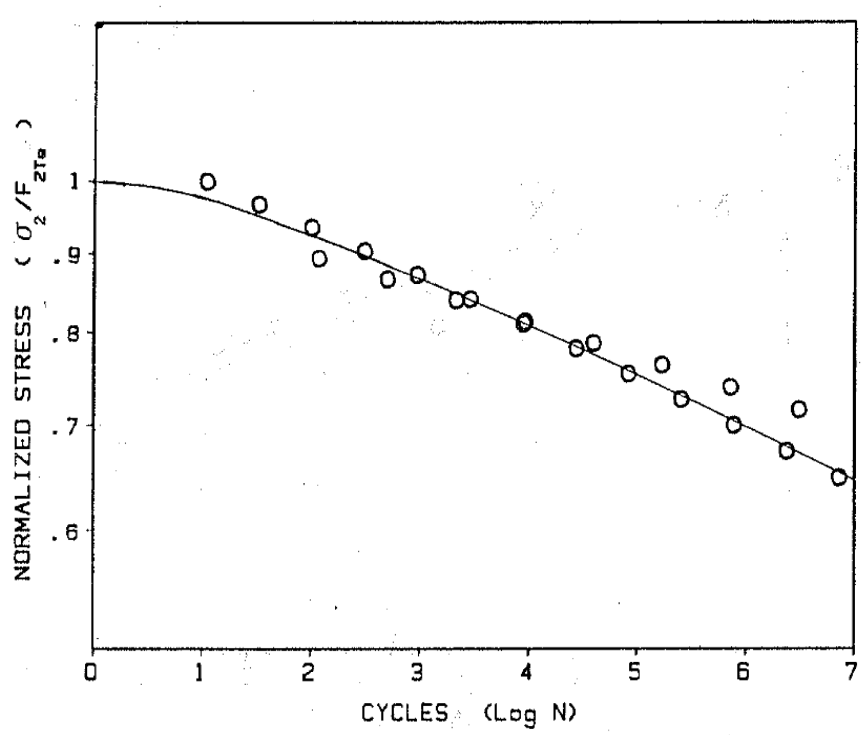

Fig. 5.1 The S-N curve of carbon/epoxy 90^o lamina. The stress is normalized by the static strength[83].

Eq. (5.7.a) which is analogous to Eq. (5.1) for the case of static loading yields the probability of failure for a given fatigue loading history. With Eq. (5.7) replacing Eq.(5.1), the procedures for simulating the cracking evolution under fatigue loading are quite similar to those for static loading described in Section 4.1. The non-interactive and interactive regimes are modeled separately.

5.2.2 Non-interactive regime

In non-interactive regime, which is the initial stage of cracking evolution, the stress perturbation by preexisting cracks is highly localized and therefore can be neglected. The local stress σ_i^u can be assumed to be the constant ply stress in uncracked laminates. Still assuming that each element with its length as l_0 can only accommodate one crack, we can obtain the crack density at cycle N from Eq. (5.7):

$$\rho = \frac{1}{l_0} * (1 - Exp\left(-\left(\frac{\sigma_{xx}}{\sigma_0 N^a}\right)^m\right) \tag{5.8}$$

where σ_{xx} is the constant transverse stress in uncracked off-axis plies. The distribution of crack space L due to the random formation of cracks is:

$$P_L(L \leq L') = 1 - exp(-\rho L') \tag{5.9}$$

5.2.3 Interactive regime

A numerical iterative is developed to model the process of multiplication of cracks. Since the increase rate of crack density $\frac{d\rho}{dN}$ varies greatly over the whole fatigue life ($\approx 10^6$ cycles), an adaptive increment for the number of cycles ΔN at each step must be used. At the stage of fast increase for crack density, ΔN can be as small as 1 to correctly capture the process while it needs to be increased to ~10^4 during the last stage for more efficient computation without compromising the accuracy.

Instead of directly counting the cracks over certain gauge length to calculate the crack density, the distribution of block length which is the crack spacing between two

neighboring cracks is monitored. The initial $P_L^{(0)}$ at step 0 for the interactive regime is given by Eq. (5.9) at the end of the non-interactive regime. For numerical computation, it has to be discretized as:

$$P_{L_i}^{(0)} = \begin{cases} P_L(L_i) - P_L(L_{i-1}) & i = 1,2,\dots,Nc-1 \\ 1 - P_L(L_{i-1}) & i = Nc \end{cases} \tag{5.10}$$

where $L_i = \mathrm{i} * \mathrm{l}_0$, and Nc should be large enough so that $P_L(L_{\mathrm{Nc}})$ is close to 1 according to Eq. (5.9). At step n, $P_{L_i}^{(n)}$ is the percentage for blocks with the length as L_{i} among all blocks.

From step n to step n+1, the cracking evolution could be tracked by examining the probability of forming new cracks in all blocks. The element at x_j within the block L_i is denoted as $x_{i,j}$.The maximum transverse stress for element $x_{i,j}$ corresponding to external fatigue loading is denoted as $\sigma_{i,j}$, which is obtained from Hashin's variational approach for cross ply laminate, and from the FE model for multidirectional laminates. For the details of the stress analysis of cracked laminates, see Section 4.

With local stress $\sigma_{i,j}$, the local loading history parameter $H_{i,j}$ can be calculated. If $\mathrm{H}_{\mathrm{i,j}}^{(\mathrm{n})}$ has been given from previous iteration, and from step n to step n+1, the increment for the number of cycles is ΔN. According to Eq. (5.6), the loading history parameter increases to:

$$H_{i,j} = H_{i,j}^{(n-1)} + \frac{\Delta N}{(\sigma_{i,j}/\sigma_0)^{1/a}} \tag{5.11}$$

Due to the increment of the loading history, elements surviving until step n could fail at step n+1, and the probability of failure at step n+1 is:

$$\lambda_{\mathrm{ij}}^{(\mathrm{n+1})} = \frac{P\left(D<1, H=H_{i,j}^{n}\right) - P\left(D<1, H=H_{i,j}\right)}{P\left(D<1, H=H_{i,j}^{n}\right)} \tag{5.12}$$

If no element fails from step n to step n+1, then the block L_{i} survives. Among all blocks with the length as L_{i}, the percentage of the surviving ones is:

$$P0_{L_i}^{(n+1)} = P_{L_i}^{(n)} * \prod_{j=1}^{i}\left(1-\lambda_{\mathrm{ij}}^{(\mathrm{n+1})}\right) \tag{5.13}$$

If only one element $\mathrm{x_{i,j}}$ fails from step n to step n+1, then block L_{i} divides into two smaller blocks with their lengths as $(j-1)l_0$ and $(i-j)l_0$. The probability is:

$$P1_{x_{i,j}}^{(n+1)} = P_{L_i}^{(n)} * \frac{\lambda_{\mathrm{ij}}^{(\mathrm{n+1})}}{1-\lambda_{\mathrm{ij}}^{(\mathrm{n+1})}} * \prod_{j=1}^{i}\left(1-\lambda_{\mathrm{ij}}^{(\mathrm{n+1})}\right) \tag{5.14}$$

If the increment ΔN is controlled carefully so that no more than one crack could form within any block, then all possibilities for the cracking evolution from step n to step n+1 have been examined by applying Eq.(5.13) and (5.14) to all blocks L_i ($\mathrm{i} = 1,2 \ldots, \mathrm{Nc}$). By adding the percentage of the long blocks, which divides into two small blocks, to the percentage of the corresponding small blocks, the probability distribution of block length could be updated at step n+1:

$$P_{L_i}^{(n+1)} = P_{L_i}^{(n)} P0_{L_i}^{(n+1)} + \sum_{k=i+1}^{N} 2\, P_{L_i}^{(n)} P1_{k,i+1}^{(n+1)} \tag{5.15}$$

where the first part of the right side is corresponding to the percentage of the blocks surviving from the additional loading, and the second part is corresponding to the percentage of those short blocks forming from the process that long blocks are divided by new cracks. Since one long blocks will generate two short blocks, there is a factor 2

in the second part. It will cause the sum of $P_{L_i}^{(n)}$ not remained as 100%. Therefore, $P_{L_i}^{(n+!)}$ has to be normalized. Once the distribution of the block length is updated at step n+1, the crack density can be easily calculated:

$$\rho^{(n+1)} = \frac{1}{\sum_{i=1}^{N} L_i * P_{L_i}^{(n+1)}} \tag{5.16}$$

It should be noted that n is the step number of the numerical iteration, rather than the number of cycles. But they are related by:

$$N = N_0 + \sum_i^n \Delta N_i \tag{5.17}$$

where N_0 is the number of cycles at the end of the non-interactive regime, and ΔN_i is the adaptive increment at each step of the iteration. Combined with Eq. (5.17), Eq. (5.16) finally gives the numerical solution of the crack density as a function of the number of cycles for the interactive regime.

The iterative at step n+1 starts with the information from step n: the probability distribution of block length $P_{L_i}^{(n)}$ and the local loading history parameter for each element, $H_{i,j}^{(n)}$. $P_{L_i}^{(n)}$ has been updated) to $P_{L_i}^{(n+1)}$ through Eq. (4.16) . To continue the iterative, $H_{i,j}^{(n)}$ also has to be updated to $H_{i,j}^{(n+1)}$.

For the elements with same location as x_{ij} at step n+1, they may have undergone different loading histories. As Fig. 5.2 shows, they may be directly from the block L_i, which survives from step n to step n+1, or from the longer ones divided by the new cracks at step n+1. Although all of them share same local stress and therefore the same

loading history after step n+1, their previous loading history are usually different. Elements from longer blocks should have the larger loading history parameter. At successive step from n+1, they would have different failure rates because of the different loading history as Eq. (5.11) and (5.12) indicate.

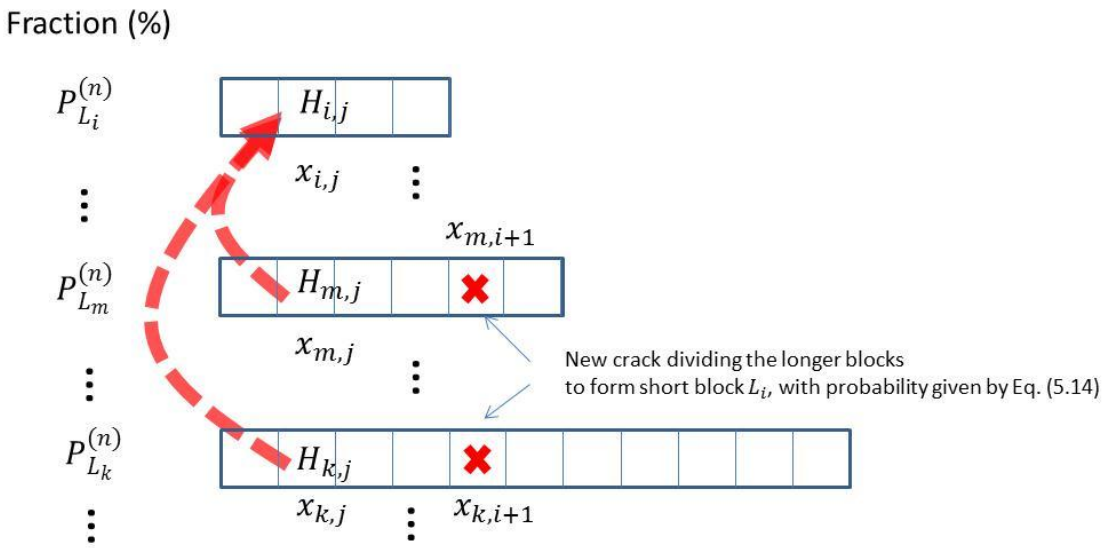

Fig. 5.2 Elements with different loading history merge together

Let us denote η_k as the fraction of elements with certain loading history parameter H_k among all elements at x_{ij} at the end of step n+1. Similar to the procedures from n to n+1, the failure rate at x_{ij} from step n+1 to step n+2 is:

$$\lambda_{i,j} = \sum_k \eta_k \frac{P(D<1,H=H_k)-P(D<1,H=H_k+\Delta H)}{P(D<1,H=H_k)} \tag{5.18}$$

where

$$\Delta H = \frac{\Delta N}{(\sigma_{i,j}/\sigma_0)^{1/a}} \tag{5.19}$$

is the increment of the loading history parameter corresponding to ΔN from step n+1 to step n+2.

It would be very difficult, if not impossible, to implement Eq. (5.18) into the numerical iteration. At each step, there are so many possibilities for H_k, and the accumulation of those possibilities keeps increasing as the iteration goes on. An alternative way is to find certain average value for the load history parameters, $H_{i,j}^{(n+1)}$, so that from step n+1 to step n+2, the following formula could be satisfied:

$$\lambda_{i,j} = \sum_k \eta_k \frac{P(D<1,H=H_k)-P(D<1,H=H_k+\Delta H)}{P(D<1,H=H_k)} = \frac{P\left(D<1,H=H_{i,j}^{(n+1)}\right)-P\left(D<1,H=H_{i,j}^{(n+1)}+\Delta H\right)}{P\left(D<1,H=H_{i,j}^{(n+1)}\right)} \quad (5.20)$$

It can be shown that $H_{i,j}^{(n+1)}$ that can satisfy Eq. (5.20) may be approximated as:

$$H_{i,j}^{(n+1)} = \left(\sum_{k=0}^{Nc-i} \eta_k \, H_k^{-(am+1)}\right)^{-1/(am+1)} \quad (5.21)$$

With the updated $H_{i,j}^{(n+1)}$ together with $P_{L_i}^{(n+1)}$ from Eq. (5.15), the iteration is completed.

5.3 Results and discussion

5.3.1 Cross ply laminate

The experimental study on the cracking evolution in carbon/epoxy cross ply laminate under fatigue tension along 0^o direction was reported by Charewica and Daniel[81]. The reported crack density data in the 90^o layer after the first cycle of loading under different maximum stress levels is equivalent to the crack density data obtained from the static tensile test. Therefore, those data are used to estimate the Weibull parameters for the

static strength distribution through the statistical model as Section 4 describes. Based on the estimated Weibull parameters, the prediction of the crack density after the first cycle of loading under different fatigue stress levels is shown in Fig. 5.3.

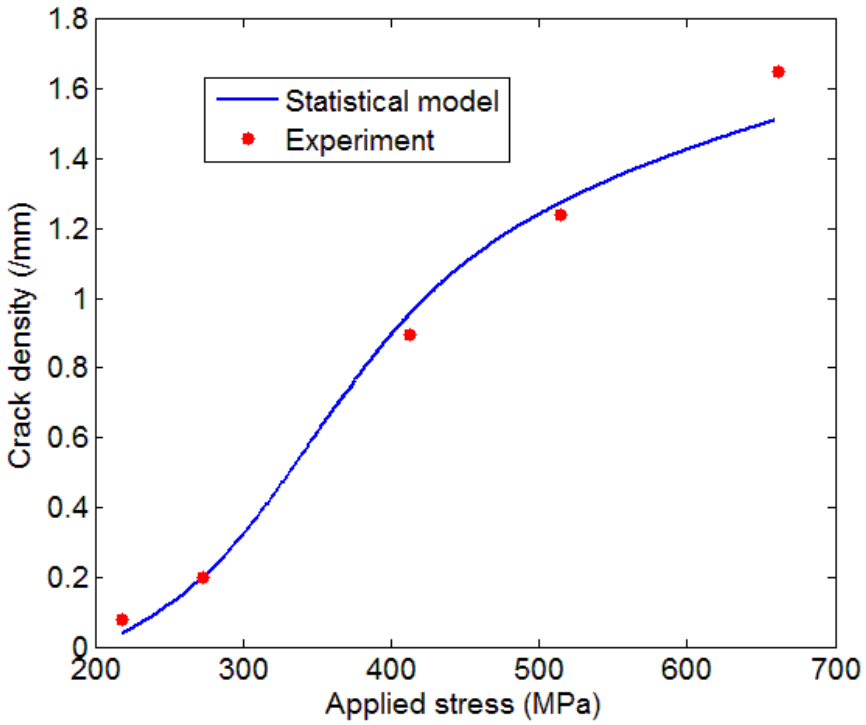

Fig. 5.3 The cracking evolution in [0/90]s laminate. The simulation is based on Weibull parameters estimated by the plotted experimental data ($\sigma_0 = 95MPa, m = 6.3$).

The two parameters, the fatigue parameter a and the fatigue limit$\sigma_{f.l.}$ in Eq. (5.2), are estimated by the experimental crack density data under one of the fatigue stress levels. Fig. 5.4 shows the crack density evolution under fatigue tension with maximum stress varying from 218 MPa to 412MPa. The experimental crack density data obtained under the fatigue tension (σ_x^{max}=412MPa) is used to estimate the two parameters through the statistical model described in Section 5.1. The same fatigue parameters are used in the

statistical model to predict the cracking evolution under other fatigue stress levels. As Fig. 5.4 shows, the prediction agrees well with the experimental data.

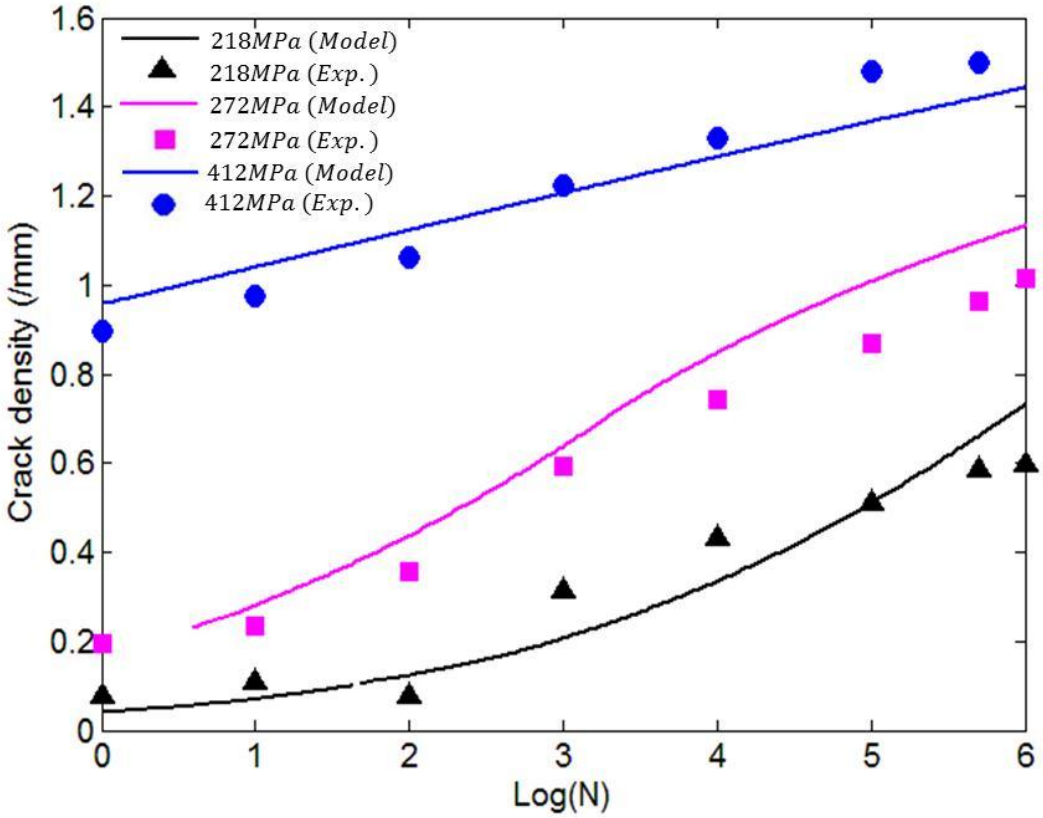

Fig. 5.4 Crack density as a function of the number of cycles.

5.3.2.Multidirectional laminates

The cracking evolution in the -60^{o} plies of glass/epoxy [*[0/+60$_2$/0/-60$_2$]s* laminates under axial fatigue tension was measured by Vivian and reported in his thesis[84]. The same specimens were obtained from Vivian for static testing, which were conducted by the author. The cracking evolution in the -60^{o} plies under static tension is presented in

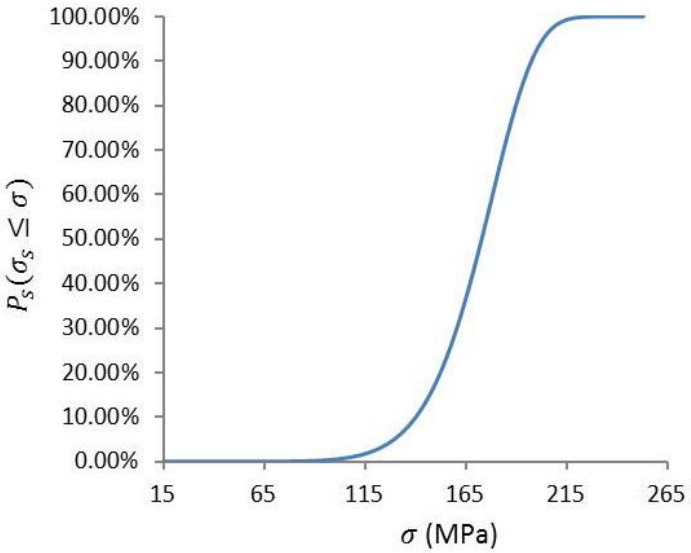

Fig. 5.5 The Weibull distribution of static strength of the -60^o plies. Two Weibull parameters: $\sigma_0 = 180MPa, m = 9$.

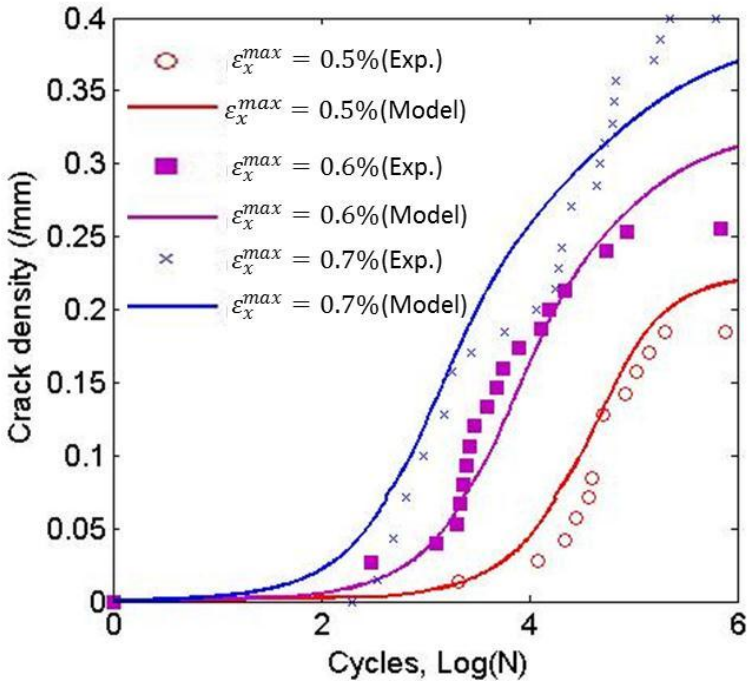

Fig. 5.6 The cracking evolution in [0/+60$_2$/0/-60$_2$]s laminates. The applied maximum strain varies from 0.5% to 0.7%. Experimental data is cited from[84]. The parameters used in the model: a=-0.09, $\sigma_{f.l.} = 40MPa$.

Section 4.2, from which the Weibull distribution of static strength (see Fig. 5.5) of the -60^o plies is estimated and used in the statistical model for fatigue case. Fig. 5.6 shows the simulation results for the stochastic cracking evolution in the -60^o plies under fatigue axial tension. The maximum applied strain varies from 0.5% to 0.7%. The parameter a and fatigue limit $\sigma_{f.l.}$ are estimated by fitting the experimental data. From Fig. 5.6, it can be seen that the simulation results agree well with the experimental data. Generally, three stages can be observed from the crack density data. The crack density increases from zero after certain cycles at a modest rate, followed by a fast increase. Finally, the cracking evolution ceases after certain cycles and the maximum crack density is obtained. In the statistical model using same parameters, these three stages of the cracking evolution are captured for different fatigue loading levels.

It is found that the fatigue limit $\sigma_{f.l.}$ has to be applied in the model otherwise the predicted crack density would keep increasing without seeing the cease of the cracking evolution. However, Fig. 5.1 shows no fatigue limit existed for the unconstrained 90^o lamina even if under extremely high cycles, i.e. 10^7 cycles. This is another difference in the cracking process of unconstrained and constrained plies. For the stand-alone 90^o plies, the fatigue failure is controlled by the weakest element that possesses the severest defect. Such a defect can be invoked as the nucleation of a crack even if the fatigue loading is extremely low. Therefore, no obvious fatigue limit can be observed from the S-N curve. For constrained plies, the weakest elements already fail at the first stage of the cracking evolution. The survived elements without severe defects would possess a

non-zero fatigue limit. Once the local stress is lower than fatigue limit because of the perturbation of cracks, the new crack cannot form, and therefore the cracking evolution ceases.

6. CONCLUSIONS AND FUTURE WORK

The experimental investigations and theoretical studies on the stochastic matrix cracking evolution in composite laminates with defects have been carried out. The presented study demonstrates the proposed modeling strategy that accounts for the statistically distributed defects in damage mechanics models for the evaluation of materials response. The experimental investigations identify the important mechanisms for the cracking evolution in composites with defects. Based on the experimental observations, the statistical model of the matrix cracking evolution is developed. In the statistical model, the influence of the distributed defects is characterized by the statistical distribution of the static strength. Based on such a statistical distribution, the statistical process for the cracking evolution is simulated. For different loading conditions, i.e. the static and fatigue loading, the modeling is unified through the strength-life equal rank assumption. The experimental investigations find that, the defects introduced by the manufacturing processes have detrimental effect on the integrity of composite laminates. The specimens with more defects possess severer damage state, i.e. higher crack density, under the same external loading condition. The non-uniform distribution of cracks measured under the optical microscopy verifies the stochastic nature of the matrix cracking evolution. Closer microscopic observations provide evidences showing that the stochastic cracking evolution is caused by the distributed defects. Also, the in-plane shear stress, which is caused by either the external loading or the intrinsic anisotropy of multidirectional laminates, enhances the matrix cracking process under the transverse tensile stress. Such effect becomes more significant for fatigue. The microscopic observations suggest that

the in-plane shear stress induces inclined microcracks, which enhance the initiation and propagation of the major matrix crack.

The statistical model of the matrix cracking evolution yields the predictions of the crack density and the statistical distribution of the crack spacing. The predictions agree well with the experimental data for both the static and fatigue loading. The statistical model deepens the understanding of the stochastic process for the multiplication of cracks. The different stages for the cracking evolution are better simulated compared to deterministic models, especially for the initial stage dominated by the effect of defects. It also provides an efficient way to evaluate the manufacturing quality of composite laminates through the Weibull distribution of the static strength. By taking the information of the multiple cracks in constrained plies, the statistical model is able to estimate the Weibull distribution of the static strength in a more reliable way compared to some traditional approaches. For low-cost composites with many defects, the statistical distribution of materials properties is very important for assessing the reliability of the structures.

As discussed in Section 2.2, the stochastic matrix cracking evolution is a multiscale problem. The presented experimental study investigates the development of a single crack on a micro-scale and the multiplication of cracks on a macro-scale. But the statistical model focuses on the multiplication of cracks on the macro-scale while the mechanisms for the formation of a single crack have been lumped into the statistical distribution of the static strength in an empirical way. Without better understanding of the mechanism on the micro-scale, the estimated statistical distribution of the static

strength for a given laminates cannot be readily converted and applied to other configurations. For the future work, the mechanism for the development of a single crack during the cracking evolution should be studied. Based on this knowledge, certain mechanistic failure criteria under multiaxial stress state for static and fatigue loading should be developed. The developed statistical model can integrate such failure criteria to complete the multiscale modeling for the cracking evolution in composite laminates.

REFERENCES

[1] Talreja R. Damage analysis for structural integrity and durability of composite materials. Fatigue and Fracture of Engineering Materials and Structures. 2006;29(7):481-506.

[2] Nairn J. Matrix microcracking in composites. Polymer matrix composites. 2000;2:403-432.

[3] Budiansky B, Fleck N. Compressive failure of fibre composites. Journal of the Mechanics and Physics of Solids. 1993;41(1):183-211.

[4] Fleck N. Compressive failure of fiber composites. Advances in Applied Mechanics. 1997;33:43-117.

[5] Han Y, Hahn H, Croman R. A simplified analysis of transverse ply cracking in cross-ply laminates. Composites Science and Technology. 1988;31(3):165-177.

[6] Highsmith A, Reifsnider K. Stiffness reduction mechanisms in composite laminates. Damage in Composite Materials. 1982;775:103-117.

[7] Talreja R. Continuum mechanics characterization of damage in composite materials. Proceedings of The Royal Society of London, Series A: Mathematical and Physical Sciences. 1985;399(1817):195-216.

[8] Talreja R. Damage mechanics and fatigue life assessment of composite materials. International Journal of Damage Mechanics. 1999;8(4):339-354.

[9] Hoa SV. Principles of the manufacturing of composite materials. Lancaster, PA 17601: DEStech Publications, Inc.; 2009.

[10] Grunenfelder L, Nutt S. Void formation in composite prepregs-effect of dissolved moisture. Composites Science and Technology. 2010;70(16):2304-2309.

[11] Bowles KJ, Frimpong S. Void effects on the interlaminar shear strength of unidirectional graphite-fiber-reinforced composites. Journal of Composite Materials. 1992;26(10):1487.

[12] Liu L, Zhang B-M, Wang D-F, Wu Z-J. Effects of cure cycles on void content and mechanical properties of composite laminates. Composite Structures. 2006;73(3):303-309.

[13] de Almeida SFM, Neto Z. Effect of void content on the strength of composite laminates. Composite Structures. 1994;28(2):139-148.

[14] Olivier P, Cottu J, Ferret B. Effects of cure cycle pressure and voids on some mechanical properties of carbon/epoxy laminates. Composites. 1995;26(7):509-515.

[15] Costa ML, Almeida SrFMd, Rezende MC. The influence of porosity on the interlaminar shear strength of carbon/epoxy and carbon/bismaleimide fabric laminates. Composites Science and Technology. 2001;61(14):2101-2108.

[16] Tang J, Lee W, Springer G. Effects of cure pressure on resin flow, voids, and mechanical properties. Journal of Composite Materials. 1987;21(5):421.

[17] Joffe R, Krasnikovs A, Varna J. COD-based simulation of transverse cracking and stiffness reduction in [S/90n]s laminates. Composites science and technology. 2001;61(5):637-656.

[18] Cairns DS, Riddle T, Nelson J. Wind turbine composite blade manufacturing: the need for understanding defect origins, prevalence, implications and reliability. Sandia National Laboratories, Albuquerque, New Mexico 87185. 2011

[19] Toft HS, Branner K, Berring P, SÃ¸rensen JD. Defect distribution and reliability assessment of wind turbine blades. Engineering Structures. 2011;33(1):171-180.

[20] Varna J, Joffe R, Berglund L, Lundström T. Effect of voids on failure mechanisms in RTM laminates. Composites science and technology. 1995;53(2):241-249.

[21] Adams DO, Hyer MW. Effects of layer waviness on the compression strength of thermoplastic laminates. Journal of Reinforced Composites. 1993;12(4):414-429.

[22] Talreja R. Defect damage mechanics: broader strategy for performance evaluation of composites. Plastics, Rubber and Composites, 38. 2009;2(4):49-54.

[23] Ricotta M, Quaresimin M, Talreja R. Mode I strain energy release rate in composite laminates in the presence of voids. Composites Science and Technology. 2008;68(13):2616-2623.

[24] Boniface L, Smith P, Ogin S, Bader M. Observations on transverse ply crack growth in a(0/90 2) s CFRP laminate under monotonic and cyclic loading. Proceedings of the 6th International Conference on Composite Materials, vol 3: London. 1987.p. 156-165.

[25] Lafarie-Frenot M, Henaff-Gardin C. Formation and growth of 90 deg ply fatigue cracks in carbon/epoxy laminates. Composites Science and Technology. 1991;40(3):307-324.

[26] Boniface L, Smith PA, Bader MG, Rezaifard AH. Transverse ply cracking in cross-ply CFRP laminates - Initiation or propagation controlled? Journal of Composite Materials. 1997;31(11):1080-1112.

[27] Garrett K, Bailey J. Multiple transverse fracture in 90 cross-ply laminates of a glass fibre-reinforced polyester. Journal of Materials Science. 1977;12(1):157-168.

[28] Kies J. Maximum strains in the resin of fiberglass composites. US Naval Research Laboratory, NRL Report 65752, 1962.

[29] Sun Z, Daniel I, Luo J. Statistical damage analysis of high temperature composite laminates. Proceedings of the 43rd AIAA/ASME/ASCE Structures, Structural Dynamics and Materials Conference, Denver,2002.

[30] Parvizi A, Garrett K, Bailey J. Constrained cracking in glass fibre-reinforced epoxy cross-ply laminates. Journal of Materials Science. 1978;13(1):195-201.

[31] Flaggs D, Kural M. Experimental determination of the in situ transverse lamina strength in graphite/epoxy laminates. Journal of Composite Materials. 1982;16(2):103.

[32] Crossman F, Wang A. The dependence of transverse cracking and delamination on ply thickness in graphite/epoxy laminates. Damage in Composite Materials. 1982:118-139.

[33] Ho S, Suo Z. Tunneling cracks in constrained layers. Journal of Applied Mechanics. 1993;60(4):890.

[34] O'Brien T, Salpekar S. Scale effects on the transverse tensile strength of graphite/epoxy composites. Composite Materials: Testing and Design. 1993;11:23.

[35] Parvizi A, Bailey J. On multiple transverse cracking in glass fibre epoxy cross-ply laminates. Journal of Materials Science. 1978;13(10):2131-2136.

[36] Reifsnider K, Highsmith A. Characteristic damage states: a new approach to representing fatigue damage in composite laminates. Materials: Experimentation and Design in Fatigue. 1981:246-260.

[37] Peters P, Chou T. On cross-ply cracking in glass and carbon fibre-reinforced epoxy laminates. Composites. 1987;18(1):40-46.

[38] Andersons J, Joffe R, Sparnins E. Statistical model of the transverse ply cracking in cross-ply laminates by strength and fracture toughness based failure criteria. Engineering Fracture Mechanics. 2008;75(9):2651-2665.

[39] Liu S, Nairn J. The formation and propagation of matrix microcracks in cross-ply laminates during static loading. Journal of Reinforced Plastics and Composites. 1992;11(2):158.

[40] Manders P, Chou T, Jones F, Rock J. Statistical analysis of multiple fracture in 0/90/0 glass fibre/epoxy resin laminates. Journal of Materials Science. 1983;18(10):2876-2889.

[41] Hashin Z. Analysis of cracked laminates: a variational approach. Mechanics of Materials. 1985;4(2):121-136.

[42] Reifsnider K. Some fundamental aspects of the fatigue and fracture response of composite materials.Proceedings 14th Annual Meeting, Society of Engineering Science. Bethlehem, PA ; 1977. p. 373-384.

[43] Fukunaga H, Chou T, Peters P, Schulte K. Probabilistic failure strength analyses of graphite/epoxy cross-ply laminates. Journal of Composite Materials. 1984;18(4):339.

[44] Nairn JA. The strain energy release rate of composite microcracking: a variational approach. Journal of Composite Materials. 1989;23(11):1106-1129.

[45] Hashin Z. Thermal expansion coefficients of cracked laminates. Composites Science and Technology. 1988;31(4):247-260.

[46] Varna J, Berglund L. Multiple transverse cracking and stiffness reduction in cross-ply laminates. Journal of Composites Technology and Research. 1991;13(2):97-106.

[47] Varna J, Berglund LA. Thermo-elastic properties of composite laminates with transverse cracks. Journal of Composites Technology and Research. 1994;16(1):77-87.

[48] Praveen G, Reddy J. Transverse matrix cracks in cross-ply laminates: stress transfer, stiffness reduction and crack opening profiles. Acta Mechanica. 1998;130(3):227-248.

[49] McCartney LN. Theory of stress transfer in a 0-90-0 cross-ply laminate containing a parallel array of transverse cracks. Journal of the Mechanics and Physics of Solids. 1992;40(1):27-68.

[50] Varna J, Berglund L. A model for prediction of the transverse cracking strain in cross-ply laminates. Journal of Reinforced Plastics and Composites. 1992;11(7):708.

[51] Noh J, Whitcomb J. Effect of various parameters on the effective properties of a cracked ply. Journal of Composite Materials. 2001;35(8):689.

[52] Li S, Singh CV, Talreja R. A representative volume element based on translational symmetries for FE analysis of cracked laminates with two arrays of cracks. International Journal of Solids and Structures. 2009;46(7-8):1793-1804.

[53] Weibull W. A statistical distribution function of wide applicability. Journal of Applied Mechanics. 1951;18:293-297.

[54] Wetherhold RC. Statistics of fracture of composite materials under multiaxial loading, Ph.D. Dissertation. Univerisity of Delaware, 1983.

[55] Wang A, Chou P, Lei S. A stochastic model for the growth of matrix cracks in composite laminates. Journal of Composite Materials. 1984;18(3):239.

[56] Vinogradov V, Hashin Z. Probabilistic energy based model for prediction of transverse cracking in cross-ply laminates. International Journal of Solids and Structures. 2005;42(2):365-392.

[57] Takeda N, Ogihara S. In situ observation and probabilistic prediction of microscopic failure processes in CFRP cross-ply laminates. Composites science and technology. 1994;52(2):183-195.

[58] Peters P. The Strength Distribution of 90^{o} Plies in 0/90/0 Graphite-Epoxy Laminates. Journal of Composite Materials. 1984;18(6):545.

[59] Sun Z, Daniel I, Luo J. Modeling of fatigue damage in a polymer matrix composite. Materials Science and Engineering A. 2003;361(1-2):302-311.

[60] Asp L, Berglund LA, Talreja R. Prediction of matrix-initiated transverse failure in polymer composites. Composites Science and Technology. 1996;56(9):1089-1097.

[61] Talreja R, Akshantala NV. An inadequacy in a common micromechanics approach to analysis of damage evolution in composites. International Journal of Damage Mechanics. 1998;7(3):238-249.

[62] Cheng Z, Redner S. Scaling theory of fragmentation. Physical Review Letters. 1988;60(24):2450.

[63] Cho C, Holmes JW, Barber JR. Distribution of matrix cracks in a uniaxial ceramic composite. Journal of the American Ceramic Society. 1992;75(2):316-324.

[64] Louis BM. Gas transport in out-of-autoclave prepreg laminates, Master thesis, 2010.

[65] Repecka L, Boyd J. Vacuum-bag-only-curable prepregs that produce void-free parts. 47th International SAMPE symposium and exhibition, Long Beach, CA;2002.

[66] Boey F, Lye S. Void reduction in autoclave processing of thermoset composites:: Part 1: High pressure effects on void reduction. Composites. 1992;23(4):261-265.

[67] Ogasawara T, Yokozeki T, Onta K, Ogihara S. Linear and nonlinear torsional behavior of unidirectional CFRP and GFRP. Composites Science and Technology. 2007;67(15-16):3457-3464.

[68] Reifsnider K. The critical element model: a modeling philosophy. Engineering Fracture Mechanics. 1986;25(5-6):739-749.

[69] Chen AS, Matthews FL. A review of multiaxial biaxial loading tests for composite-materials. Composites. 1993;24(5):395-406.

[70] Swanson S, Messick M, Tian Z. Failure of carbon/epoxy lamina under combined stress. Journal of Composite Materials. 1987;21(7):619.

[71] Found M. A review of the multiaxial fatigue testing of fiber reinforced plastics. ASTM International; 1985:381.

[72] Hashin Z, Rotem A. A fatigue failure criterion for fiber reinforced materials. Journal of Composite Materials. 1973;7(4):448.

[73] Sims D, Brogdon V. Fatigue behavior of composites under different loading modes. Fatigue of filamentary composite materials. 1977:185–205.

[74] Awerbuch J, Hahn H. Off-axis fatigue of graphite/epoxy composite. ASTM International; 1981:243.

[75] Sun C, Vaidya R. Prediction of composite properties from a representative volume element. Composites science and Technology. 1996;56(2):171-179.

[76] Li S, Wongsto A. Unit cells for micromechanical analyses of particle-reinforced composites. Mechanics of Materials. 2004;36(7):543-572.

[77] Whitcomb J, Chapman C, Tang X. Derivation of boundary conditions for micromechanics analyses of plain and satin weave composites. Journal of Composite Materials. 2000;34(9):724.

[78] Li S. Boundary conditions for unit cells from periodic microstructures and their implications. Composites Science and Technology. 2008;68(9):1962-1974.

[79] Chou P, Croman R. Residual strength in fatigue based on the strength-life equal rank assumption. Journal of Composite Materials. 1978;12(2):177.

[80] Degrieck J, Van Paepegem W. Fatigue damage modeling of fibre-reinforced composite materials: review. Applied Mechanics Reviews. 2001;54:279.

[81] Charewicz A, Daniel IM. Damage mechanisms and accumulation in graphite/epoxy laminates. Composite Materials: Fatigue and Fracture, ASTM STP 907; 1986. p. 274-297.

[82] Miner MA. Cumulative damage in fatigue. Journal of Applied Mechanics. 1945;12(3):159 -164.

[83] Lee J, Daniel I, Yaniv, G. Fatigue life prediction of cross-ply composite laminates. Composite Materials: Fatigue and Fracture, ASTM STP 1012; 1989. P.19-28.

[84] Vivian L. Damage analysis on composite laminates under fatigue loading, Master thesis. University of Padova, 2011.

VITA

Yongxin Huang was born in Sichuan, China. He obtained his B.S. degree in Modern Mechanics at University of Science and Technology of China in 2006. In fall 2009, he obtained his M.S. degree in Aerospace Engineering at Texas A&M University. He received his Ph.D degree at Texas A&M University in 2012. Mr. Huang can be reached at iamhyx@tamu.edu. His contact address is:

Yongxin Huang

Texas A&M University

Department of Aerospace Engineering

H.R. Bright Building, Rm 701, Ross Street

College Station TX 77840